

**UNCLASSIFIED**

**D 4 3 8 0 1 7**

**DEFENSE DOCUMENTATION CENTER**

**FOR**

**SCIENTIFIC AND TECHNICAL INFORMATION**

**CAMERON STATION, ALEXANDRIA, VIRGINIA**

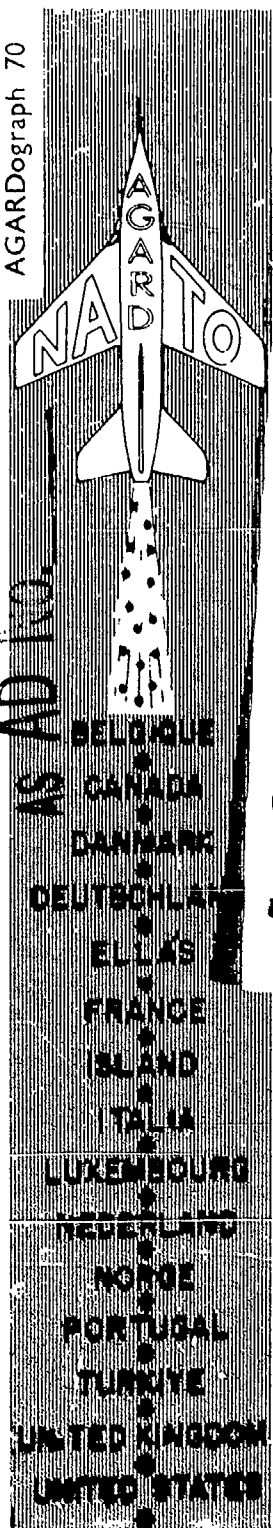


**UNCLASSIFIED**

NOTICE: When government or other drawings, specifications or other data are used for any purpose other than in connection with a definitely related government procurement operation, the U. S. Government thereby incurs no responsibility, nor any obligation whatsoever; and the fact that the Government may have formulated, furnished, or in any way supplied the said drawings, specifications, or other data is not to be regarded by implication or otherwise as in any manner licensing the holder or any other person or corporation, or conveying any rights or permission to manufacture, use or sell any patented invention that may in any way be related thereto.

CATALOGUE NO. 438017

AGARDograph 70



438017

AGARDograph 70

# AGARDograph

## FLOW VISUALIZATION IN WIND TUNNELS USING INDICATORS

Compiled by

R. L. MALTBY

APRIL 1962

NO OTS

NORTH ATLANTIC TREATY ORGANIZATION  
ADVISORY GROUP FOR AERONAUTICAL RESEARCH AND DEVELOPMENT

AGARDograph 70

NORTH ATLANTIC TREATY ORGANIZATION  
ADVISORY GROUP FOR AERONAUTICAL RESEARCH AND DEVELOPMENT  
(ORGANISATION DU TRAITE DE L'ATLANTIQUE NORD)

FLOW VISUALIZATION IN WIND TUNNELS  
USING INDICATORS

APRIL 1962

Compiled by

R.L. Maltby

Royal Aircraft Establishment, Bedford, England

This is one of a series of publications by the AGARD - NATO Fluid Dynamics Panel.

Professor Wilbur C. Nelson of The University of Michigan is the Editor.

533.6.071.3

358h6

## FLOW VISUALIZATION IN WIND TUNNELS USING INDICATORS

compiled by

R.L. Maltby\*

### PREFACE

Throughout the history of aerodynamic and hydrodynamic research it has been necessary to devise methods of making the flow visible to the experimenter so that he may understand its general nature before proceeding with detailed measurement or mathematical analysis. As the knowledge of the subject has advanced and the demands of aircraft design have changed new methods of flow visualization have had to be developed; the use of smoke and tufts for the study of separated flows, chemical and evaporative techniques for the identification of boundary layer transition, electric sparks for the measurement of velocity profiles, and so on. Most methods involve introducing some disturbing influence as indicators into the air flow and quantitative measurement becomes suspect, but these difficulties are avoided in the pure optical methods which play such a large part in investigations on compressible flows. These optical methods have been discussed by Holder, North and Wood in AGARDograph 23 and the present AGARDograph is intended to examine some of the other flow visualization techniques in current use in British wind tunnel practice.

Many of the techniques which are well established have already been fully described and a bibliography of these descriptions is included in Part V. Other techniques which have been devised and developed over the last few years to deal with current problems - particularly in relation to the understanding of separated flow regimes - have not always been described in as much detail as they deserve. Indeed, since they must be regarded only as a means to an end, few who make use of them have troubled to examine their validity or to understand the physical principles involved. This is particularly true of two of the most valuable methods for investigating three-dimensional flow structures, namely the vapour screen technique and the surface oil flow technique and the authors have therefore concentrated on these problems rather than on including detailed descriptions of techniques already adequately described elsewhere.

A Bibliography of indicator techniques is given in Part V which is intended to give references over the whole range of indicator techniques, particularly those techniques which are already well established. Reference numbers given in the text are prefixed with the Part number to distinguish them from Bibliography items.

The AGARDograph is based on four papers already published by the Royal Aircraft Establishment. Section 1.2 and Part IV have also been published in the Journal of Fluid Mechanics.

---

\* Royal Aircraft Establishment, Bedford, England

## CONTENTS

	Page
PREFACE	iii
LIST OF FIGURES	v
PART I	
THE SURFACE OIL FLOW TECHNIQUE	
L. C. Squire, R. L. Maltby, R. F. A. Keating and A. Stanbrook	1
PART II	
TECHNIQUES FOR LOCATING BOUNDARY LAYER TRANSITION	75
PART III	
SMOKE TECHNIQUES FOR USE IN LOW SPEED WIND TUNNELS	
R. L. Maltby and R. F. A. Keating	83
PART IV	
DEVELOPMENT OF THE VAPOUR SCREEN METHOD OF FLOW VISUALIZATION IN A 3 FT x 3 FT SUPERSONIC WIND TUNNEL	
I. McGregor	111
PART V	
BIBLIOGRAPHY	165
DISTRIBUTION	

LIST OF FIGURES

PART I		Page
Fig. I. 1	Co-ordinate system	50
Fig. I. 2	Variation of the thickness of the oil sheet at a stagnation point	50
Fig. I. 3	Variation of the ratio $H(= \delta_1/l')$ with $\alpha$ and $\gamma$	51
Fig. I. 4	Variation of the ratio $l \left( = \frac{l'^2}{u_0} \left( \frac{\partial u}{\partial z} \right)_0 \right)$ with $\alpha$ and $\gamma$	52
Fig. I. 5	Variation of the skin-friction on a surface for different values of the parameter $\gamma$ .	53
Fig. I. 6	Oil streamline pattern on a yawed wing	54
Fig. I. 7	Percentage reduction in apparent separation distance for different oil sheet thicknesses ( $h_0$ ) and aerofoil chords with speed	55
Fig. I. 8	Surface flow patterns on $A = 1$ delta wing at $\alpha = 15^\circ$ (chryseno, kerosene, U-V light)	56
Fig. I. 9	Surface flow pattern on yawed wing. Indication of vortex breakdown	57
Fig. I. 10	Surface flow pattern. Formation of wavelets in flocculent mixture	57
Fig. I. 11	Details of mobilometer	58
Fig. I. 12	Typical mobilometer results on $TiO_2$ - oil mixture	58
Fig. I. 13	The effect of an additive on a mixture of $TiO_2$ and kerosene	59
Fig. I. 14	Photographic data for use in RAE low speed wind tunnels	60
Fig. I. 15	Flow $45^\circ$ delta wing, $\alpha = 30^\circ$ , lampblack-kerosene	61
Fig. I. 16	Transition wedges shown by $TiO_2$ - kerosene mixture	61
Fig. I. 17	Surface flow on portion of $25^\circ$ swept wing ('Dayglo' in U-V light)	62
Fig. I. 18	Surface flow pattern on $55^\circ$ swept wing. (Anthracene-kerosene; U-V light)	63

	Page	
Fig. I. 19	(a) Examples of oil flow patterns	64-65
	(b) Examples of oil flow patterns (continued)	65-66
	(c) Examples of oil flow patterns (concluded)	67
Fig. I. 20	Typical effects of varying the amount of $TiO_2$ on the development of a pattern	68
Fig. I. 21	Typical oil flow patterns on a $15^\circ$ wedge	69
Fig. I. 22	Patterns obtained with different degrees of dispersion	69
Fig. I. 23	Flow patterns obtained with and without oleic acid in the oil mixture	70
Fig. I. 24	Effect of the proportions of the mixture on the time taken to form a pattern	71
Fig. I. 25	Theoretical variation of oil sheet thickness with time	72
Fig. I. 26	Correlation of time taken to form an oil flow pattern in various tunnels	73
Fig. I. 27	Viscosity/temperature relationship for various oils in use	74
PART II		
Fig. II. 28	Transition indicated by china clay technique (NPL)	81
PART III		
Fig. III. 29	Titanium tetrachloride smoke on slender delta wing (Harvey)	97
Fig. III. 30	Cambridge University version of Preston and Sweeting smoke generator	98
Fig. III. 31	Luminosity of mists	99
Fig. III. 32	$TiCl_4$ smoke generator	99
Fig. III. 33	Condensation in vortex cores	100
Fig. III. 34	Flow in edge vortex shown by soap bubble traces	100
Fig. III. 35	Brooks resin smoke generator	101

	Page	
Fig. III.36	Paper smoke generator	102
Fig. III.37	The smoke tube method	103
Fig. III.38	Vortex breakdown using the smoke tube method	103
Fig. III.39	Arrangement for smoke screen tests	104
Fig. III.40	Details of light source	104
Fig. III.41	Smoke screen technique	105
Fig. III.42	Flow pattern on flat plate. $\alpha = 25^\circ$	106
Fig. III.43	Smoke screen technique using linear flash tube	107
Fig. III.44	Smoke screen technique. Vortex development on delta wing	108
Fig. III.45	Smoke screen technique. Vortex development on delta wing	109
<b>PART IV</b>		
Fig. IV.46	Illumination system for vapour screen experiments	145
Fig. IV.47	Total temperature probe	146
Fig. IV.48	Variation of total temperature across the working section before and after overhaul of the aftercooler	146
Fig. IV.49	Relation between quantity of water added to the tunnel and the frostpoint	147
Fig. IV.50	Effect of Mach number on quantity of water required to produce a satisfactory vapour screen. Total pressure = 12 in. Hg. total temperature = 45°C	148
Fig. IV.51	Density of saturated water vapour as a function of temperature	149
Fig. IV.52	Effect of total pressure on the quantity of water required to produce a satisfactory vapour screen at a Mach number of 1.41	150
Fig. IV.53	Effect of humidity on working section static pressure at nominal Mach numbers of 1.51 and 1.81	151

	Page	
Fig. IV.54	Effect of humidity on actual Mach number and static pressure in the working section at nominal Mach numbers of 2.00 and 1.51	152
Fig. IV.55	Schlieren photographs of Mach waves used to determine the actual Mach number in the working section	153
Fig. IV.56	Vapour screen photographs of the flow behind a cambered delta wing at $M = 1.51$	154
Fig. IV.57	Vapour screen photographs of the flow behind a cambered delta wing at $M = 1.88$ ( $M_{dry} = 2.00$ )	155
Fig. IV.58	Vapour screen photographs of the flow over the upper surface of a plane wing at $M = 1.75$ ( $M_{dry} = 1.81$ )	156
Fig. IV.59	Comparison of surface oil-flow and vapour screen results on a plane wing at $M = 1.51$ , $\alpha = 8^\circ$	157
Fig. IV.60	Comparison of surface oil-flow and vapour screen results on a cambered wing at $M = 1.51$ , $\alpha = 8^\circ$	158
Fig. IV.61	Vapour screen photographs taken at $M = 1.32$ showing the 'blue line' phenomenon	159
Fig. IV.62	Vapour screen photographs of the flow behind a delta wing at $M = 0.85$ , $\alpha = 4^\circ$	160
Fig. IV.63	Vapour screen photographs of the flow behind a delta wing at $M = 0.85$ , $\alpha = 8^\circ$	161
Fig. IV.64	Saturated vapour density of some organic liquids suitable for vapour screen experiments	162
Fig. IV.65	Vapour screen photographs of the flow just behind a delta wing, using carbon tetrachloride vapour. $M = 1.96$	163
Fig. IV.66	Vapour screen photographs of the flow just behind a delta wing, using water vapour. $M = 1.83$ ( $M_{dry} = 2.00$ )	164

PART I

THE SURFACE OIL FLOW TECHNIQUE

## CONTENTS

	Page
LIST OF FIGURES	4
I. 1 INTRODUCTION	6
I. 2 THE MOTION OF A THIN OIL SHEET UNDER THE BOUNDARY LAYER ON A BODY	7
I. 2. 1 INTRODUCTION	7
I. 2. 2 EQUATIONS GOVERNING THE MOTION OF A THIN OIL SHEET	7
I. 2. 2. 1 Equations for the Oil-Flow Direction	7
I. 2. 2. 2 Equation Governing the Thickness of the Oil Sheet	11
I. 2. 3 OIL MOTION NEAR A STAGNATION POINT IN TWO-DIMENSIONAL FLOW	12
I. 2. 4 GENERAL SOLUTIONS OF THE EQUATIONS OF SECTION I. 2. 2	14
I. 2. 4. 1 Effect of the Oil on a Two-Dimensional Boundary Layer with an Arbitrary Pressure Gradient	14
I. 2. 4. 2 Variation of the Thickness of the Oil Sheet with Time	18
I. 2. 5 OIL STREAMLINE DIRECTIONS	19
I. 2. 6 EXTENSION OF THE RESULTS TO TURBULENT, AND COMPRESSIBLE, BOUNDARY LAYERS	21
I. 2. 6. 1 Turbulent Boundary Layers	21
I. 2. 6. 2 Boundary Layers in Compressible Flow	22
I. 2. 7 APPLICATION OF THE RESULTS OBTAINED TO THE INTERPRETATION OF TUNNEL OIL FLOW PATTERNS	22
I. 2. 8 CONCLUSIONS	23
NOTATION	24
APPENDIX I. 2. 1	26
APPENDIX I. 2. 2	27
REFERENCES	28
I. 3 THE SURFACE OIL FLOW TECHNIQUE FOR USE IN LOW SPEED WIND TUNNELS	29
I. 3. 1 INTRODUCTION	29
I. 3. 2 COMPOSITION OF THE PAINTS	29
I. 3. 2. 1 General Principles	29
I. 3. 2. 2 The Oil Medium	30
I. 3. 2. 3 Additives	31
I. 3. 2. 4 Pigments	32

	Page
1.3.3 APPLICATION OF PAINTS	34
1.3.4 RECIPES	34
1.3.5 PHOTOGRAPHIC RECORDING	35
1.3.6 INTERPRETATION OF OIL FLOW PATTERNS	36
REFERENCES	38
1.4 THE SURFACE OIL FLOW TECHNIQUE FOR USE IN HIGH SPEED WIND TUNNELS	39
1.4.1 INTRODUCTION	39
1.4.2 EXPERIMENTAL STUDY OF THE DEVELOPMENT OF THE PATTERN	39
1.4.2.1 Effect of the Pigment Concentration	39
1.4.2.2 Oleic Acid Additive	40
1.4.2.3 The Thickness of the Oil Sheet	42
1.4.3 COMPARISON OF THE VARIOUS FORMS OF THE TECHNIQUE	42
1.4.3.1 General Comments	42
1.4.3.2 Correlation of Running Times	44
1.4.4 MULTIPLE PATTERNS DURING A SINGLE RUN	45
1.4.5 CONCLUDING REMARKS - RECOMMENDED MIXTURE	45
APPENDIX 1.4.1	47
REFERENCES	49
FIGURES	50

## LIST OF FIGURES

		Page
Fig. I. 1	Co-ordinate system	50
Fig. I. 2	Variation of the thickness of the oil sheet at a stagnation point	50
Fig. I. 3	Variation of the ratio $H(= \delta_1/\theta)$ with $\alpha$ and $\gamma$	51
Fig. I. 4	Variation of the ratio $l \left( = \frac{\theta^2}{u_0} \left( \frac{\partial u_1}{\partial z} \right)_e \right)$ with $\alpha$ and $\gamma$	52
Fig. I. 5	Variation of the skin-friction on a surface for different values of the parameter $\gamma$ .	53
Fig. I. 6	Oil streamline pattern on a yawed wing	54
Fig. I. 7	Percentage reduction in apparent separation distance for different oil sheet thicknesses ( $h_0$ ) and aerofoil chords with speed	55
Fig. I. 8	Surface flow patterns on $A = 1$ delta wing at $\alpha = 15^\circ$ (chryseno, kerosene, U-V light)	56
Fig. I. 9	Surface flow pattern on yawed wing. Indication of vortex breakdown	57
Fig. I. 10	Surface flow pattern. Formation of wavelets in flocculent mixture	57
Fig. I. 11	Details of mobilometer	58
Fig. I. 12	Typical mobilometer results on $TiO_2$ - oil mixture	58
Fig. I. 13	The effect of an additive on a mixture of $TiO_2$ and kerosene	59
Fig. I. 14	Photographic data for use in RAE low speed wind tunnels	60
Fig. I. 15	Flow $45^\circ$ delta wing, $\alpha = 20^\circ$ , lampblack-kerosene	61
Fig. I. 16	Transition wedges shown by $TiO_2$ - kerosene mixture	61
Fig. I. 17	Surface flow on portion of $35^\circ$ swept wing ('Davglo' in U-V light)	62
Fig. I. 18	Surface flow pattern on $55^\circ$ swept wing. (Anthracene-kerosene; U-V light)	63

Fig. I. 19	(a) Examples of oil flow patterns	64 - 65
	(b) Examples of oil flow patterns (continued)	65 - 66
	(c) Examples of oil flow patterns (concluded)	67
Fig. I. 20	Typical effects of varying the amount of $TiO_2$ on the development of a pattern	68
Fig. I. 21	Typical oil flow patterns on a $15^\circ$ wedge	69
Fig. I. 22	Patterns obtained with different degrees of dispersion	69
Fig. I. 23	Flow patterns obtained with and without oleic acid in the oil mixture	70
Fig. I. 24	Effect of the proportions of the mixture on the time taken to form a pattern	71
Fig. I. 25	Theoretical variation of oil sheet thickness with time	72
Fig. I. 26	Correlation of time taken to form an oil flow pattern in various tunnels	73
Fig. I. 27	Viscosity/temperature relationship for various oils in use	74

## PART I. THE SURFACE OIL FLOW TECHNIQUE

## I.1 INTRODUCTION

The surface oil-flow technique is intended to enable the nature of the flow over the surface of a wind tunnel model to be investigated quickly and easily. The surface is coated with a specially prepared paint consisting of a finely powdered pigment, a suitable oil medium and, in some cases, a dispersing agent. The air flowing over the surface carries the oil with it and a streaky deposit of the powder remains to mark the direction of flow (Fig I.8). The patterns made by the streaks indicate directly the local directions of flow at the surface and by implication the general flow structure in the three-dimensional field above it. In some circumstances the position of transition from laminar to turbulent boundary layers may also be indicated.

On the face of it then, the technique offers a great amount of valuable information with very much less effort than would be required by other means and it is therefore important to examine its reliability. Doubts of its validity are sometimes raised on the score that the paint film will interfere with the flow in the boundary layer and also that the streaks do not necessarily lie in the local flow direction because of gravitational and pressure gradient effects. Although there is, undoubtedly, some substance in these objections, experience has shown that the effects are small and that the method gives reliable information in many complex conditions. Nevertheless it is of interest to know to what extent the presence of the oil affects the flow, and also what the pattern represents. As a basic step in the understanding of the oil-flow technique the theoretical motion of a thin oil sheet, of non-uniform thickness, on a surface under a boundary layer is studied in the next Section. The application of the technique to experiments in low-speed and high-speed wind tunnels is described subsequently.

## 1.2 THE MOTION OF A THIN OIL SHEET UNDER THE BOUNDARY LAYER ON A BODY

L.C. Squire

### I.2.1 INTRODUCTION

The main parameter in the problem is the ratio of the viscosity of the fluid in the boundary layer to the viscosity of the oil. The solutions obtained are valid for all values of this ratio likely to be found in practice. Numerical results have been produced for infinite wings with velocity distributions outside the boundary layer of the form  $U = ax$  or  $U = \beta_0 - \beta_1 x$ . The parameters have been related to typical pressure distributions and are calculated in Appendix I.2.1.

The numerical methods apply for incompressible laminar boundary layers; the extension of the results to compressible and turbulent layers is discussed in Section I.2.6.

### I.2.2 EQUATIONS GOVERNING THE MOTION OF A THIN OIL SHEET

#### I.2.2.1 Equations for the Oil-Flow Direction

The thickness of the oil sheet,  $h$ , is a function of surface position and time. It is generally not greater than about 0.05 in., and in the following analysis will be assumed to be of the same order as the boundary layer thickness. Then the motion of the oil is governed by the equations of slow viscous motion:

$$\frac{\partial u_2}{\partial t} = \nu_2 \nabla^2 u_2 - \frac{1}{\rho_2} \frac{\partial p_2}{\partial x} \quad (I.1)$$

$$\frac{\partial v_2}{\partial t} = \nu_2 \nabla^2 v_2 - \frac{1}{\rho_2} \frac{\partial p_2}{\partial y} \quad (I.2)$$

$$\frac{\partial w_2}{\partial t} = \nu_2 \nabla^2 w_2 - \frac{1}{\rho_2} \frac{\partial p_2}{\partial z} \quad (I.3)$$

together with the continuity equation

$$\frac{\partial u}{\partial x} + \frac{\partial v}{\partial y} + \frac{\partial w}{\partial z} = 0. \quad (I.4)$$

The co-ordinate system, and velocity components are defined in Figure I.1. The suffix 2 refers to motion in the oil and suffixes 0 and 1 refer to free-stream and boundary layer flow respectively. The boundary conditions are (i) that the oil velocities are equal to those in the boundary layer at the surface of the oil, (ii) that the viscous stresses in the oil and the air are also equal at the oil/air surface, and (iii) that at the body surface the oil is stationary. These conditions may be written:

$$\left. \begin{aligned} u_1 &= u_2; & v_1 &= v_2; & w_1 &= w_2 & \text{at } z = h \\ u_2 &= v_2 = w_2 = 0 & & & & & \text{at } z = 0 \end{aligned} \right\} \quad (I.5)$$

$$\mu_1 \frac{\partial u_1}{\partial z} = \mu_2 \frac{\partial u_2}{\partial z}; \quad \mu_1 \frac{\partial v_1}{\partial z} = \mu_2 \frac{\partial v_2}{\partial z} \quad \text{at } z = h. \quad (\text{I.6})^*$$

Equations (I.1) to (I.3) will now be simplified by order of magnitude considerations, taking account of two small quantities, the boundary layer thickness,  $\delta$ , and the ratio of the viscosities of air and oil,  $\frac{\mu_1}{\mu_2}$  ( $= \lambda$ , say) †.

By standard boundary layer theory,

$$\frac{\partial u_1}{\partial z} \text{ and } \frac{\partial v_1}{\partial z} \text{ are } O\left(\frac{1}{\delta}\right).$$

Thus by Equation (I.6),

$$\frac{\partial u_2}{\partial z} \text{ and } \frac{\partial v_2}{\partial z} \text{ are } O\left(\frac{\lambda}{\delta}\right).$$

At  $z = 0$ ,  $u_2$  and  $v_2$  are zero, thus within the oil  $u_2$  and  $v_2$  are  $O(\lambda)$ ; their derivatives with respect to  $x$  and  $y$  are also of the same order.

From the continuity equation, it then follows that  $\frac{\partial w}{\partial z}$  is  $O(\lambda)$  and, since  $w_2 = 0$  at  $z = 0$ , that  $w_2$  is  $O(\lambda \delta)$ . Differentiating the continuity equation with respect to  $z$  then shows that  $\frac{\partial^2 w_2}{\partial z^2}$  is  $O\left(\frac{\lambda}{\delta}\right)$ .

The order of the terms  $\frac{\partial u_2}{\partial t}$ ,  $\frac{\partial v_2}{\partial t}$  will now be considered. It has already been shown that  $u_2$ ,  $v_2$  are  $O(\lambda)$ , and so their influence on the boundary layer will be small. In this case Equations (I.1) to (I.6) represent the motion of an oil sheet under a steady boundary layer, in which the only variation with time enters through the boundary conditions (I.5) and (I.6), since  $h$  is a function of time. Therefore the derivatives under consideration may be written

$$\frac{\partial u_2}{\partial t} = \frac{\partial u_2}{\partial h} \frac{dh}{dt}; \quad \frac{\partial v_2}{\partial t} = \frac{\partial v_2}{\partial h} \frac{dh}{dt}.$$

At the edge of the layer  $w_2 = \frac{dh}{dt}$ , thus  $\frac{dh}{dt}$  is  $O(\delta \lambda)$  while  $\frac{\partial u_2}{\partial h}$ ,  $\frac{\partial v_2}{\partial h}$  have the same order as  $\frac{\partial u_2}{\partial z}$ ,  $\frac{\partial v_2}{\partial z}$ , namely  $O\left(\frac{\lambda}{\delta}\right)$ . Thus the time derivatives of  $u_2$  and  $v_2$

\* For the derivation of this boundary condition see Appendix I.2.2.

† For the range of oils used in tunnels  $\lambda$  lies in the range  $10^{-2}$  to  $10^{-4}$ .

are  $O(\lambda^2)$ . Similarly, the derivative  $\frac{\partial w_2}{\partial t}$  is  $O(\lambda^2 \delta)$ . When the orders of the terms in Equation (1.3) are considered it is found that the pressure change through the oil layer is  $O(\lambda \delta)$ . Thus the pressure may be regarded as constant through the oil layer, and since by standard boundary layer theory

$$p_0(x, y) = p_1(x, y)$$

then

$$p_2(x, y) = p_1(x, y) = p_0(x, y). \quad (1.7)$$

If Equations (1.1) and (1.2) are now divided by  $\nu_2$ , the pressure terms may be written (remembering  $\rho_0 = \rho_1$ ):

$$\frac{1}{\mu_2} \frac{\partial p_2}{\partial x} = \frac{\lambda}{\mu_1} \frac{\partial p_0}{\partial x} - \frac{\lambda}{\nu_1} \frac{1}{\rho_0} \frac{\partial p_0}{\partial x} \quad (1.8)$$

$$\frac{1}{\mu_2} \frac{\partial p_2}{\partial y} = \frac{\lambda}{\mu_1} \frac{\partial p_0}{\partial y} = \frac{\lambda}{\nu_1} \frac{1}{\rho_0} \frac{\partial p_0}{\partial y}. \quad (1.9)$$

By boundary layer theory  $\delta$  is  $O(\nu_1^{1/2})$ , while by Bernoulli's equation  $\frac{1}{\rho_0} \frac{\partial p_0}{\partial x}$  and  $\frac{1}{\rho_0} \frac{\partial p_0}{\partial y}$  are  $O(1)$ . Thus the pressure terms in Equations (1.8) and (1.9) are  $O\left(\frac{\lambda}{R^2}\right)$ . Equations (1.1) and (1.2) may now be simplified by retaining terms of the highest order only, when they become

$$v_2 \frac{\partial^2 u_2}{\partial z^2} = \frac{1}{\rho_2} \frac{\partial p_0}{\partial x} \quad (1.10)$$

$$v_2 \frac{\partial^2 v_2}{\partial z^2} = \frac{1}{\rho_2} \frac{\partial p_0}{\partial y}. \quad (1.11)$$

In Equations (1.10) and (1.11) the pressure terms are known from the external flow so that the equations are ordinary second order equations for  $u_2$  and  $v_2$ . These equations must be solved, in conjunction with the boundary layer equations

$$\left. \begin{aligned} u_1 \frac{\partial u_1}{\partial x} + v_1 \frac{\partial u_1}{\partial y} + w_1 \frac{\partial u_1}{\partial z} &= -\frac{1}{\rho_1} \frac{\partial p}{\partial x} + \nu_1 \frac{\partial^2 u_1}{\partial z^2} \\ u_1 \frac{\partial v_1}{\partial x} + v_1 \frac{\partial v_1}{\partial y} + w_1 \frac{\partial v_1}{\partial z} &= -\frac{1}{\rho_1} \frac{\partial p}{\partial y} + \nu_1 \frac{\partial^2 v_1}{\partial z^2} \\ u_1 \frac{\partial w_1}{\partial x} + v_1 \frac{\partial w_1}{\partial y} + w_1 \frac{\partial w_1}{\partial z} &= -\frac{1}{\rho_1} \frac{\partial p}{\partial z} + \nu_1 \frac{\partial^2 w_1}{\partial z^2} \end{aligned} \right\} \quad (1.12)^*$$

\* See footnote on page 10.

$$u_1 \frac{\partial v_1}{\partial x} + v_1 \frac{\partial v_1}{\partial y} + w_1 \frac{\partial v_1}{\partial z} = - \frac{1}{\mu_1} \frac{\partial p}{\partial y} - \gamma_1 \frac{\partial^2 v_1}{\partial z^2} \quad (I.12)^*$$

$$\frac{\partial u_1}{\partial x} + \frac{\partial v_1}{\partial y} + \frac{\partial w_1}{\partial z} = 0, \quad (I.13)^*$$

to satisfy the boundary conditions (I.5) and (I.6). A simple iterative approach used here, is to find solutions of Equations (I.10) and (I.11) satisfying the conditions

$$u_2 = v_2 = 0 \quad \text{at } z = 0$$

and

$$\mu_1 \frac{\partial u_1}{\partial z} = \mu_2 \frac{\partial u_2}{\partial z}; \quad \mu_1 \frac{\partial v_1}{\partial z} = \mu_2 \frac{\partial v_2}{\partial z} \quad \text{at } z = h.$$

The third condition is then satisfied by finding a solution of the boundary layer equations such that at  $z = h$ ,  $u_1 = (u_2)_{z=h}$ ,  $v_1 = (v_2)_{z=h}$ , where  $(u_2)_{z=h}$  and  $(v_2)_{z=h}$  are found from the solution of the oil flow equations. This process is iterative since  $\left(\frac{\partial u_1}{\partial z}\right)_{z=h}$  and  $\left(\frac{\partial v_1}{\partial z}\right)_{z=h}$  depend on  $(u_2)_{z=h}$  and  $(v_2)_{z=h}$ . However,

since these velocities are  $O(\lambda)$  the changes in  $\left(\frac{\partial u_1}{\partial z}\right)_{z=h}$  and  $\left(\frac{\partial v_1}{\partial z}\right)_{z=h}$  are also small and so the process should converge quickly.

By direct integration of Equations (I.10) and (I.11) solutions which satisfy the two boundary conditions are:

$$\left. \begin{aligned} u_2 &= \lambda \left\{ \left( \frac{1}{\mu_1} \frac{\partial p}{\partial x} \right) \left( \frac{z^2}{2} - h z \right) + \left( \frac{\partial u_1}{\partial z} \right)_{z=h} z \right\} \\ v_2 &= \lambda \left\{ \left( \frac{1}{\mu_1} \frac{\partial p}{\partial y} \right) \left( \frac{z^2}{2} - h z \right) + \left( \frac{\partial v_1}{\partial z} \right)_{z=h} z \right\} \end{aligned} \right\} \quad (I.14)$$

At the oil surface,  $z = h$ ,

$$(u_2)_{z=h} = \lambda \left\{ - \frac{h^2}{2} \left( \frac{1}{\mu_1} \frac{\partial p}{\partial x} \right) + h \left( \frac{\partial u_1}{\partial z} \right)_{z=h} \right\} \quad (I.15)$$

\* Equations (I.12) and (I.13) apply only for a flat surface, but they may be used on slightly curved surfaces. On more highly curved surfaces the full equations must be used (see Ref. 1.2.4).

The boundary condition  $w_2 = w_1$  should also be applied but as  $w_2$  is  $O(\lambda^2)$  this condition is replaced by  $w_1 = 0$  at  $z = h$ .

$$(v_2)_{z=h} = \lambda \left\{ -\frac{h^2}{2} \left( \frac{1}{\mu_1} \frac{\partial p}{\partial y} \right) + h \left( \frac{\partial v_1}{\partial z} \right)_{z=h} \right\} \quad (I.15)$$

and these are the velocities needed in the solution of the boundary layer equations.

The investigation of the boundary layer with the boundary conditions  $u_1 = u_2$ ,  $v_1 = v_2$  is carried out in Sections I.2.3 and I.2.4, where it is shown that the change in the boundary layer skin-friction is small.

It should be noted that the oil film, in addition to giving the boundary layer a non-zero velocity at the oil surface, also effectively changes the body shape, and hence the external flow. The latter effect, however, is small for thin oil films and is ignored. Then the boundary layer equations can be solved for the original pressure distribution with the non-zero velocity condition transferred to the body surface, that is

$$u_1 = (u_2)_h, \quad v_1 = (v_2)_h \quad \text{at } z = 0.$$

It is advisable at this point to consider the range of validity of the order of magnitude analysis made in this section. Goldstein (Ref. I.2.1) has shown that the approximations of boundary layer theory break down in the immediate neighbourhood of separation, consequently the equations for the oil flow, which are based on this theory, will also be invalid in this condition. As the main interest is in determining the position of separation it is important to know how close to separation the simplified equations hold. A numerical study of the boundary layer solution for a linearly retarded mainstream (Ref. I.2.3) has shown that the equations are valid for 99.5% of the distance to separation. It is reasonable to assume that the simplified oil flow equations are also valid in the same region.

#### 1.2.2.2 Equation Governing the Thickness of the Oil Sheet

So far the oil thickness,  $h$ , has been regarded as an arbitrary function of surface position and time. The equation satisfied by this function will now be determined. Consider the area ABCD in Figure 1; then in time  $\delta t$  the increase in height multiplied by the area  $\delta x \delta y$  is equal to the amount of oil which has moved on to the base ABCD less the amount which has moved off this area. In the limit, when  $\delta x$ ,  $\delta y$  and  $\delta t$  tend to 0, the equation for  $h$  becomes

$$\frac{\partial h}{\partial t} = -\frac{\partial}{\partial x} \int_0^h u_1 dz - \frac{\partial}{\partial y} \int_0^h v_1 dz. \quad (I.16)$$

Substituting for  $u_1$  and  $v_1$  from Equation (I.14) this becomes

$$\begin{aligned} \frac{1}{\lambda} \frac{\partial h}{\partial t} = & -\frac{\partial}{\partial x} \left\{ \left( \frac{\partial u_1}{\partial z} \right)_{z=0} \frac{h^2}{2} - \frac{1}{\mu_1} \frac{\partial p}{\partial x} \frac{h^3}{3} \right\} \\ & - \frac{\partial}{\partial y} \left\{ \left( \frac{\partial v_1}{\partial z} \right)_{z=h} \frac{h^2}{2} - \frac{1}{\mu_1} \frac{\partial p}{\partial y} \frac{h^3}{3} \right\}. \end{aligned} \quad (I.17)$$

Equation (I.17) is a non-linear partial differential equation where the functions  $\left(\frac{\partial u_1}{\partial z}\right)_{z=h}$  and  $\frac{\partial p}{\partial x}, \frac{\partial p}{\partial y}$  are, in general, of numerical form. Thus solutions will usually have to be found by numerical methods. However, one simple solution has been found corresponding to flow near a stagnation point in two-dimensional flow. This solution is described in Section I.2.3; the result of a direct numerical integration of Equation (I.17) will be described in Section I.2.4.2.

### I.2.3 OIL MOTION NEAR A STAGNATION POINT IN TWO-DIMENSIONAL FLOW

Near a two-dimensional stagnation point the velocity distribution in the stream-wise direction outside the boundary layer is of the simple form  $u = ax$ ; the oil flow in this case is of special interest because both the modified boundary layer equations and Equation (I.17) can be solved. Making, as in standard boundary layer theory, the transformation  $u_1 = ax f'(\eta)$ , where  $\eta = \left(\frac{a}{\nu_1}\right)^{1/2} z$  and the prime denotes differentiation with respect to  $\eta$ , the two-dimensional boundary layer equations

$$u_1 \frac{\partial u_1}{\partial x} + w_1 \frac{\partial u_1}{\partial z} = -\frac{1}{\rho_1} \frac{\partial p}{\partial x} + \nu_1 \frac{\partial^2 u_1}{\partial z^2} \quad (I.12)$$

$$\frac{\partial u_1}{\partial x} + \frac{\partial w_1}{\partial z} = 0 \quad (I.13)$$

reduce to

$$f'''(\eta) + f''(\eta)f(\eta) = (f'(\eta))^2 - 1 \quad (I.14)$$

(see Ref. I.2.2, page 139).

At the wall,  $z = 0$ ,  $f'(0) = \frac{(u_z)_h}{ax}$ , instead of the more usual value  $f'(0) = 0$ .

The other boundary conditions remain the same, i.e.  $f(0) = 0$ ,  $f'(\infty) = 1$ . The value of  $(u_z)_h$  can be found from Equation (I.15) to be

$$(u_z)_h = \lambda \left\{ \frac{a^2 h^2}{\nu_1} + \left(\frac{a^2}{\nu_1}\right)^{1/2} h f''(0) \right\} x, \quad (I.15)$$

so

$$f'(0) = \lambda \left\{ \frac{a h^2}{\nu_1} + \left(\frac{a}{\nu_1}\right)^{1/2} h f''(0) \right\} = \gamma \quad (\text{say}). \quad (I.16)$$

In practice Equations (I.14) and (I.16) must be solved by iteration, but before this is possible it is necessary to find  $h$ , which (by substituting Equation (I.15) in Equation (I.17)) is given as the solution of the equation

$$\begin{aligned}
 \frac{\partial h}{\partial t} &= -\lambda \frac{\partial}{\partial x} \left\{ \left( \frac{a^3}{\nu_1} \right)^{\frac{1}{2}} f''(0) \frac{h^2}{2} + \frac{a^2}{\nu_1} \frac{h^3}{3} \right\} x \\
 &= -\lambda \left\{ \left( \frac{a^3}{\nu_1} \right)^{\frac{1}{2}} f''(0) \frac{h^2}{2} + \frac{a^2}{\nu_1} \frac{h^3}{3} \right\} \\
 &= -Ah^2 - Bh^3 \quad (\text{say}), \tag{I.21}
 \end{aligned}$$

provided  $h$  is independent of  $x$ , which is true if  $h$  is constant at time  $t = 0$ .

Equations (I.18), (I.20) and (I.21) now depend on the three parameters  $\gamma$ ,  $A$  and  $B$ , where  $\gamma$  and  $A$  are functions of  $f''(0)$ . Equations (I.18) and (I.21) can, however, be solved for arbitrary values of these parameters and the solutions can be combined iteratively with Equation (I.20) to find the solution of any particular problem.

First consider Equation (I.18). As  $(u_1)_h$  is  $O(\lambda)$  this equation can be linearized by putting  $f'(\eta) = f'_0(\eta) + \gamma g'(\eta)$ , where  $f'_0(\eta)$  is the standard two-dimensional solution and where  $g'(0) = 1$ ;  $g(0) = 0$ ;  $g'(\infty) \rightarrow 0$ . Then  $g'(\eta)$  satisfies the equation

$$g'''(\eta) + f_0(\eta) g''(\eta) + f_0''(\eta) g'(\eta) - 2f_0'(\eta) g'(\eta) = 0. \tag{I.22}$$

This equation has been solved by standard numerical techniques to give the solution tabulated below:

$\eta$	$g'(\eta)$	$\eta$	$g'(\eta)$
0	1.000	2.0	0.053
0.2	0.840	2.2	0.034
0.4	0.686	2.4	0.021
0.6	0.547	2.6	0.012
0.8	0.425	2.8	0.007
1.0	0.322	3.0	0.004
1.2	0.238	3.2	0.002
1.4	0.171	3.4	0.001
1.6	0.119	3.6	0.000
1.8	0.081		

$g''(0) = -0.810.$

The solution of Equation (I.21) is readily obtained as

$$At = \frac{1}{h} - \frac{1}{h_2} + \frac{h}{A} \log \frac{h}{h_2} \left[ \frac{A + B h_2}{A + B h} \right] \tag{I.23}$$

$$Ah_z t = \left( \frac{1}{K} - 1 \right) + C \log K \left\{ \frac{1+C}{1+CK} \right\} \quad (I.24)$$

where  $C = h_z \frac{B}{A}$ ,  $K = \frac{h}{h_z}$  and  $h_z$  is the oil height at  $t = 0$ .  $K$  is plotted against  $Ah_z t$  in Figure 1.2 for various values of  $C$ .

These solutions for  $f(\eta)$  and  $h_z$  can now be combined to find the oil and boundary layer flow in the following particular case. The initial oil thickness is assumed to be 0.018 inch with  $\lambda = 1 \times 10^{-4}$  and the kinematic viscosity of air as  $2 \times 10^{-4}$  ft/sec. The external velocity is assumed to be of the form  $U = 10^2 x$  ft/sec (i.e.  $a = 10^4$ /sec). This corresponds, for example, to an aerofoil in an airstream of 120 ft/sec with the flow outside the boundary layer attaining the main-stream velocity at 0.144 inch behind the stagnation point.

Consider the oil flow at the start of the motion. In the first stage of the iteration use is made of the standard two-dimensional solution  $f_0''(0)$  (Ref. 1.2.2), from which  $f''(0) = f_0''(0) = 1.232$  and so  $\gamma = 4.3 \times 10^{-3}$  (Eqn (I.20)). With this value the second approximation for  $f''(0)$  becomes 1.228 and there is no change in  $\gamma$ . Thus in this case, with a rather thick oil layer, the skin-friction (which is proportional to  $f''(0)$ ) is reduced by less than  $\frac{1}{2}\%$ .

Now consider the motion after 10 seconds. Using  $f''(0) = 1.230$  and the above values of  $h_z$  and  $a$ , it follows that  $C = 5.8$  and  $Ah_z t = 65$ , so that from Equation (I.24)  $K$  is approximately 0.015 and so the oil thickness has been reduced to less than one sixtieth of its original value. This example, although of rather academic interest, is of value from two points of view. In the first place the numerical results can be used to check the magnitude of the terms ignored in Equations (I.1), (I.2) and (I.3). Also in this case the change in oil thickness is quite rapid so that it is possible that the unsteady boundary layer equations should have been used. However, in the ten seconds considered,  $\gamma$  changes from  $4.3 \times 10^{-3}$

to almost zero. Thus  $\frac{d\gamma}{dt} \approx 4.3 \times 10^{-4}$  per second and, since  $u_1 = ax(f'(\eta) + \gamma g'(\eta))$ ,

$\frac{du_1}{dt} \approx ax \times 4.3 \times 10^{-4}$ . In Equation (I.12) the dominant terms near  $x = 0$  are  $\frac{1}{\rho_1} \frac{\partial p}{\partial x}$

and  $\nu_1 \frac{\partial^2 u_1}{\partial x^2}$ , and  $\frac{1}{\rho_1} \frac{\partial p}{\partial x} = -a^2 x$ . Thus the ratio of the unsteady term,  $\frac{\partial u_1}{\partial t}$ ,

compared with the dominant terms is  $a^{-1} \times 10^{-4}$  or  $O(10^{-6})$ , confirming that use of the steady equation is justified.

## 1.2.4 GENERAL SOLUTIONS OF THE EQUATIONS OF SECTION 1.2.2

### 1.2.4.1 Effect of the Oil on a Two-Dimensional Boundary Layer with an Arbitrary Pressure Gradient

In this Section the effect of the oil on two-dimensional boundary layers is considered. The extension to three-dimensional boundary layers would involve considerr-

able numerical work which has not been carried out as the analysis of the present section suggests that the effect of the oil is extremely small for cases which are likely to arise in practice. The method used is based on the momentum equation; it is first shown that this equation is unaltered by the changed inner boundary condition\* and then that the velocity can be represented by a modified Pohlhausen profile.

Integrating the two-dimensional form of the boundary layer equations, (I.12) and (I.13) with respect to  $z$ , the following equation is obtained:

$$\int_0^{\delta} u_1 \frac{\partial u_1}{\partial z} dz + \int_0^{\delta} w_1 \frac{du_1}{dz} dz = \int_0^{\delta} u_0 \frac{\partial u_0}{\partial x} dz - \nu_1 \left[ \frac{\partial u_1}{\partial z} \right]_0 \quad (\text{I.25})$$

where  $\frac{1}{\rho_1} \frac{\partial p}{\partial x}$  has been replaced by  $u_0 \frac{\partial u_0}{\partial x}$ .

Using the continuity equation the term  $\int_0^{\delta} w_1 \frac{du_1}{dz} dz$  is eliminated by writing

$$\begin{aligned} \int_0^{\delta} w_1 \frac{\partial u_1}{\partial z} dz &= [w_1 u_1]_0^{\delta} - \int_0^{\delta} u_1 \frac{\partial w_1}{\partial z} dz \\ &= [w_1 u_1]_0^{\delta} + \int_0^{\delta} u_1 \frac{\partial u_1}{\partial x} dz \end{aligned} \quad (\text{I.26})$$

The lower limit of the term in square brackets is 0, since, at  $z = 0$ ,  $w_1 = 0$ ; (this is true although  $u_1 \neq 0$ ). At

$$z = \delta, \quad w_1 = \int_0^{\delta} \frac{\partial w}{\partial z} dz = - \int_0^{\delta} \frac{\partial u_1}{\partial x} dz.$$

Thus Equation (I.25) becomes

$$2 \int_0^{\delta} u_1 \frac{\partial u_1}{\partial x} dz - u_0 \int_0^{\delta} \frac{\partial u_1}{\partial x} dz - \int_0^{\delta} u_0 \frac{\partial u_0}{\partial x} dz = - \nu_1 \left[ \frac{\partial u_1}{\partial z} \right]_{z=0} \quad (\text{I.27})$$

This equation is exactly the same as the standard two-dimensional equation and will be written

$$\frac{\partial(\delta^2)}{\partial x} = 2 \frac{\delta^2}{u_0} \frac{\partial u_0}{\partial x} (2 + H) - \frac{2 \nu_1 l}{u_0} \quad (\text{I.28})$$

\* For convenience the inner boundary condition will be applied at  $x' = 0$  rather than  $x = h$ , and the prime dropped subsequently.

where

$$\theta = \int_0^\delta \left(1 - \frac{u_1}{u_0}\right) \frac{u_1}{u_0} dz; \quad \delta_1 = \int_0^\delta \left(1 - \frac{u_1}{u_0}\right) dz$$

$$H = \delta_1/\theta; \quad l = \frac{\theta}{u_0} \left(\frac{\partial u_1}{\partial z}\right)_{z=\delta}$$

Equation (I.28) may be solved in the usual manner by regarding  $\frac{u_1}{u_0}$  as a polynomial function of  $\frac{z}{\delta}$ , satisfying certain boundary conditions. These conditions will now be considered. At the edge of the boundary layer,  $z = \delta$ ,  $u_1$  tends smoothly to  $u_0$ . Thus, as in the standard method

$$\frac{u_1}{u_0} = 1, \quad \frac{\partial}{\partial z} \left(\frac{u_1}{u_0}\right) = 0, \quad \frac{\partial^2}{\partial z^2} \left(\frac{u_1}{u_0}\right) = 0 \quad \text{at } z = \delta.$$

At  $z = 0$ ,  $u_1 = (u_2)_h$  (i.e. the oil velocity). Thus  $\frac{u_1}{u_0} = \frac{(u_2)_h}{u_0} = \gamma$ , where  $\gamma$  may be a function of  $x$ . At  $z = 0$ ,  $w_1 = 0$ ; thus in Equation (I.12)

$$\nu_1 \left(\frac{\partial^2 u_1}{\partial z^2}\right)_{z=0} = (u_1)_h \frac{\partial (u_2)_h}{\partial x} - u_0 \frac{\partial u_0}{\partial x}$$

but

$$\nu_1 \frac{\partial^2 u_1}{\partial z^2} = \nu_1 \frac{u_0}{\delta^2} \frac{\partial^2 \left(\frac{u_1}{u_0}\right)}{\partial \left(\frac{z}{\delta}\right)^2}$$

therefore

$$\left[ \frac{\partial^2 \left(\frac{u_1}{u_0}\right)}{\partial \left(\frac{z}{\delta}\right)^2} \right]_{z=0} = \frac{\delta^2}{\nu_1} \left\{ \gamma \frac{\partial (u_2)_h}{\partial x} - \frac{\partial u_0}{\partial x} \right\} = \Lambda \quad (\text{say}). \quad (\text{I.29})$$

A Pohlhausen profile modified to satisfy these boundary conditions is:

$$\frac{u_1}{u_0} = \gamma + (1 - \gamma) \left\{ 2 \left(\frac{z}{\delta}\right) - 2 \left(\frac{z}{\delta}\right)^3 + \left(\frac{z}{\delta}\right)^4 \right\} + \frac{\Lambda}{6} \left[ 1 - \left(\frac{z}{\delta}\right)^3 \right] \left(\frac{z}{\delta}\right). \quad (\text{I.30})$$

Then by integration of this function

$$\theta = \frac{\delta}{315} \left\{ (1 - \gamma) \left( 37 + \frac{115}{2} \gamma \right) - \frac{\Lambda}{\delta} \left( 1 + \frac{55}{8} \gamma \right) - \frac{5}{144} \Lambda^2 \right\} \quad (I.31)$$

$$\delta_1 = \frac{\delta}{120} \{ 36(1 - \gamma) - \Lambda \} \quad (I.32)$$

$$\left( \frac{\partial u_1}{\partial z} \right)_{z=0} = \frac{1}{\delta} \left[ 2(1 - \gamma) + \frac{\Lambda}{6} \right]. \quad (I.33)$$

These values could be substituted into Equation (I.28) to give an equation for  $\Lambda$ . Instead a slightly different approach is used as it leads to less numerical work. In this approach  $H$  and  $l$  are regarded as functions of the parameters

$$\frac{\theta^2}{u_0} \left( \frac{\partial^2 u_1}{\partial z^2} \right)_{z=0} = \left\{ \frac{\theta^2}{\delta^2} \Lambda = \alpha \quad (\text{say}) \right\} \quad \text{and } \gamma.$$

These functions, obtained from Equations (I.31) and (I.32), are plotted in Figures I.3 and I.4.

The method has been used to study the boundary layer developed by an external velocity of the form  $u_0 = \beta_0 - \beta_1 x$ . The following values have been assumed for  $\gamma$ :  $\gamma = 0$ ,  $\pm 0.05$ , and  $\gamma$  varying linearly from  $+0.05$  at the leading edge to  $-0.05$  at the trailing edge.\* The resulting skin-friction curves are plotted in Figure I.5. From comparison with the no-oil curve ( $\gamma = 0$ ) it will be seen that the major effect of the oil is where the skin-friction approaches zero, that is in the vicinity of separation; the distance to separation is changed by at most 9%. In Appendix I.2.1 values of  $\gamma$  likely to be found in practice are investigated and it is found that maximum values of  $\gamma$  are of order 0.01. Thus in general the oil will only have a small influence on the boundary layer, changing the distance to separation by at most 2%. It should be noted that  $\gamma$  increases as the oil viscosity decreases, and thus the influence of the oil on the boundary layer increases with a decrease in oil viscosity.

The accuracy of the present analysis for the boundary layer on a moving surface, as compared with the accuracy of the Pohlhausen method for a stationary surface, has been investigated briefly. For the case of zero pressure gradient the skin-friction as given by Equations (I.28) and (I.30) has been compared with an exact solution of the problem (Ref. I.2.4). The skin-friction values given by the two methods are in close agreement for all values of  $\gamma$  between 0 and 1. With an adverse pressure gradient the accuracy is more difficult to estimate; however, it has been found that for the velocity distributions  $u = \beta_0 - \beta_1 x$  and  $\gamma \geq 0.15$  the separation point begins to move towards the leading edge as  $\gamma$  is increased, thus reversing the trend

\* Too many parameters enter a practical case to use an actual distribution of  $\gamma$ . However, in all cases  $\gamma$  is positive at the leading edge and negative at separation.

shown in Figure I.5 for  $\gamma < 0.05$ . This forward movement of separation is contrary to the expected physical action of the moving surface and suggests that the Pohlhausen method becomes less accurate for large values of  $\gamma$ .

#### I.2.4.2 Variation of the Thickness of the Oil Sheet with Time

The variation of the oil thickness,  $h$ , with time and position is determined by the solution of Equation (I.17). Only one solution of this equation has been found, and this for the rather restricted case of the two-dimensional stagnation point. From the form of the equation it can be seen that in two dimensions a steady oil state is impossible, for in the steady state  $\frac{\partial h}{\partial t} = 0$  and this would imply that

$$\frac{\partial}{\partial x} \int_0^h u_2 dz = 0$$

or

$$\int_0^h u_2 dz = \text{constant} . \quad (\text{I.34})$$

It would then follow that the amount of oil passing any point is constant, but since at the leading edge  $u_2$  is zero, no oil passes that point and the constant in Equation (I.34) is zero. Thus by Equation (I.17)

$$\frac{1}{2} h^2 \left( \frac{\partial u_1}{\partial z} \right)_0 - \frac{h^3}{3} \frac{1}{\mu_1} \frac{\partial p}{\partial x} = 0$$

so

$$h = 0 \quad \text{or} \quad \frac{3}{2} \left( \frac{\partial u_1}{\partial z} \right)_0 \left/ \frac{1}{\mu_1} \frac{\partial p}{\partial x} \right. . \quad (\text{I.35})$$

The non-zero form of  $h$  is infinite at the pressure minimum, and so there is no steady form of  $h$  except  $h = 0$ . (This result is also true on infinite yawed wings

since in this case  $\frac{\partial}{\partial y} \int_0^h v_2 dz = 0$ ).

In general, then,  $h$  is a variable function of time. No approximate method has been found to determine  $h$  and it would appear that the only method is the direct numerical integration of Equation (I.17). (Expansion in powers of  $t$  was found to be only slowly convergent, even for very small values of  $t$ .)

A numerical integration of Equation (I.17) has been carried out for the oil thickness under a two-dimensional boundary layer with an external velocity distribution of the form  $u_0 = \beta_0 - \beta_1 x$ . In this case Equation (I.17) may be written:

$$\frac{\partial h'}{\partial \left( \frac{t}{\sqrt{\beta_1}} \right)} = - \frac{\partial}{\partial \xi} \left\{ (1 - \xi) \left[ \frac{(h')^2}{2} f(\xi) - \frac{(h')^3}{3} \right] \right\} \quad (\text{I.36})$$

where  $\xi = \frac{\beta_1}{\beta_0} x$ ,  $h' = \left(\frac{\beta_1}{\nu_1}\right)^{1/2} h$  and  $f(\xi)$  is the non-dimensional skin-friction given by Howarth (Ref.I.2.3). The boundary condition is  $h' = 0.5$ , for all  $\xi$ , at  $t = 0$ .

The numerical integration of Equation (I.36) is very long and laborious and so only coarse steps have been used to determine the trends of the solution. In general the oil leaves the leading edge very quickly and flows downstream. Over the rear half of the region between the leading edge and the boundary layer separation the oil thickness is almost uniform, but increases steadily with time. The indication from this rough calculation is that the actual amount of oil on the surface appears to increase, suggesting that there may be an inflow of oil from downstream of separation.

### I.2.5 OIL STREAMLINE DIRECTIONS

In this section the oil flow direction on a general surface is considered. From the oil velocities given in Equation (I.14) the oil streamline direction is:

$$\frac{dy}{dx} = \frac{\left(\frac{\partial v_1}{\partial z}\right)_{z=0} + \frac{1}{\nu_1} \left(\frac{1}{\rho_1} \frac{\partial p}{\partial y}\right) \left\{\frac{z}{2} - h\right\}}{\left(\frac{\partial u_1}{\partial z}\right)_{z=0} + \frac{1}{\nu_1} \left(\frac{1}{\rho_1} \frac{\partial p}{\partial x}\right) \left\{\frac{z}{2} - h\right\}} \quad (I.37)$$

This direction varies between

$$\frac{\left(\frac{\partial v_1}{\partial z}\right)_{z=0} - \frac{h}{\nu_1} \left(\frac{1}{\rho_1} \frac{\partial p}{\partial y}\right)}{\left(\frac{\partial u_1}{\partial z}\right)_{z=0} - \frac{h}{\nu_1} \left(\frac{1}{\rho_1} \frac{\partial p}{\partial x}\right)}$$

at the wall and

$$\frac{\left(\frac{\partial v_1}{\partial z}\right)_{z=0} - \frac{h}{2\nu_1} \left(\frac{1}{\rho_1} \frac{\partial p}{\partial y}\right)}{\left(\frac{\partial u_1}{\partial z}\right)_{z=0} - \frac{h}{2\nu_1} \left(\frac{1}{\rho_1} \frac{\partial p}{\partial x}\right)}$$

at the oil surface.

The direction of the boundary layer surface streamlines in the absence of the oil is

$$\left(\frac{\partial v_1}{\partial z}\right)_{z=0} / \left(\frac{\partial u_1}{\partial z}\right)_{z=0}$$

In general the pressure term is small compared with the skin-friction term and so has only a small influence on the oil direction except near points of small skin-friction, for example, near separation. In Figure I.6 the oil streamlines at the wing surface and at the oil surface on an infinite swept wing are drawn. The chord-wise velocity on this wing was assumed to be of the form\*  $u = \beta_0 - \beta_1 x$ ; the skin-friction was then found by Howarth's power series solution (Ref. I. 2.3), and the cross-flow by the methods of Reference I.2.4. The oil streamlines were considered for a stage when the oil height varied linearly† from zero at the leading edge to twice its original height at the separation point (starting from an initial uniform height of 0.001 inch). It will be seen in Figure I.6 that the two oil streamlines closely follow the surface streamline with no oil on the surface, except that the oil streamlines become parallel to the leading edge before the surface streamline.

Eichelbrenner and Oudart (Ref. I.2.5) have shown that on a general surface the surface streamlines form an envelope at the separation line, and an envelope of the oil streamlines is usually taken as indicating separation. On a yawed infinite wing the envelope is parallel to the leading edge. Thus, in Figure I.6, the oil tends to indicate separation too early.

Changes in oil thicknesses, forward speeds, and velocity distributions do not affect the shape of the curves but merely the relative position at which the curves become parallel to the leading edge; the actual positions are given by the two points at which

$$\left(\frac{\partial u_1}{\partial z}\right)_0 - \frac{h}{\nu_1 \rho_1} \frac{\partial p}{\partial x} = 0$$

and

$$\left(\frac{\partial u_1}{\partial z}\right)_0 - \frac{h}{2\nu_1 \rho_1} \frac{\partial p}{\partial x} = 0.$$

Taking the mean of these two points as the separation point indicated by the oil, the reduction in separation distance, as a percentage of the chord, for various speeds and model sizes is plotted in Figure I.7.

These curves, which are independent of the oil viscosity, are useful as guides to the thickness of oil which should be used. For example, with a velocity normal to the leading edge of 800 ft/sec and a chord of 6 in. an oil height of less than 0.0005 in. must be used to keep the separation line indicated by oil within 1% of the true separation line. For a chord of 24 in. and the same velocity the oil thickness can be doubled while still giving results of the same accuracy.

---

\* The constants  $\beta_0$  and  $\beta_1$  are related to the velocity recovery of an RAE.104 aerofoil,  $C_L = 0.2$ ; details are given in Appendix I.2.1.

† The oil thickness at other conditions, i.e. with a non-linear variation along the surface, did not greatly affect the results as plotted.

## I. 2. 6 EXTENSION OF THE RESULTS TO TURBULENT, AND COMPRESSIBLE, BOUNDARY LAYERS

### I. 2. 6. 1 Turbulent Boundary Layers

So far the analysis has been confined to laminar layers since the calculation of the boundary layer in this case is relatively simple. In this section the flow under a turbulent boundary layer is studied in a qualitative manner. Within the oil layer the equations of motion, and the boundary conditions are unaltered provided that the boundary condition defining equality of stress is written:

$$\mu_2 \frac{\partial u_2}{\partial z} = (\tau_x)_1 ; \quad \mu_2 \frac{\partial v_2}{\partial z} = (\tau_y)_1 \quad (I. 38)$$

where  $(\tau_x)_1$  and  $(\tau_y)_1$  are the x and y components of the mean\* skin-friction in the turbulent boundary layer. With this form of boundary condition the oil velocity components become:

$$u_2 = \frac{1}{\mu_2} \left\{ \frac{\partial p}{\partial x} \left( \frac{z^2}{2} - h z \right) + (\tau_x)_1 z \right\} \quad (I. 39)$$

$$v_2 = \frac{1}{\mu_2} \left\{ \frac{\partial p}{\partial y} \left( \frac{z^2}{2} - h z \right) + (\tau_y)_1 z \right\} \quad (I. 40)$$

with corresponding forms for the streamlines.

To make use of these equations would involve the calculation of  $(\tau_x)_1$  and  $(\tau_y)_1$ , and so far no method is available for such a calculation in the general case. Even for the case of the infinite yawed wing experimental results show that the chordwise flow is not sufficiently independent of the cross-flow to be found by two-dimensional methods. Thus even in this simple case two-dimensional values may not strictly be used in Equation (I.39) to determine the apparent separation line. However, such results are probably adequate to indicate the order of the distance between apparent and actual separation. For this purpose experimental results quoted in Reference I.2.2 for a cylinder and an aerofoil ( $t/c = 15\%$ ) are used in Equations (I.39) and (I.40). These experimental results give values of the skin-friction and the pressure distributions on a cylinder of 5.89 in. diameter at Reynolds numbers between  $1 \times 10^5$  and  $2.5 \times 10^5$ . Similar measurements are given for the aerofoil at various incidences.

From the results quoted for the aerofoil (and the cylinder at the higher Reynolds numbers), it is found, for oil thicknesses of 0.005 in. and less, that the change in the separation point as indicated by the oil is of the same order as in laminar flows. Since on the wing the flow is now attached over most of the surface the ratio of apparent attached flow to actual attached flow will be closer to unity for turbulent boundary layers than for laminar flows.

The flow on the cylinder is initially laminar, but becomes turbulent before separation. The skin friction on the cylinder increases with distance from the

---

\* 'mean' with respect to time.

stagnation point, reaches a maximum near the minimum pressure point, and then decreases again. At transition the turbulence causes the skin-friction to increase again, before it finally becomes zero at the separation point. At the lower Reynolds numbers the skin friction at transition is quite low, whereas the pressure gradient is quite large, and substitution of the quoted values in Equation (I.39) shows that  $u_2$  could be zero at the transition point for an oil thickness of about 0.005 in. So on a yawed cylinder the oil streamlines could form an envelope at the transition line. In the absence of any other information this pattern could be erroneously interpreted as a laminar separation followed possibly by a turbulent reattachment.

#### I.2.6.2 Boundary Layers in Compressible Flow

In Section I.2.2 it has been shown that the velocity is very much smaller in the oil than in the external flow, thus even in cases where the external flow is supersonic the oil flow is still governed by the equations of slow viscous motion, and the solution is as in Equation (I.14). It thus seems probable that the oil pattern will be similar to that discussed in Section I.2.5 for incompressible flows. However, the flow may now be complicated by the presence of shock waves. The pressure rise through a shock may be sufficient to separate the boundary layer (Ref. I.2.6) and the inferences made about the oil motion in the region of separation in Section I.2.5 will also apply to such shock induced separations. In Section I.2.5 it was shown that near separation the oil velocity becomes zero before the boundary layer skin-friction is zero, and in this case, also, the oil may be expected to indicate an earlier separation. For a linear adverse pressure gradient it has been shown that the oil indication underestimates the distance to separation by, at most, 5%. As the upstream influence of the shock wave in the boundary layer is of the order of one hundred boundary layer thicknesses, it would appear that the error in indicated separation will be of the order of 5 boundary layer thicknesses.

Another effect at higher speeds is that of aerodynamic heating, and heat transfer. In general the heating will change the oil viscosity and so the ratio  $\lambda$  will become a variable depending on the state of the boundary layer. However, provided this change in  $\lambda$  is not too great, the main effect on the oil pattern will be small since, as shown in Section I.2.5, the actual pattern is independent of oil viscosity.

#### I.2.7 APPLICATION OF THE RESULTS OBTAINED TO THE INTERPRETATION OF TUNNEL OIL FLOW PATTERNS

In this Report the motion of a thin oil sheet has been studied, as the first stage in the understanding of the oil-flow patterns obtained in model testing. If the oil actually moved as a sheet the resultant oil pattern would supply only limited indication of the oil motion; the only features to be seen would be separation, where the oil would pile up up-stream, and regions of high skin-friction, such as under a vortex, where the surface would be cleared of oil. Generally in practice the oil, although applied as a sheet, moves in filaments, which provide more detailed information on the direction of the oil motion. The motion of these filaments depends on a different set of equations to those considered in this Report. However, the mechanism of the motion is probably similar; that is, the resultant force acting on the oil is a balance between the pressure gradient outside the boundary layer and the stress due to the boundary layer skin-friction. Thus it may reasonably be supposed that the description

of the oil film motion also applies qualitatively to the motion of the filaments, and that the orders of magnitude of the changes in separation point are similar in both cases. Stalker (Ref. I.2.7) has studied the mechanism which results in the formation of the filaments, and by order of magnitude considerations shows that these filaments do in fact follow the surface streamlines except near separation.

#### I.2.8 CONCLUSIONS

A solution has been obtained for the motion of a thin oil sheet moving on a surface under the influence of a boundary layer. The following deductions are made from the analysis.

(a) *The motion of the oil relative to the boundary layer*

The oil follows the boundary layer surface streamlines except near separation where it tends to form an envelope upstream of the true separation envelope. This early indication of separation is expected to occur for both compressible and incompressible flow; it is less marked for turbulent than laminar layers. The distance by which separation is apparently altered depends on the oil thickness, and the model size, but it is independent of the oil viscosity (provided this viscosity is much greater than the viscosity of the fluid of the boundary layer).

(b) *The effect of the oil flow on the motion of the boundary layer*

This effect is very small in most practical cases but increases as the oil viscosity decreases.

(c) *Interpretation of the oil pattern at low Reynolds number*

Results at low Reynolds number should be treated with caution as transition could be erroneously interpreted as separation.

## NOTATION IN SECTION 1.2

a	constant for flow at the stagnation point; $u = ax$
A, B, C	functions used in the determination of the oil height
	$A = \lambda \left( \frac{a}{\nu_1} \right)^{1/2} \frac{f''(0)}{2}, \quad B = \lambda \frac{a^2}{3\nu_1}, \quad C = h_z B/A$
$f'(\eta), g'(\eta)$	boundary layer velocity profiles
H	ratio of displacement to momentum thicknesses of the boundary layer $\delta_1/\theta$
$h(x, y, t)$	thickness of the oil sheet
K	ratio of oil height at any time to height at zero time
l	non-dimensional form related to the skin-friction $= \frac{\theta}{u_0} \left( \frac{\partial u_1}{\partial z} \right)_{z=0}$
p	static pressure
u, v, w x, y, z	velocity components } see Figure I.1 co-ordinate system
$\alpha$	parameter used to calculate the boundary layer $= \frac{\beta^2}{u_0} \left( \frac{\partial^2 u_1}{\partial z^2} \right)_{z=0}$
$\beta_0, \beta_1$	constants in a linear velocity field $u_0 = \beta_0 - \beta_1 x$
$\gamma$	ratio of the oil velocity to the velocity outside the boundary layer
$\delta$	boundary layer thickness
$\delta_1$	boundary layer displacement thickness $= \int_0^\delta \left( 1 - \frac{u_1}{u_0} \right) dz$
$\eta$	non-dimensional ordinate normal to the body surface $= \left( \frac{a}{\nu_1} \right)^{1/2} z$
$\theta$	boundary layer momentum thickness $= \int_0^\delta \left( 1 - \frac{u_1}{u_0} \right) \frac{u_1}{u_0} dz$
$\lambda$	ratio of the viscosity of the working fluid to the viscosity of the oil

$\Lambda$  parameter in the polynomial velocity profile

$$= \frac{\delta^2}{\nu_1} \left\{ \gamma \frac{\partial(u_2)_h}{\partial x} - \frac{\partial u_0}{\partial x} \right\} \text{ (Equation (I.29))}$$

$\xi$  non-dimensional co-ordinate along the surface in the linear velocity field =  $\frac{\hat{x}}{\hat{x}_0}$

$\mu$  viscosity

$\nu$  kinematic viscosity

$\rho$  density

#### *Suffixes*

0 refers to conditions outside the boundary layer

1 refers to conditions inside the boundary layer

2 refers to conditions inside the oil layer

h refers to conditions at the top of the oil layer

z refers to conditions at zero time.

## APPENDIX I. 2. 1

Values of the Constants  $\beta_0$ ,  $\beta_1$  (Sections I.2.4 and I.2.5)  
and the Constant  $\gamma$  (Equ. (I.20))

In most of the boundary layer problems in this Report the velocity outside the boundary layer has been assumed to have linear variation along the chord of the form  $u_0 = \beta_0 - \beta_1 x$ . The constants can be related to the velocity distributions on the upper surface of the R.A.E. aerofoil sections (Ref. I.2.8), if it is assumed that the velocity varies linearly from the value at the maximum suction point to the value at the trailing edge. For all sections with lift coefficients in the range  $0.2 \leq C_L \leq 0.6$

it has been found that  $1.2u_0 \leq \beta_0 \leq 1.8u_0$  and  $0.3 \frac{u_0}{C} \leq \beta_1 \leq 0.9 \frac{u_0}{C}$ . All calcula-

tions have been carried out with the typical values,  $\beta_0 = 1.5u_0$ ,  $\beta_1 = 0.6 \frac{u_0}{C}$ .

The constant  $\gamma$  (Equ. (I.20)) may be evaluated for the external flow  $u_0 - \beta_0 - \beta_1 x$ . Using the skin-friction,  $f(\xi)$ , quoted in Reference I.2.2, the oil velocity at the oil surface (Equ. (I.15)) becomes:

$$\lambda \left\{ \beta_0 (1 - \xi) \frac{\beta_1^4}{\nu_1} f(\xi) h - \frac{1}{\nu_1} \beta_0 \beta_1 (1 - \xi) h^2 \right\} \quad (I.41)$$

where  $\xi = \frac{\beta_1}{\beta_0} x$ .

Then  $\gamma$ , the ratio of the oil velocity to the mainstream velocity, becomes:

$$\gamma = \lambda \left\{ \frac{\beta_1^4}{\nu_1} f(\xi) h - \frac{\beta_1}{\nu_1} h^2 \right\} \quad (I.42)$$

This parameter has been used in the calculation of the effect of the oil on the boundary layer flow, and a maximum value of this parameter is required. It is not possible to find the maximum by standard methods as the variation of  $h$  with  $\xi$ ,

(or  $x$ ) is not known. However, with practical oil thicknesses and  $\beta_1 = 0.6 \frac{u_0}{C}$  it

is found that  $\left( \frac{\beta_1}{\nu_1} h^2 \right)$  is at most 1. Also  $f(\xi)$  is  $O(1)$  except close to the

leading edge. Thus the maximum value of  $\gamma$  is  $O(\lambda)$ . The maximum value of  $\lambda$  found in practice is 0.02 for paraffin in a wind tunnel; for the type of heavy oil used in high-speed tunnels  $\lambda$ , and hence  $\gamma$ , are  $O(10^{-4})$ .

## APPENDIX I.2.2

## The Equality of Viscous Stress at the Air/Oil Interface

Equation (I.6) states the conditions that the viscous stresses shall be equal across the air/oil face. The condition given is strictly valid only for an oil surface parallel to the body surface, i.e.  $z = \text{constant}$ . However, this Report is concerned with oil layers with thicknesses varying with position, that is the oil surface is given by  $z = f(x, y)$ . The purpose of this Appendix is to show that

Equation (I.6) is valid for such surfaces provided  $\frac{\partial z}{\partial x}, \frac{\partial z}{\partial y}$  are  $o(1/\delta)$ .

The proof will be given for a surface  $z = f(x)$ . Then at a point on this surface the direction cosines to the surface normal, in the plane  $y = \text{constant}$ , are  $l$  and  $n$  and the velocity along the surface in this plane is

$$u l - w n. \quad (I.43)$$

The derivative of this velocity along the surface normal is

$$l^2 \frac{\partial u}{\partial z} + l n \left( \frac{\partial u}{\partial x} - \frac{\partial w}{\partial z} \right) - n^2 \frac{\partial w}{\partial x}. \quad (I.44)$$

Thus the strict boundary condition at the interface is

$$\begin{aligned} & \mu_1 \left( l^2 \frac{\partial u_1}{\partial z} + l n \left( \frac{\partial u_1}{\partial x} - \frac{\partial w_1}{\partial z} \right) - n^2 \frac{\partial w_1}{\partial x} \right) \\ & = \mu_2 \left( l^2 \frac{\partial u_2}{\partial z} + l n \left( \frac{\partial u_2}{\partial x} - \frac{\partial w_2}{\partial z} \right) - n^2 \frac{\partial w_2}{\partial x} \right). \end{aligned} \quad (I.45)$$

In the boundary layer  $\frac{\partial u_1}{\partial z}$  is  $o(1/\delta)$ ,  $\frac{\partial u_1}{\partial x}$ ,  $\frac{\partial w_1}{\partial z}$  are  $o(1)$  and  $\frac{\partial w_1}{\partial x}$  are  $o(\delta)$ . Thus provided  $\frac{n}{l}$  is  $o(1/\delta)$  the dominant term on the left hand side of Equation (I.45)

is  $\mu_1 l^2 \frac{\partial u_1}{\partial z}$ . In the oil flow  $\frac{\partial w_2}{\partial x}$ ,  $\frac{\partial u_2}{\partial x}$  are the same order by the continuity Equation and  $u_1 = u_2$ ,  $w_1 = w_2$  at the oil surface. Thus we might expect the terms on the right hand side of Equation (I.45) to have a similar relationship to each other. In this case Equation (I.45) reduces to Equation (I.6). The use of Equation (I.6) in Section I.2.3 gives a solution which confirms that the terms in Equation (I.45) can be dropped. Thus Equation (I.6) holds for the surface  $z = f(x)$  provided the ratio of  $\frac{n}{l}$ , or  $\frac{\partial z}{\partial x}$ , is  $o(1/\delta)$ . A similar result holds for  $z = f(x, y)$ .

The analysis of this Appendix again breaks down in the vicinity of the separation point. However, the region affected is the same as that for the analysis of Section I.2.2 so that the region of validity is not reduced further.

## LIST OF REFERENCES IN SECTION I.2

- I.2.1 Goldstein, S. *On Laminar Boundary Layer Flow Near a Point of Separation.* Quar. Jour. Mech. and App. Maths. Vol.1, 1948.
- I.2.2 Goldstein, S. *Modern Developments in Fluid Dynamics.* Oxford University Press, 1938.
- I.2.3 Howarth, L. *On the Solution of the Laminar Boundary Layer Equations.* Proc. Roy. Soc. vol.164, 1938.
- I.2.4 Squire, L.C. *On Approximate Calculation of Three-Dimensional Boundary Layers.* Ph.D. Thesis, University of Bristol, 1956.
- I.2.5 Eichelbrenner, E.A.  
Oudart, A. *Le Décollement Laminaire en Trois Dimensions.* La Recherche Aéronautique No.47, 1955.
- I.2.6 Godd, G.E.  
et alii *An Experimental Investigation of the Interaction Between Shock Waves and Boundary Layers.* Proc. Roy. Soc. Vol.226., 1954.
- I.2.7 Stalker, R.J. *A Study of the China-Film Technique for Flow Indication.* A.R.L. Report A.96., Oct., 1955.
- I.2.8 Pankhurst, R.C.  
Squire, H.B. *Calculated Pressure Distribution on the RAF 101-114 Aerofoil Sections.* CP 80, March, 1950.

### I.3 THE SURFACE OIL FLOW TECHNIQUE FOR USE IN LOW SPEED WIND TUNNELS

R.L. Maltby and R.F.A. Keating

#### I.3.1 INTRODUCTION

In Section I.2 it has been shown that there is good reason to expect that the flow of a thin layer of oil under a boundary layer will be in the direction of the boundary layer streamlines except in the immediate neighbourhood of areas of separated flow and, furthermore, there is only a very small effect of the oil flow on the motion of the boundary layer. The main problems in the experimental technique are to select and apply a paint which will leave a clearly defined pattern of streaks to indicate the direction of flow of its oil medium in the particular conditions of test and to interpret the pattern in terms of the three-dimensional flow structure.

Although patterns suitable for visual study can be achieved fairly easily, it is quite difficult to produce patterns of consistently good photographic quality. Since the value of an experiment is enormously enhanced when clear permanent records are available for unhurried consideration and consultation, the extra effort necessary to produce patterns of the highest quality is fully justified. Unfortunately the conditions of test and the materials available vary so much between one laboratory and another that refinements in the technique have taken on a very personal character and an atmosphere of 'mystique' reminiscent of 'haute cuisine' has grown up in the preparation of paints and the interpretation of patterns. In examining various recipes in use one is invariably faced with the problem of assessing the exact meaning of subjective qualities such as streakiness, runniness, clarity and spread - a problem which is familiar to rheologists and paint technologists. In fact Dr. Scott-Blair in his book 'A Survey of General and Applied Rheology' found it necessary to write a dedication in the following terms:

"This book is dedicated to Bill - Bill in every land wherever he may be. When they want to know what to do next, they send for Bill. Bill squeezes the stuff in his fingers, sniffs it, holds it to his ear, and squeezes again. Then he looks wise and says 'O.K.' or 'Leave it another ten minutes'."

If in the following paragraphs there is a lack of precision in the instructions, it is because precision appears to be inconsistent with the problem; at least it is so for the authors and, no doubt, for those of the readers who are also not paint technologists. For those wishing to use any technique which involves an element of craft the best advice is always to learn by watching Bill.

#### I.3.2 COMPOSITION OF THE PAINTS

##### I.3.2.1 General Principles

The object is to prepare a paint of such consistency that, under the conditions prevailing in the test, it will run with the surface oil flow and leave behind streaks of pigment indicating the direction of flow. The patterns made by the streaks must be

bold enough to be examined and photographed easily and yet fine enough to record all significant detail (Fig. I.8). Ideally the paint should not begin to run until the desired wind speed has been reached and after a convenient time of running, the pattern should be sufficiently dry to be unaffected by gravity after the air flow has stopped.

The process leading to the formation of streaks can be studied by applying paint to the window of a wind tunnel and watching the motion from the other side of the glass with a microscope. The clearest patterns are formed by a silting process behind small concentrations of pigment in the paint. The paint flows round those concentrations and some of the pigment is subsequently deposited in the wakes behind them. The deposits continue to grow into long streaks in the direction of flow as more pigment is deposited behind the concentrations until all the oil has been blown from the surface. The fully developed pattern is then left on the surface in a reasonably dry condition.

If the composition of the paint is slightly different, the process described by Stalker (Ref. I.3.1) can be observed. Here U-shaped wavelets form in the oil and travel slowly in the stream direction. The pigment is deposited from the tails of the U, and since the wavelets tend to form roughly one behind another, the streaks are reinforced with the passage of subsequent wavelets. If the paint is too stiff the wavelets become large and a coarse pattern is formed from which it is difficult to disperse the oil. When there is a large variation of surface shear over the surface of the model it will be difficult to choose a paint consistency to give uniform results with this method (Fig. I.10) and it is usually better to mix a paint which will silt easily.

The stiffness of the paint and the formation of streaks depends on the size of the particles in the pigment and the forces of attraction between them (Ref. I.3.2) as well as the viscosity of the oil. Materials for pigments applied as crystals or other large particles require to be ground and sifted to the correct size and those supplied as very fine powders may tend to form conglomerations (flocs) in the oil, the size of which must be controlled by the use of additives (see I.3.2.3).

Large pigment particles or large flocs tend to produce bolder streaks if the thickness of the oil layer is sufficient to keep them in motion during the silting process. In conditions of high shear the oil thickness is reduced rapidly and this will determine the maximum usable particle size.

#### I.3.2.2 The Oil Medium

The choice of the oil medium for use with a particular pigment is determined by the time that is allowed for the pattern to develop in the prevailing conditions of air flow and surface shear. The factors affecting the rate of flow are the skin friction, the thickness of the oil sheet, the boundary layer thickness, the oil viscosity, the pigment content and the properties of the pigment in suspension. However the major factors appear to be the oil viscosity and the skin friction and it is suggested in Section I.4 that the approximate time to complete a pattern can be indicated by  $36,000 \eta_{oil}/\tau$  where  $\tau$  is the skin friction at the trailing edge. The oils normally used are, in ascending order of viscosity: kerosene, light diesel oil and light transformer oil. With one of these oils it is usually possible to mix

a satisfactory paint which will start to flow at about 75% of the test speed and produce a fully developed pattern in about 2 minutes.

Although a mineral oil is most commonly used as a medium, water containing a wetting agent such as household synthetic detergent is in occasional use. The principal advantage is that it is a cleaner material to handle but it makes it very much more difficult to control the quality of the pattern.

#### I.3.2.3 Additives

The need to use an additive in some paints to control the size of the flocs leads to difficulties and uncertainties in the technique partly because of the great sensitivity of the suspension to small quantities of additive and partly because of the variable chemical nature of the oils and the additives themselves. The following simple account of oleic acid used as an additive in a titanium dioxide-kerosene paint illustrates the principles.

The stiffness of a paint can be measured with a mobilometer (Ref. I.3.3) (Fig. I.11) which consists of a glass cylinder containing a sample of the paint through which a plunger, with a small clearance at the side, is allowed to travel. The plunger is driven by weights placed on its top end and its time of travel between two fixed marks is measured. The stiffness of the paint is measured by a curve of the reciprocal of the time of travel against the load on the plunger.

Figure I.12 shows such curves plotted for some tests on a titanium dioxide-kerosene mixture. A mixture of typical proportions without additive produced curve D in which there is a large threshold of no movement following by an almost linear portion. The effect of adding 0.6% of oleic acid (curve C) was some dispersion of the pigment which reduced the threshold to about one sixth and increased the subsequent rate of movement. Further concentration of oleic acid to 10% (curve E) completely removes the threshold and brings the rate of movement to nearly that of the neat oil, suggesting that the pigment is now fully dispersed. Curve E shows that the resistance of fully dispersed paint can be increased by increasing the proportion of pigment although the threshold is not restored until the proportion of additive relative to pigment is sufficiently reduced.

Thus in preparing a paint of this kind one must first choose an oil to provide the desired rate of flow and add pigment until sufficient colour density is produced. The boldness of the streaks is then adjusted by partial dispersion of the mixture with additive. The additive will also reduce the threshold of the paint and this must be taken into account when choosing the oil.

Some laboratories use the additive to adjust the necessary threshold and accept the resulting quality of streaks. This is a simple approach but it sometimes leads to patterns of poor contrast and the more careful approach is recommended when patterns of high photographic quality are required.

The effect of oleic acid on the appearance of this paint and the resulting streaks is shown in Figure I.13. The photomicrographs show the increasing dispersion of the flocs as the oleic acid is added and the flow pictures show the expected changes in clarity. It will be noticed that with no additive the large threshold has prevented

flow except in the areas of high shear. With an excess of additive, the dispersed pigment provides a finely detailed pattern but of poor contrast.

Flocculation is affected by the mutual attraction of particles carrying electric charges generated in suspension in the dielectric medium. The additives control the extent of flocculation by modifying the charges and may either increase or decrease it depending on the constituents of the paint. For instance linseed oil will cause mild flocculation of 'Dayglo' pigment in diesel oil, yet will disperse titanium dioxide.

Of the many possible additives oleic acid and linseed oil give excellent results in the various paints in common use and, being readily available, they are to be recommended. Nevertheless they are crude products which vary in their chemical composition when new and oxidise when stored; trial and error methods are inevitable when they are used.

A more detailed account of additives and their effects will be found in References I.3.4 and I.3.5.

#### I.3.2.4 Pigments

The pigment must be chosen to have the correct flow characteristics as already described and to make a clear pattern against the background provided by the model. Thus a white powder like titanium dioxide or china clay would be used on a dark model and a black powder like lampblack on a light model. Fluorescent pigments illuminated with ultra-violet light can provide a high contrast pattern irrespective of the background colour and they give very high quality photographs without difficulties. The properties of some common pigments are listed below.

##### *Titanium dioxide (TiO<sub>2</sub>)*

This is the whitest of pigments used by paint manufacturers and is at the same time the most opaque; it is therefore suitable for making high contrast patterns on a dark background. It is non toxic and reasonably clean to use.

The particle size in material supplied for paint manufacture is about 0.2 micron although the powder used for medical purposes is somewhat coarser. It flocculates when suspended in mineral oils and requires an additive for partial dispersion of the flocs in order to produce clear streaks.

##### *China clay (Kaolin)*

This is a complex mineral which in a pure form is a hydrated silicate of alumina ( $Al_2O_3 \cdot 2 SiO_2 \cdot 2H_2O$ ). When dry it is white but when wetted with an oil of about the same refractive index it becomes transparent. For this reason China clay-oil patterns have to be dried thoroughly before they become clear except in the special case where an indication of transition is required. Here the luminal region remains wet and the turbulent region is dried.

##### *Lampblack*

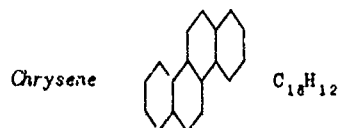
Lampblack is a common greyish carbon pigment with a basic particle diameter of order 0.1 micron. As normally supplied the aggregated particles are much larger and

these neither disperse nor flocculate appreciably in an oil suspension although oleic acid has a small effect in reducing the boldness of the pattern.

Carbon black pigments can be obtained with very much smaller basic particle sizes and a blacker appearance. It is possible that better results may be obtained with these in conjunction with a suitable additive.



This is a fluorescent hydro-carbon derived from coal tar. It is supplied in the form of grey crystals or powder and must be ground and sifted to the correct particle size. It is a variable product and the colour of fluorescence, which depends on the impurities present, varies from blue to green. The paint appears colourless in natural light and the pattern must be observed in ultra-violet light.



This material is similar to anthracene except that it is more consistent in quality and fluoresces blue with greater energy than anthracene. Unfortunately chrysene is a carcinogen and therefore there is some risk of cancer if it is used as a pigment without protection to the skin.

#### "Dayglo" pigments\*

These are the pigments used in the manufacture of fluorescent paints and printing inks and they are believed to be composed of a resin dyed with fluorescent colours. The particle size of the powder is about 1 micron and is suitable for the production of fine patterns without the use of additives. The patterns are clearly visible in natural light and photograph very well in ultra-violet light. Paints made with Dayglo are particularly easy to use and are to be recommended. The pigments may be obtained in a range of colours of which 'Saturn Yellow' and 'Neon Red' are the most suitable for visual works and 'Saturn Yellow' for monochrome photography. The red and yellow may be used together to show regions of flow mixing.

The pigment can also be obtained in pea-sized chunks which may be ground in a ball mill to produce powders of larger particle sizes.

---

\* Dayglo pigments are marketed in America by

Switzer Bros., Inc.,  
Cleveland,  
Ohio.

and in England by

Dane & Co. Ltd.,  
1-2 Sugar House Lane,  
Stratford,  
London, E. 15.

### I. 3. 3 APPLICATION OF PAINTS

The application of the paint to the surface of the model is a simple matter although care is needed to produce the best results.

The surface must first be thoroughly wetted with the medium by rubbing it with a soaked rag. On large surfaces the paint is best applied with a domestic roller, preferably of the foam plastic type. The roller is loaded with paint in the usual way but it is applied to the model with its axis slewed slightly to the direction of motion. By this means an even film is produced and the old pattern from a previous test is erased. A final finish is given by a light application of the roller. Some trials will be required to determine the correct thickness of the coating.

When a brush is used, an even coating is produced if it is moved in small circles rather than with the conventional painting motion.

### I. 3. 4 RECIPES

With the foregoing principles in mind the following three recipes are suggested as a basis for adaptation to local conditions.

#### (1) *Simple mix*

Use as pigment anthracene, chrysene\*, Dayglo pigment or coarse lampblack. Grind and sift the pigment if necessary to a mean particle size in the range 1 to 10 microns and mix with about three times its weight of oil and store in a bottle. The pigment settles rapidly and the bottle must be shaken before use. No additives are required.

Apply the mixture as described in Section I.3.3. If the roller absorbs too much oil dilute the paint with more oil.

This mixture keeps indefinitely and is very easy to use except that there is very little control on the boldness of the streaks.

#### (2) *Flocculent mix*

Mix together thoroughly 1 part by weight of titanium dioxide with 3 parts of oil. This may be done with a brush but more consistent results are obtained if a laboratory stirrer is used. Add a few drops of oleic acid or linseed oil and make a test run. If the pattern is too coarse use more additive. If it is too fine, the proportion of additive must be reduced but it must be remembered that the size of smaller models will impose a limit on the boldness of the patterns. If the paint does not run use an oil of lower viscosity, increase the wind speed or add neat oil.

The paint should be made shortly before use since it deteriorates in storage.

The paint in an old pattern need not be removed for each test but the surface must be restored with a roller containing oil only since the amount of additive is linked

---

\* See medical note in Section I.3.2.4.

with the pigment rather than the oil. After a few tests the surface should be cleaned with a rag soaked in oil containing an excess of additive.

(3) *Titanium dioxide wash*

Mix together thoroughly 1 part by weight of titanium dioxide, 1 part linseed oil and 4 parts oil. Here the pigment is almost fully dispersed and a very fine pattern of low contrast is produced which is suitable for photographing only on small models although it is useful for visual work when transition must be determined at the same time as the flow pattern.

The paint keeps well in an airtight bottle.

### I.3.5 PHOTOGRAPHIC RECORDING

The main difficulty in photographing patterns in normal light is to avoid highlights arising from reflections and uneven lighting. With evenly diffused lighting and a slow, high-contrast emulsion there are no special precautions required in taking photographs of high quality white patterns on black models. If the model is coloured, the contrast is improved if a suitable filter or an emulsion insensitive to the background colour is used. Thus a model finished in natural wood colour is best photographed with an 'ordinary' emulsion, that is one sensitive to blue only.

If the model can be taken out of the wind tunnel, lighting becomes easier. The model with a lampblack pattern illustrated in Figure I.15 was removed from the wind tunnel and placed in a tent made of white fabric. The tent was illuminated from outside and produced a uniform lighting effect on the model.

With a fluorescent pattern illuminated only by ultra-violet light, the difficulties connected with the appearance of the surface of the model and with reflections are overcome. The tunnel is blacked out and the fluorescence is excited by a lamp\* emitting the mercury 3650Å line. Only the pattern is seen, both the model surface and the background remaining invisible. Reflections of the light source in the surface are eliminated by fitting an ultra-violet filter (Wratten 2B) to the camera and the visible fluorescence is photographed on a medium speed panchromatic plate (Ilford F.P.4). Although the exposure time is quite long, it cannot be shortened by using a faster plate because of the greater reciprocity failure, and similar difficulties are found with colour emulsions.

The intense blue fluorescence of chrysenes\*\* allows an 'ordinary' emulsion to be used without loss of speed. Negatives of brilliant quality are obtained which can be processed under a red safe light (Fig.I.8).

In order to avoid the long exposure times required with fluorescent pigments an electronic flash tube can be used instead of a continuous burning lamp if a window of

---

\* An ordinary U-V 'sun ray' lamp is suitable.

\*\* See medical note in section I.3.2.4.

Wood's Glass (sometimes called blackglass) is fitted to the gun. The flash factor is reduced because only the ultra-violet content of the flash is transmitted; for instance, a 100 Joule unit used with 'Saturn Yellow' gives a flash factor of about 10 with 50 ASA film. Colour photographs are easily obtainable in this way.

Ultra-violet light is injurious to the eyes and suitable glasses must be worn when it is being used.

Figure I.14 gives the photographic data used in the 13 ft x 9 ft low speed wind tunnel at the Royal Aircraft Establishment, Bedford.

### I.3.6 INTERPRETATION OF OIL FLOW PATTERNS

The objections that are raised against the surface oil flow technique are often the result of careless interpretation or attempts to read too much into the details of the pattern. It is, of course, impossible to give detailed instructions in interpretation as it must depend on a thorough understanding of aerodynamic features of the model under test. Some examples of flow patterns are discussed below to assist in the recognition of common flow conditions but it must be remembered that under different circumstances they might appear in a different form. In the notes given below, familiarity with the aerodynamics of separated flow regimes is assumed. Clarification will be found in Reference I.3.6.

Figure I.16 shows the flow pattern on a swept wing at  $0^\circ$  incidence made with a titanium dioxide flocculent paint. The difference in appearance between the laminar and turbulent regions can be seen, especially in the turbulent wedges from the disturbances near the leading edge where the high shear has led to fine streaks.

Figure I.17 shows the flow on part of a  $25^\circ$  swept wing at three angles of incidence using Dayglo and ultra-violet light. At  $\alpha = 2^\circ$  there is a laminar separation and reattachment at about the half-chord position. In the separated region there is an accumulation of paint which has been drifting slowly towards the tip, leaving a clear area on either side. At several places turbulent wedges have broken through the separation area and some of the accumulated oil is drifting towards the trailing edge through these gaps. The large V-shaped pattern near the inboard end of the wing is the wake from a supporting wire.

At  $\alpha = 6^\circ$  the laminar separation region and reattachment are visible at the leading edge of the wing and the turbulent boundary layer nearer the trailing edge is beginning to drift towards the tip.

At  $\alpha = 10^\circ$  there is still a laminar separation region with reattachment at the leading edge and there is now a turbulent separation near the trailing edge. The surface flow direction behind this separation is forwards from the trailing edge. The wake from the supporting wire is having a large local effect on this flow.

The main features associated with vortex flows from edge separations are illustrated by the flow over a flat, sharp-edged delta wing with an aspect ratio of 1. The pattern in Figure I.8 is produced by chrysene and kerosene photographed in ultra-violet light. The coiled vortex sheets springing from the separations along the

leading edges produce the characteristic 'herring-bone' pattern. on each side of the centre-line. The suction peak on the wing surface associated with the vortex above, lies close to the point of inflexion of the S-shaped lines in the herring-bone pattern. The point of inflexion is often closer to the leading edge than a casual inspection may suggest. Measurements of surface flow direction by other methods on this model confirmed that the streaks gave a reliable indication.

The secondary separation line is indicated by the dark line outboard of the herring-bone pattern. In the early stages of the development of the pattern this region contained an accumulation of paint and it appeared then as a white line. As the development progressed, this accumulation was blown off the trailing edge leaving the wing surface bare as it is in the photograph. Regions of separation are, therefore, indicated either by white patches or dark patches according to the conditions and the state of development of the pattern.

Outboard of the secondary separation line is a region of secondary flows including a further separation line.

In flow regimes of this kind the shape of the secondary separation line can often give indirect indications of the state of flow elsewhere. For instance, a transition from laminar to turbulent flow on the surface of the middle of the wing is sometimes accompanied by a sudden outboard bend of the secondary separation lines. Also, during a study of the breakdown of the vortex core, it was noticed that there was also a change in direction of the separation line. Figure I.9, which illustrates this phenomenon, is also an example of the poor pattern which is obtained when the size of particles of pigment (in this case anthracene) is too large.

The part-span vortex flow on a  $55^\circ$  swept wing at  $\alpha = 8^\circ$  is illustrated in Figure I.18. In this case the secondary separation line is white because the paint has not cleared away. At  $\alpha = 16^\circ$  on the same wing the vortex flow has spread all along the leading edge. Under the vortex, the angle of sweepback of the surface flow is less than that of the wing trailing edge. At a point further inboard, the surface flow is tangential to the trailing edge and a new vortex forms from the trailing edge outboard of this point. When this happens, oil which has accumulated on the trailing edge is drawn over the surface of the wing in a curved line and this line is often a valuable indication that the new vortex has formed. The herring-bone pattern associated with this vortex is sometimes found on the upper surface near the trailing edge, but this is not very evident in Figure I.18.

On wings with highly swept edges the vortex flow breaks down near the tips at high angles of incidence and a forward flow on the surface results. The incidence at which this breakdown occurs decreases with the sweep angle and it is a common feature of the flow on wings of moderate sweep. Figure I.15 shows the surface flow pattern obtained with lampblack and kerosene on a  $45^\circ$  delta wing at  $\alpha = 20^\circ$ . The vortex flow is clearly shown near the front of the wing but, nearer the tip, the flow is mainly in a forward direction which leads to a rotating flow in the surface plane. The centre of the rotation is usually plainly marked and indicates the rearward extremity of the normal vortex flow.

## LIST OF REFERENCES IN SECTION I.3

- I.3.1 Stalker, R.J.      *A Study of the China-Clay Film Technique for Flow Indication.* Australia ARL Report A96, 1955.
- I.3.2 Remington, J.S.  
Francis, W.      *Pigments, Their Manufacture, Properties and Use.* Leonard Hill Ltd., London, 1954.
- I.3.3 Perry, J.H.      *Chemical Engineers' Handbook.* McGraw-Hill, 1941.
- I.3.4 Chatfield      *Paint and Varnish Manufacture.* Newnes, 1955.
- I.3.5 Sagarin      *Cosmetics, Science and Technology.* Interscience Publishing Inc., New York, 1957.
- I.3.6 Thwaites, B.      *Incompressible Aerodynamics.* Oxford University Press, 1959.

## 1.4 THE SURFACE OIL FLOW TECHNIQUE FOR USE IN HIGH SPEED WIND TUNNELS

A. Stanbrook

### 1.4.1 INTRODUCTION

The principles of the surface oil flow technique in high speed wind tunnels are similar to those for low speed tunnels (Section I.3) but more emphasis is placed on the choice of the oil medium to suit the running time required. Again, the exact compositions of the paint mixtures used in various laboratories have individual characters based on the local conditions and the personal preferences of the experimenters concerned. The purpose of this Section is to collate the experience from separate tunnels, to explain variations in the technique and to provide a guide for the development of oil mixtures for specific purposes.

Typical examples of oil flow patterns from a high speed tunnel are presented in Figure I.19. Figure I.19(a) shows the types of pattern obtained when the flow, separating from the leading edge, forms either a bubble or a vortex. The third photograph shows the appearance of transition in oil flow patterns. (Comparisons between oil flow and sublimation visualization of transition position are discussed in Reference I.4.1; the sublimation technique is described further in Reference I.4.2.) Figure I.19(b) shows flow deflection, and separation, at shock waves, together with the appearance of a tip vortex. The uppermost photograph in Figure I.19(c) shows a typical result of the application of too much oil mixture. During the run oil accumulated behind the separation line and formed a blob which stood up from the wing. As the tunnel flow was stopped this blob collapsed and the oil spread over an appreciable region on the wing, obliterating details of the flow.

The other three photographs in Figure I.19(c) show various stages in the development of oil patterns. The first shows an early stage at which the filaments are just forming. In the second, filaments have formed but are running together to form rivers of oil which are obscuring detail. The third was taken after the completion of this same run, when the rivers had flowed downstream, off the model, and a large amount of fine detail could be observed.

### 1.4.2 EXPERIMENTAL STUDY OF THE DEVELOPMENT OF THE PATTERN

#### 1.4.2.1 Effect of the Pigment Concentration

To provide background information on the importance of precise proportions of the oil mixture, a series of tests was made on a wedge of  $15^\circ$  total angle and 2.5 in. chord in a 3 in. square supersonic wind tunnel with a short starting time (approximately 3 seconds). The oils referred to in this and in other parts of the note are classified in Appendix I.4.1.

Figure I.20 shows a typical\* graph of the variations of the time taken to form a pattern with the proportion of titanium dioxide to a given oil/oleic acid mixture by volume\*\*, at a free stream Mach number of 1.4 (a local Mach number on the wedge of 1.12) with atmospheric total temperature and pressure. It will be seen that there was a minimum concentration of pigment below which no filaments were observed, the limit being lower with turbulent flow (for which the skin friction is higher). Above this minimum a filament pattern was observed. The time taken for the pattern to develop was independent of the pigment concentration up to a certain limit, above which the time increased rapidly. At the lower concentrations, the pattern formed was eventually lost as the oil mixture moved downstream and off the model. The time taken for this to happen also increased with pigment concentration and there appeared to be a limit above which some trace of the pattern remained on the model indefinitely.

Typical photographs, shown in Figure I.21, compare the development of the pattern with both laminar and turbulent boundary layers for one particular oil mixture. (These photographs show 1/2 in. wide chordwise strips of the wedge.)

#### I.4.2.2 Oleic Acid Additive

The function of oleic acid as an additive to titanium dioxide prints to control the boldness of the filament lines by controlling the degree of agglomeration of the particles is discussed in Section I.3.2. The following tests made in the 3 in. supersonic tunnel illustrate the effects under high speed flow conditions.

Figure I.22 shows flow patterns obtained on the wedge in the 3 in. tunnel using mixtures containing different amounts of dispersing agent. The uppermost pattern was obtained with no dispersing agent (3 ccs OM-108 oil + 2 ccs  $TiO_2$ ). The skin friction in the laminar flow region was too low to move the coagulated oil sheet. However, irregularities in the oil sheet caused transition further downstream and the higher skin friction was sufficient to move the oil. The second photograph shows a pattern obtained with a small amount of oleic acid present (1 drop in 3 ccs OM-108 oil + 2 ccs  $TiO_2$ ), with which an acceptable filament pattern was obtained. Since the further addition of sufficient oleic acid to ensure complete dispersion of the pigment would probably have altered the viscosity, a proprietary oil of the same viscosity containing the highest available proportion of detergent additive (Shell Rimula 30) was used. The result is shown in the third pattern in Figure I.22. Since dispersion was complete, the pigment particles were each completely separate and no filaments were observed.

It is seen from the uppermost pattern in Figure I.23 that where the skin friction is high enough (e.g. in the turbulent boundary layer) it is possible for an oil mixture not containing oleic acid to flow. In the particular case shown in Figure I.22 the filament pattern is indistinct. Figure I.23 shows a comparison between flow patterns on a wing from mixtures with and without oleic acid (1 drop in

\* These results are for OM-108 oil but tests with other oils show variations similar in type.

\*\* Volume of titanium dioxide refers to the loosely packed powder as scooped from the jar. Its density has been found to be approximately 0.75 gm/cc., compared with the true density of titanium dioxide of 3.8-4.2 gm/cc.

1½ ccs oil + 1 cc TiO<sub>2</sub>). The skin friction was sufficient to move the oil near the leading edge and the root and, in this case, the advantage gained from the addition of oleic acid was only marginal, flow lines being visible in both cases, but more distinct when oleic acid was present. (The flow was attached around the leading edge of the wing and then separated from the surface at a shock wave.) Further downstream, in the region of separated flow, the skin friction and, hence, the rate of flow of oil were low. The test was not continued for long enough to see whether the oil would move in this region; to do this would have resulted in loss of the remainder of the pattern.

Whether or not filament patterns may be obtained without oleic acid will depend on the viscosity of the oil, on the quantity of pigment added and on the skin friction intensity in the flow. This may be seen from the following table which shows limiting pigment concentrations with various oils for laminar and turbulent flow (from tests in the 3 in. tunnel):

Oil	Viscosity at surface temperature (Stokes)	Limiting pigment concentration (cc TiO <sub>2</sub> /cc oil)	
		Laminar	Turbulent
Shell Limea 931	4	0.5	-
OM-108	6	-	0.6
OM-108	9	0.45	-
Shell Vitrea 72	14	0.3	-

For lower concentrations than these the link between the pigment particles in the coagulated network was sufficiently weak to be readily broken by the skin friction.

Now, if some dispersing agent were added a certain amount of the pigment would be dispersed. It is reasonable to suppose that further pigment could be added until the same degree of coagulation was reached. Some tests to study this effect were made using varying proportions of oleic acid to oil. The results (Fig. I.24) show that an appreciable increase\* in the limiting pigment concentration was produced by the addition of a small proportion of oleic acid (0.08 drop/cc of oil). This improvement did not increase in proportion to the amount of oleic acid added, presumably owing to additional factors such as the reduction in spacing of individual pigment particles (relative to their size) at the increased pigment concentrations involved.

At moderate pigment concentrations (0.2 to 0.6, Fig. I.24) increase of the proportion of oleic acid first decreases the time taken to form a pattern and then increases it. The initial decrease is probably due to the increased ease of movement of the oil mixture brought about by a small degree of dispersion and the consequent break-up of the coagulated network. As the degree of dispersion increased the

\* The quantitative results obtained may only be applied to the particular sample of oleic acid, because of possible differences of quality and deterioration.

size of the coagulated clusters of particles decreases and more time is required for them to collect together into filaments.

The discussion above shows that oleic acid may be used to extend the workable range of pigment concentrations. However, it is not advisable to use a mixture which is near to the limiting pigment concentration, since the limit depends upon the actual skin friction intensity. With a complex flow pattern the range of skin friction would be large, from very high values in the regions scoured by vortices to very low values in the neighbourhood of separation. Then, if a mixture with a pigment concentration near the limit were used it is probable that there would be extensive regions in which the skin friction intensity was insufficient to break up the coagulated network of pigment particles.

#### 1.4.2.3 The Thickness of the Oil Sheet

Some tests were made with various initial thicknesses of oil on the wedge, using pairs of feeler gauges and a straight-edge to 'scrape' the oil sheet to a required thickness. No variation in the time taken to develop a filament pattern was observed over the range of thicknesses from 0.0005 in. to 0.005 in. It was also found that the normal application of oil mixture used in the tests was approximately 0.002 in. thick.

The distribution of oil film thickness over a surface during the running period is given by Equation (1.17) which may be solved numerically for laminar and turbulent flow on a two-dimensional flat plate assuming that the presence of the oil does not affect the surface skin-friction intensity. Calculations have been made for the conditions of the tests in the 3 in. tunnel described in Section 1.4.2.1 and for initial thicknesses of the oil sheet of 0.005 in. and 0.001 in. The results are shown in Figure 1.25 in the form of thickness distributions across the wedges at various times after the start of the motion.

It will be seen that the oil sheet thickness varies about five times as fast for the turbulent boundary layer as for the laminar, and that after about 30 seconds for laminar flow (and 6 seconds for turbulent flow) the thickness is virtually independent of the initial thickness.

The photographs reproduced in Figure 1.21 were taken at various times in the development of the oil filaments. In the laminar flow pattern at 4 minute filaments have formed 3/4 in. from the leading edge while at 24 minutes there are filaments over the entire chord. Filaments formed over 0.8 of the chord in 4 minute of turbulent flow. Comparison with the theoretical thickness distributions at the corresponding points and times suggests that in these tests the filaments formed when the sheet thickness was approximately 0.0002 in. (irrespective of the initial thickness of the oil sheet).

### 1.4.3 COMPARISON OF THE VARIOUS FORMS OF THE TECHNIQUE

#### 1.4.3.1 General Comments

Some general comments may be made from information supplied by the staffs of various tunnels.

The majority of the mixtures used have from 2/5 to 2/3 cc pigment/cc of oil although concentrations vary; from 1/5 to 3 are also in use. (The stiffer mixes have been used where it is required to limit the movement of the pattern during tunnel shut-down. The times taken are not comparable with those for the more common proportions.) Titanium dioxide is used fairly consistently as pigment - it is, after all, the whitest pigment available. Antimony dioxide has been tried (by Lee and Berry of the National Physical Laboratory) with less satisfactory contrast in the results. Lampblack is used in low speed tunnels, but appears to have been used little in high speed tunnels (the only case found was in some early tests by Fairbairn in an intermittent tunnel at Armstrong Whitworth Aircraft). Another pigment in use (by Igglesden (Ref. I.4.5) of the Royal Aircraft Establishment) is Prussian Blue (supplied in paste form, ready mixed with Shell Caraca 35 oil by Henry Stuart, Sons & Co., as 'Micrometer' brand engineer's blue marking). Fluorescent powders have been used in low speed tunnels, and could also be used in high speed tunnels provided that their use was restricted to large models (because of the large particle size).

The choice of oil is largely determined by tunnel running conditions. For instance, a light oil or hydraulic fluid would be used in an intermittent tunnel to reduce the time taken to form a pattern (e.g. OM-15 is used in an intermittent tunnel at Armstrong Whitworth Aircraft). On the other hand, a heavy oil would be used in a tunnel which takes a long time to reach operating conditions, to lengthen the time taken to form a pattern and hence to limit the effect on the oil flow of the incorrect running conditions (e.g. Shell Nassa 87 oil has been used in the 3 ft and 8 ft tunnels at the Royal Aircraft Establishment, Bedford). In tunnels where the temperature is raised to avoid moisture condensation (e.g. De Havilland Aircraft, English Electric Aviation and Handley Page) a silicone fluid is generally used in place of oil. This has the advantage of avoiding excessive viscosity at atmospheric temperature, thereby making application of the mixture easier. Castor oil has been used (in the 8 ft x 6 ft tunnel at the Royal Aircraft Establishment) on metal models with an extremely high standard of surface finish. Trouble was experienced with other oils on these models, castor oil was tried because of its high adhesion to metal surfaces.

Oleic acid is used to limit coagulation in nearly all cases, although it has not been necessary to add any dispersing agent to mixtures based on natural animal or vegetable oils (such as castor oil) since sufficient fatty acids are present in these oils. In some cases, dispersing agents have been omitted from mixtures based on mineral oils and some form of pattern has been produced. However, the standard of the pattern could possibly have been improved by the addition of oleic acid. In other cases, the oil viscosity has been varied by blending two oils, one of which already contains a dispersing agent. They were not always mixed in the same proportion and the consequent variation in the degree of dispersion resulted in the standard of pattern formed not being repeatable. It would be preferable in such a case to choose two oils, neither of which contains additives.

By varying the degree of coagulation (i.e. changing the relative proportions of pigment and dispersing agent) it is possible to alter the size of the filaments and, hence, the scale of the pattern. Thus, a greater degree of coagulation is necessary on large models than on smaller models.

The smallest size of filament to be attained is determined by the resolution of the photographic system used and by the method to be used for the reproduction of the

results, if any. Although considerably more fine detail may be obtained on a large model than on a small one, this may be useless if it cannot be recorded.

Cleansing of the surface of the model with solvent and rubbing over with oil is held by some to be essential for the production of good oil flow patterns while others consider it to be completely unnecessary. Whether it is essential or not, it does serve the useful purpose of removing finger-prints (which may be acidic) and of providing a clean, uniformly oily surface. No one considers cleaning to be necessary between the individual runs of a series of oil flow studies, respreading of the mixture with, possibly, further application of the oil mixture being sufficient in this case.

The method of application varies between spray, paint-roller, brush and hand according to the viscosity of the mixture and the size of the model. The thicker mixtures are applied by hand and it is thought that the rubbing action of the finger on the surface improves the initial dispersion of pigment.

#### I.4.3.2 Correlation of Running Times

In addition to providing details of the oil mixtures used in their tunnels, the various staffs were invited to quote times for the formation of flow patterns on typical models. The data provided are for a large variety of tunnels, varying from low speed to high supersonic speed and including both intermittent and continuous running. They apply to models of wings and of wing/body combinations. Total temperatures vary from 15°C to 140°C. The oils used range from kerosene to steam cylinder oils and include silicone fluids.

In Figure I.26 these running times are correlated in terms of the parameter

$$\mu_{oil}/qc_f$$

where  $\mu_{oil}$  is the viscosity of the oil  
 $q$  is the dynamic head  
 $c_f$  is the local skin friction coefficient,

which has the dimension of time and which is implicit in the theoretical treatment in Section I.2). It may also be recalled that the time taken for a pattern to develop was found (experimentally, with some further theoretical justification) to be independent of the initial thickness of the oil sheet.

For the correlation, the oil viscosity has been taken at the surface recovery temperature for zero heat transfer (Ref.I.4.3), while the local skin friction coefficient,  $c_f$ , has been calculated at the trailing edge of a typical chord, using Cope's data for flat plates (Ref.I.4.4) at the free stream Mach number. It will be seen that the correlation is reasonable, the majority of the data lying in the range

$$t = (36,000 \pm 12,000) \left( \frac{\mu_{oil}}{qc_f} \right).$$

(Note that in Figure I.26, for convenience, the ordinate is measured in minutes while the abscissa is measured in seconds.)

Results for the flow on the simple flat wedge in the 3 in. tunnel are also plotted in Figure I.26 (as filled points). The times quoted are for the initial formation of filaments, which then remained on the wedge for a considerable time (see Section I.4.2.1). The fact that these times ( $t \approx 7500 \mu_{oil}/qc_f$ ) are minima in itself accounts for them being less than the general values quoted, where time has been allowed to ensure that the pattern is fully established. Further, in the general case the skin friction will differ from the flat plate value, being higher in some regions and lower in others. Consequently, it is to be expected that filaments will form quickly in some regions (e.g. beneath strong vortices) while in others the formation will be delayed and time has to be allowed for the pattern to develop in all regions.

#### I.4.4 MULTIPLE PATTERNS DURING A SINGLE RUN

Various attempts have been made to obtain more than one oil flow pattern during a single run. It has been found to be possible in certain cases, given some pre-knowledge of the type of flow patterns that are going to be obtained. For example it is helpful to know in advance that at one of the incidences to be tested, there will be a major flow separation on the wing. If this is then selected as the first condition (and a suitable condition chosen to follow) sufficient oil may be left on the wing to be redistributed in the later condition. It is also possible to interpose a dissimilar pattern between two similar patterns at different conditions in order to ensure that the second of the like patterns is freshly obtained. This method has been used by Ormerod in studies of the vortex flow over slender wings, where the pattern changes little with Mach number at fixed incidence.

Multiple patterns may also be used successfully when studying one particular and localised feature of the flow. For example (Ref. I.4.6), in obtaining the Mach number and flow deflection boundary for shock-induced separation of the boundary layer separated and attached flows were investigated alternately and the type of flow was clear even though fine details were confused by traces from earlier patterns.

For permanent records in all these cases it is, of course, essential to be able to photograph the flow pattern during the run.

#### I.4.5 CONCLUDING REMARKS - RECOMMENDED MIXTURE

From a correlation of available data on the oil flow technique it is possible to recommend the following procedure for the determination of an oil mixture.

- (1) The running time to develop a pattern is first decided, by consideration of the operating conditions of the tunnel.
- (2) This time is divided by 30,000 to give an approximate value for the parameter  $\mu_{oil}/qc_f$ .
- (3) A value of  $qc_f$ , calculated at the trailing edge of a typical chord from boundary layer theory for a flat plate, is used to determine the required oil viscosity at the temperature of the surface. With simple models, or if the correct

lowest value of  $qc_f$  on the model is used, this may under-estimate the viscosity required (Section I.4.3.2).

(4) A suitable oil may be chosen from Figure I.27, or similar data.

(5) The mixture should contain from 2/5 to 2/3 parts of titanium dioxide powder to 1 part of oil (by volume or weight, since the densities are almost identical).

(6) The amount of oleic acid, or other dispersing agent, must be determined by experiment, since the factors involved are so variable (e.g. the oleic acid may deteriorate, the oil may already contain a dispersing agent or, in some cases, a dispersing agent may be unnecessary).

## APPENDIX I.4.1

## Characteristics of the Various Oils in Use

A brief description of some oils in use is given below and graphs of the variation of kinematic viscosity with temperature are given in Figure I.27. The SAE motor oil classifications are also shown in Figure I.27 for convenient reference.

## SERVICE OILS (Ref.I.4.7)

OM - 13	A light mineral oil of low pour point ( $-46^{\circ}\text{C}$ ) containing 0.05 to 0.10% of stearic acid.
OM - 15	Aviation hydraulic fluid; petroleum base, with an oxidation inhibitor, viscosity index improver and an anti-wear agent (pour point $-59^{\circ}\text{C}$ ).
OM - 108	A refined filtered mineral oil of SAE 30 grade (pour point $-18^{\circ}\text{C}$ ).
OM - 160	A refined mineral oil (pour point $-12^{\circ}\text{C}$ ).
OM - 270	A plain mineral oil (pour point $-12^{\circ}\text{C}$ ).

## PROPRIETARY OILS

## Shell Group oils\*

Carnea 35	A plain mineral oil (pour point $-12^{\circ}\text{C}$ ). Specific gravity at $15.6^{\circ}\text{C}$ = 0.933.
Limea 931	A plain mineral oil (pour point $-12^{\circ}\text{C}$ ). Specific gravity at $15.6^{\circ}\text{C}$ = 0.935.
Macoma 76	A mineral oil with mild E.P. additive in the form of soap (pour point $-7^{\circ}\text{C}$ ). Specific gravity at $15.6^{\circ}\text{C}$ = 0.936.
Nassa 79	A plain mineral oil (pour point $10^{\circ}\text{C}$ ). Specific gravity at $15.6^{\circ}\text{C}$ = 0.905.
Nassa 87	A plain mineral oil (pour point $7^{\circ}\text{C}$ ). Specific gravity at $15.6^{\circ}\text{C}$ = 0.908.
Rimula 30	A mineral oil of SAE 30 grade with polar detergent additive (pour point $-18^{\circ}\text{C}$ ). Specific gravity at $15.6^{\circ}\text{C}$ = 0.912. Viscosity as for OM - 108.

---

\* Details kindly supplied by Shell-Mex and B.P. Ltd.

Vitreia 72

A plain mineral oil (pour point  $-7^{\circ}\text{C}$ ). Specific gravity at  $15.6^{\circ}\text{C} = 0.880$ .

**Edgar Vaughan & Co.Ltd., Oils**

EVCO Medium turbine oil Specific gravity at  $15.6^{\circ}\text{C} = 0.880$ .

EVCO NPL 4

(No details available).

**OTHER OILS**

Various vegetable oils, such as castor oil and linseed oil, are in use. They all contain fatty acids.

Various paraffins are in use.

**SILICONE FLUIDS (Ref.I.4.8)**

Midland Silicone MS 200/500 cs

MS 200/1000 cs

MS 200/12,500 cs

} Dimethyl silicone fluids  
with characteristically high  
viscosity index.

## LIST OF REFERENCES IN SECTION I.4

- I.4.1 Winter, K.L.  
et alii *Methods of Determination and of Fixing Boundary Layer Transition on Wind Tunnel Models at Supersonic Speeds.* CP.212, September 1954.
- I.4.2 Pankhurst, R.C.  
Holder, D.W. *Wind-Tunnel Techniques.* Pitman, London, 1952.
- I.4.3 Howarth, L. (Ed.) *Modern Developments in Fluid Dynamics. High Speed Flow.* Oxford University Press, 1953.
- I.4.4 Cope, W.F. *The Turbulent Boundary Layer in Compressible Flow.* R & M 2840, November 1943.
- I.4.5 Igglesden, M.S. *Wind Tunnel Measurements of the Lift-Dependent Drag of Thin Conically Cambered Slender Delta Wings at Mach Numbers 1.4 and 1.8.* ARC. CP.519.
- I.4.6 Stanbrook, A. *An Experimental Study of the Glancing Interaction Between a Shock Wave and a Turbulent Boundary Layer.* ARC CP.555
- I.4.7 - *Handbook of Service Lubricants and Temporary Protectives.* H.M.S.O., London, 1958.
- I.4.8 - *M.S. Silicone Fluids.* Midland Silicones Technical Data Sheet G.1 (Edition 6), October 1959.

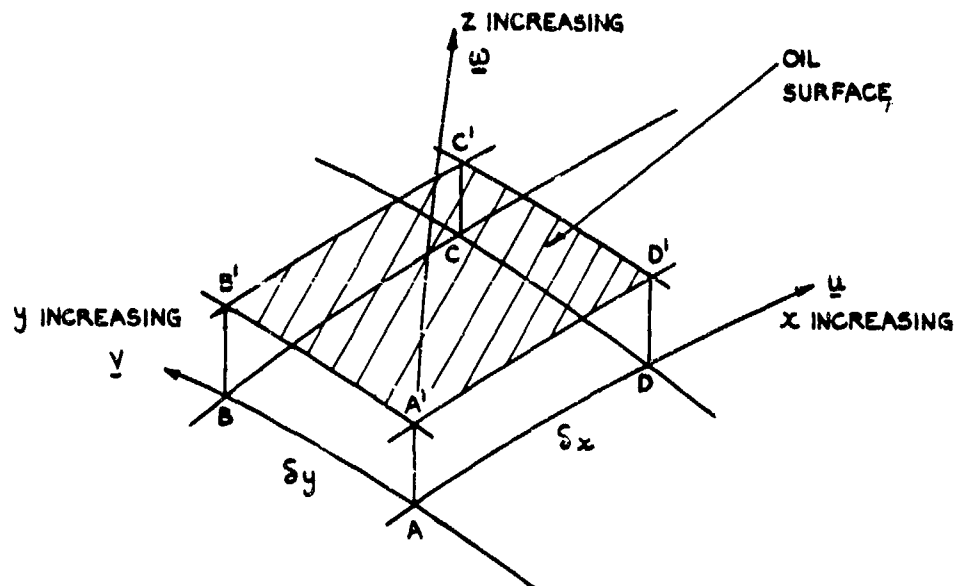


Fig.I.1 Co-ordinate system

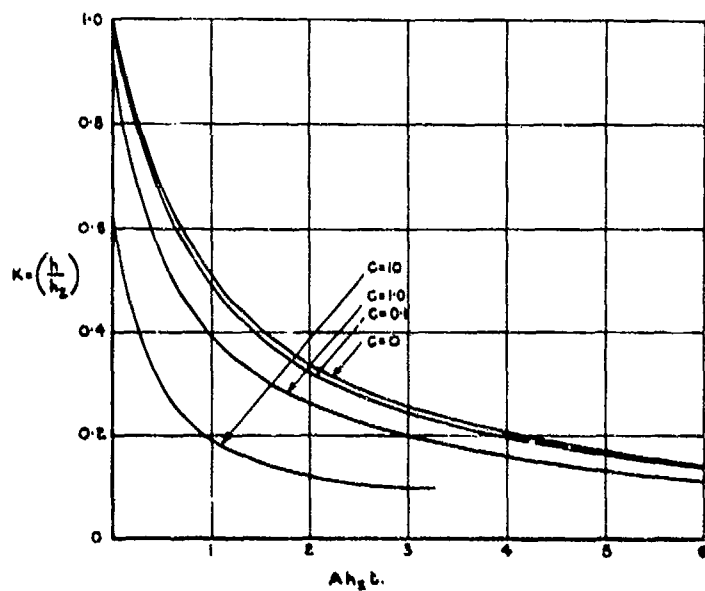


Fig.I.2 Variation of the thickness of the oil sheet at a stagnation point:

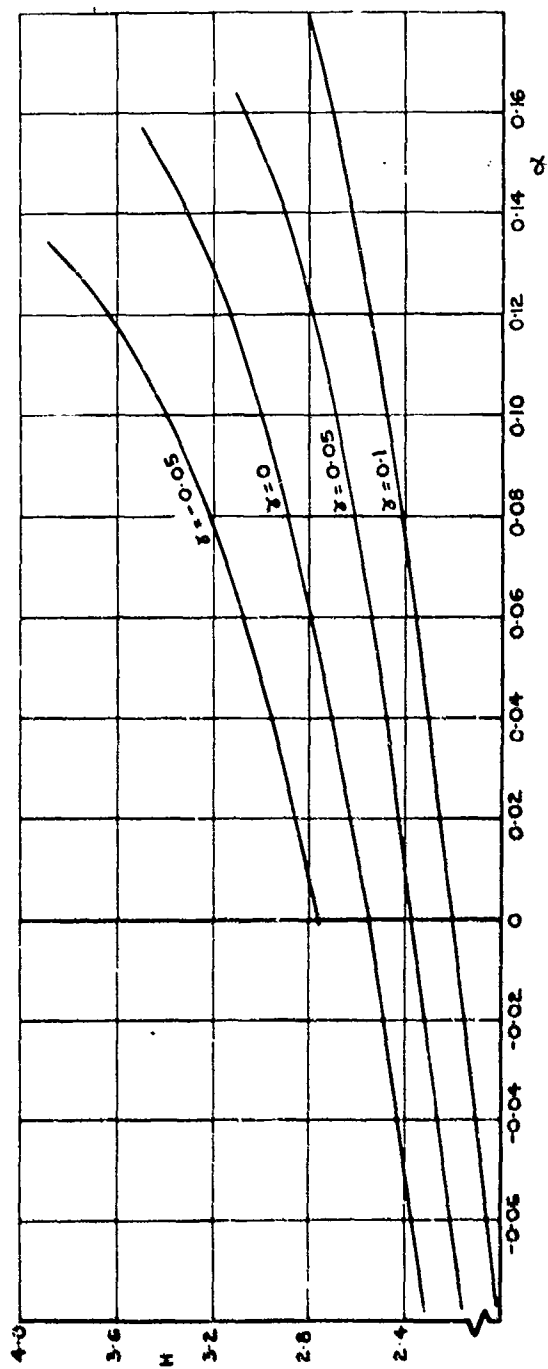


Fig. I.3 Variation of the ratio  $H(= c_i/b)$  with  $\alpha$  and  $\gamma$

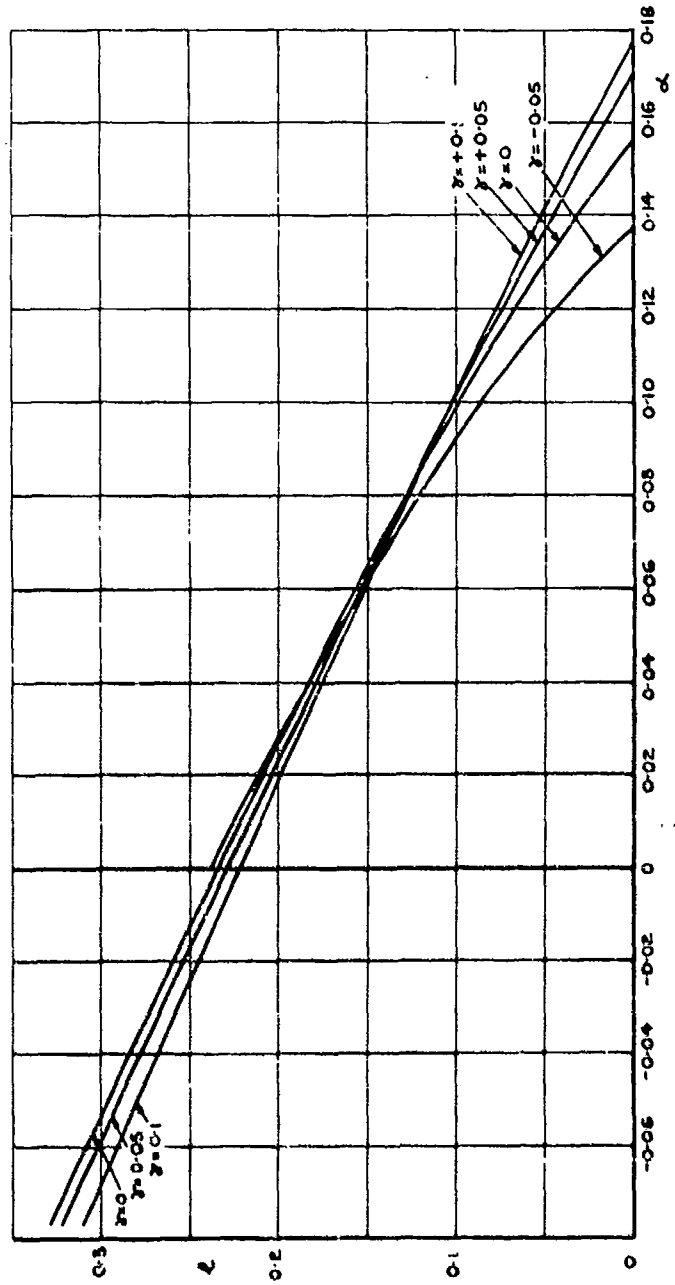


Fig. I.4 Variation of the ratio  $l \left( = \frac{G^2 \partial u_1}{u_0 \partial z} \right)_0$  with  $\alpha$  and  $\gamma$

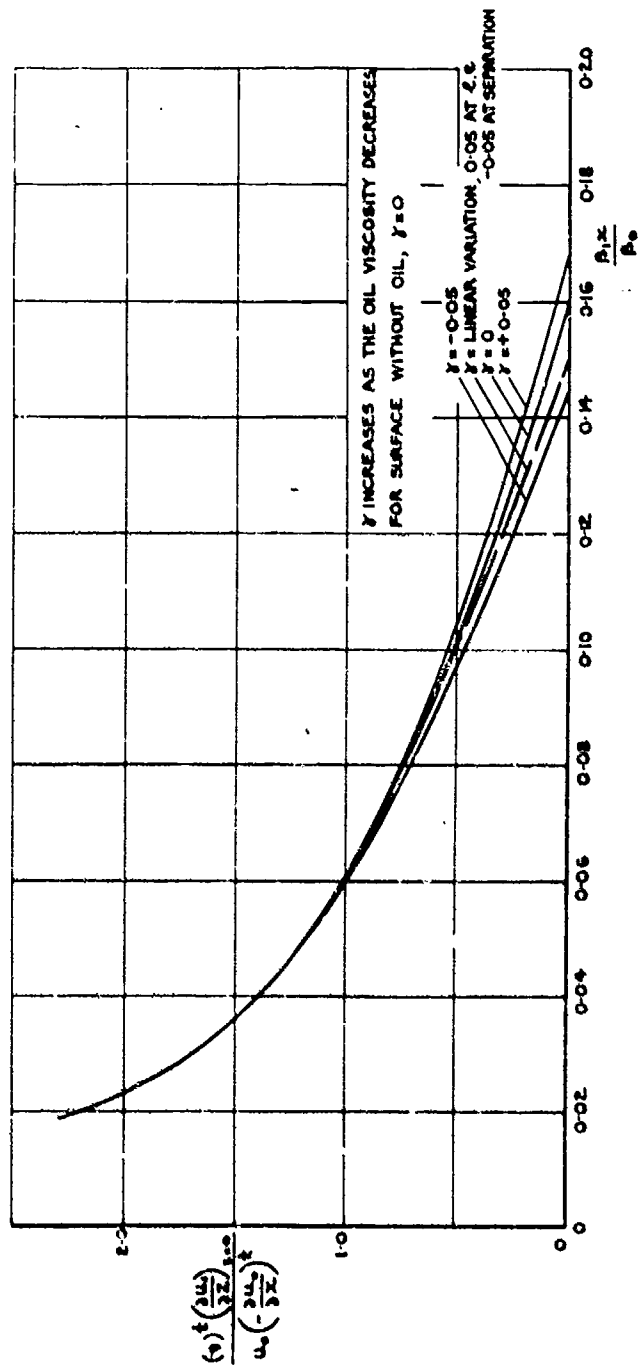


Fig. I.5 Variation of the skin-friction on a surface for different values of the parameter  $\gamma$

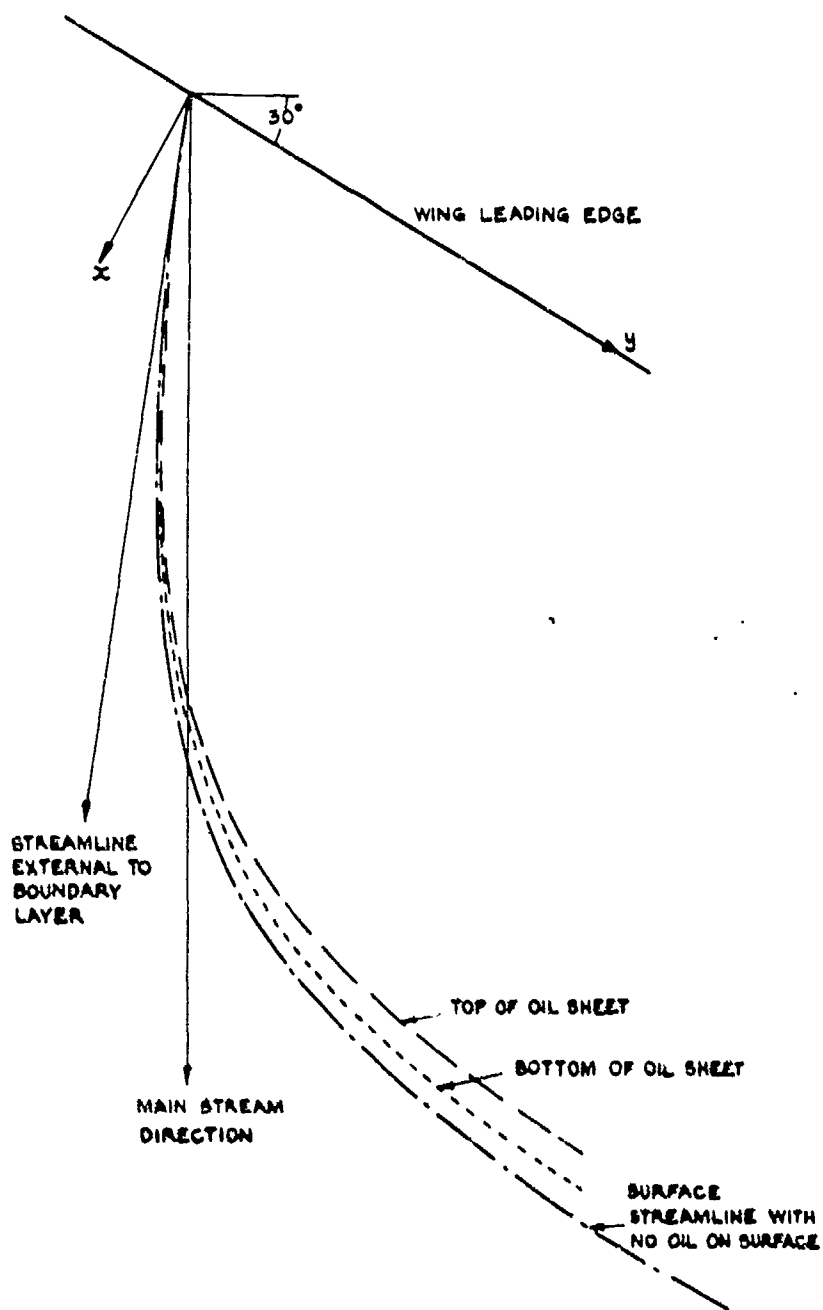


Fig. 1.6 Oil streamline pattern on a yawed wing

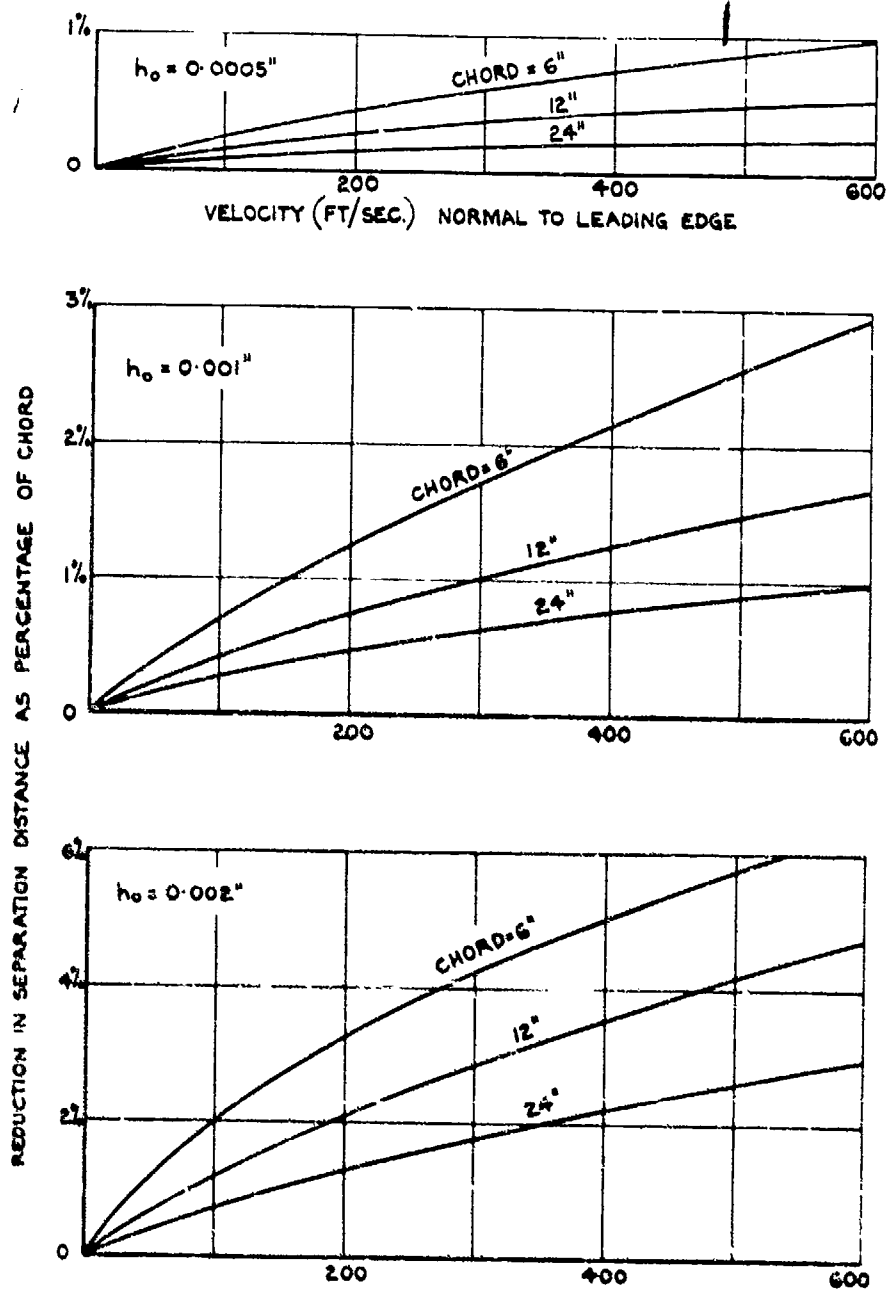


Fig. 1.7 Percentage reduction in apparent separation distance for different oil sheet thicknesses ( $h_o$ ) and aerofoil chords with speed

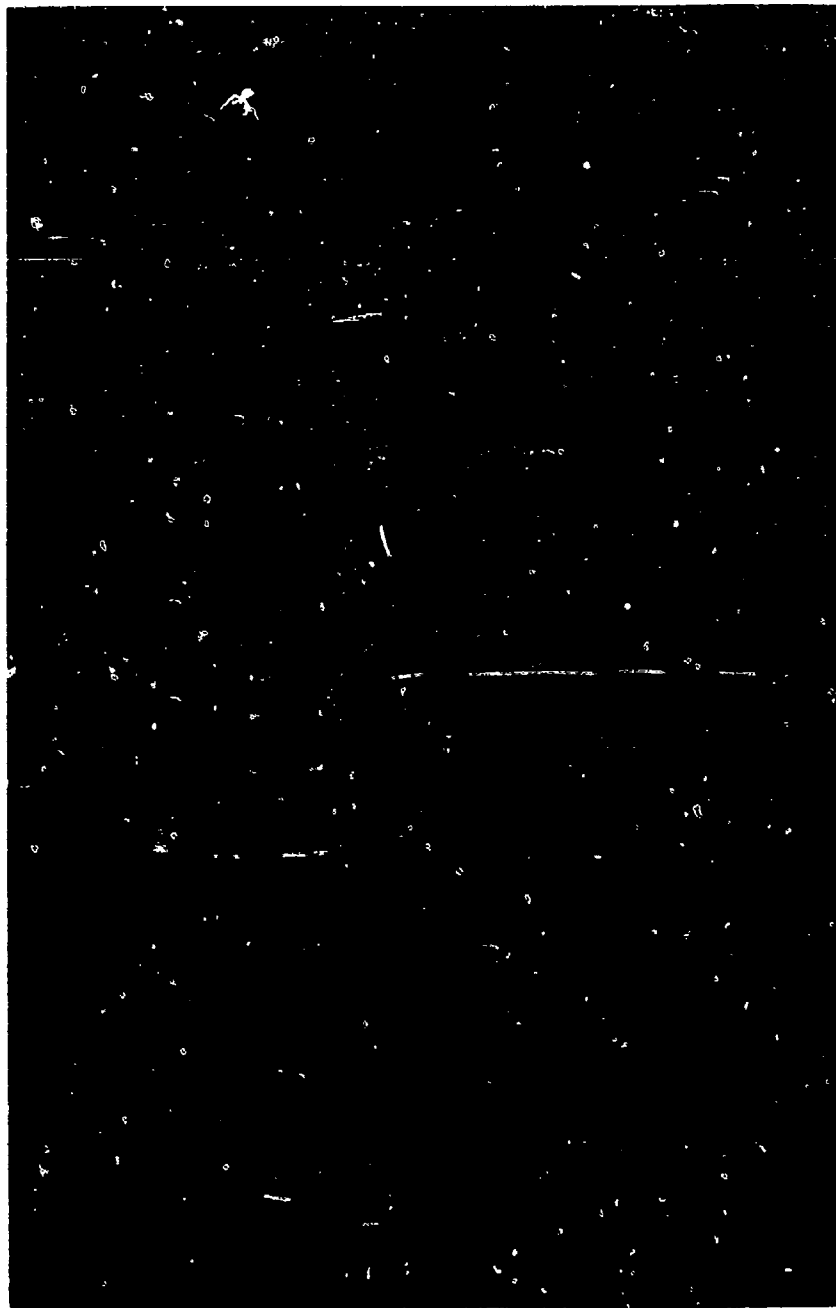


Fig.1.8 Surface flow patterns on  $\Lambda = 1$  delta wing at  $\alpha = 15^\circ$  (chrycene, kerosene, U-V light)

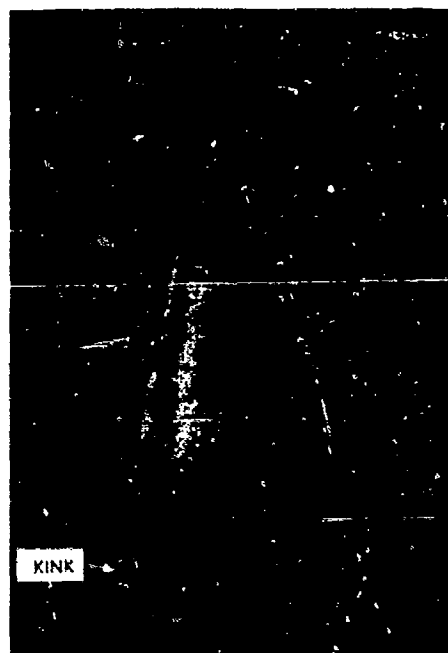


Fig.1.9 Surface flow pattern on yawed wing. Indication of vortex breakdown



Fig.1.10 Surface flow pattern. Formation of wavelets in flocculent mixture

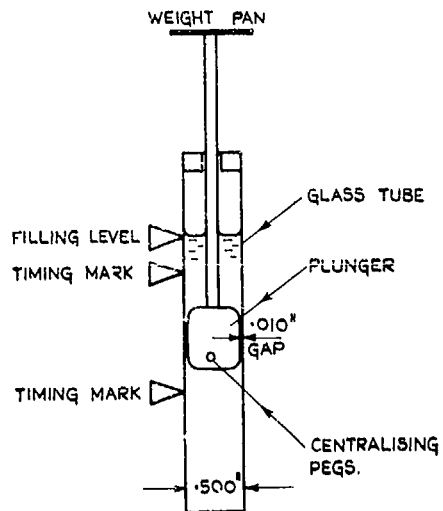
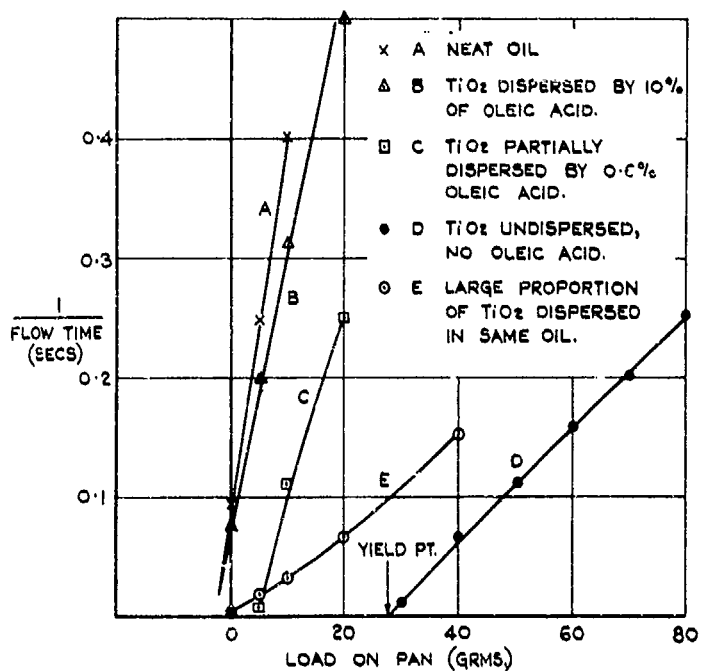


Fig. I.11 Details of mobilometer

Fig. I.12 Typical mobilometer results on  $TiO_2$  - oil mixture

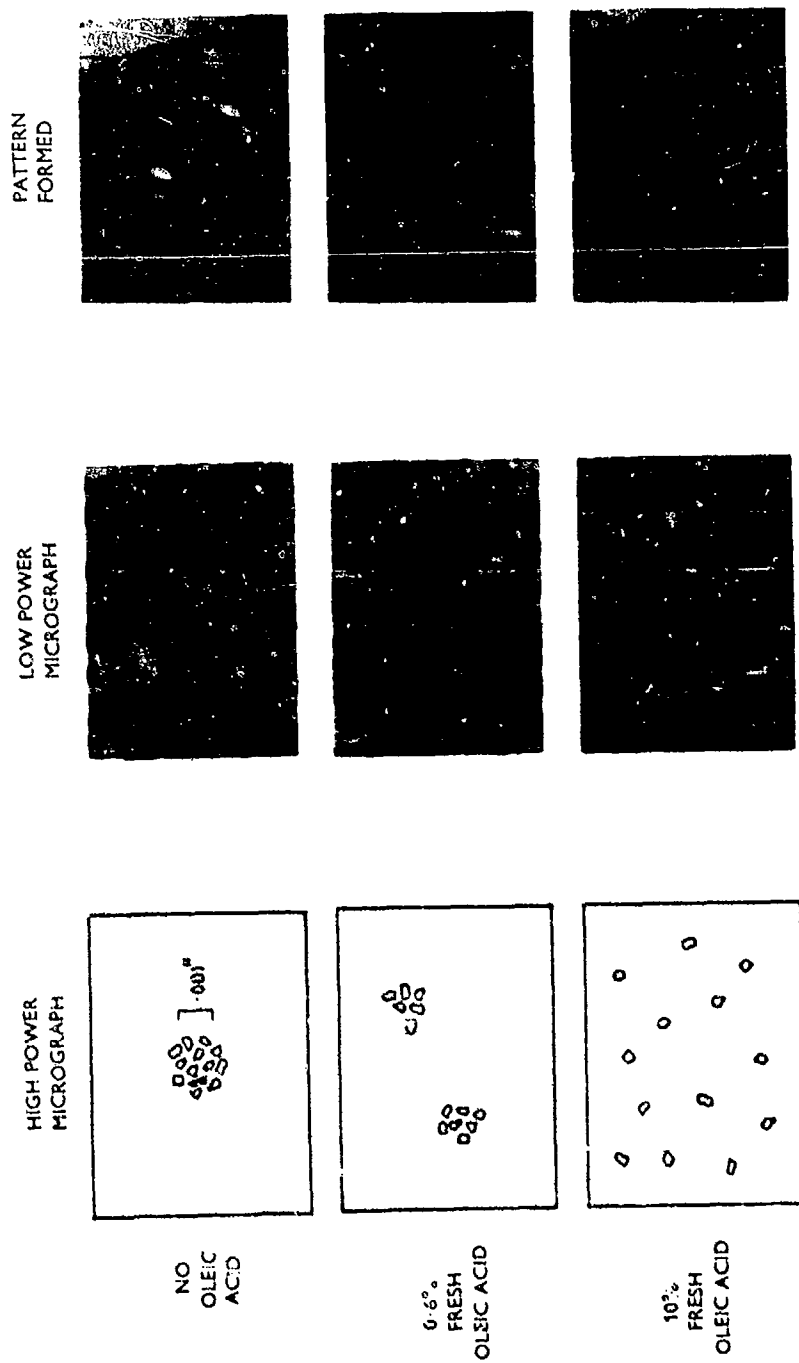


Fig. I. 13 The effect of an additive on a mixture of  $TiO_2$  and kerosene

Pigment	Photographic Technique	Lighting Arrangement	Photographic Film	Filter	Aperture No.	Exposure Time	Remarks
Anthracene	Fluorescence	125 watt U. V. Lamp 4 ft from model	Medium speed Pan (160 ASA)	2B	22	6 mins	Fluorescence varies with quality
			Blue sensitive ordinary (3 ASA)	2B	22	6 mins	
Chrysene	Fluorescence	125 watt U. V. Lamp 4 ft from model	Medium speed Panchromatic	2B	22	3 mins	Intense blue fluorescence
			Blue sensitive ordinary	2B	22	3 mins	
Satin Yellow Dye Pigment	Fluorescence	125 watt U. V. Lamp 4 ft from model	Medium speed Panchromatic	2B	22	3 mins	Bright lime-green fluorescence (recommended)
	Fluorescent flash	600 joules flash, with black glass 4 ft from model	Medium speed Panchromatic	2B	8	One flash	
Titanium Dioxide	Reflected light	500 watt floor lights	Slow, contrast Pan (80 ASA)	-	22	½ min	Dark model
	Reflected light	500 watt floor lights	Slow, contrast Panchromatic	-	22	½ min	White model
Lamp Black	Light tent	500 watt outside white fabric tent	Slow, contrast Panchromatic	-	22	approx 2 mins	Metal, white or polished model

Fig. I. 14 Photographic data for use in RAE low speed wind tunnels

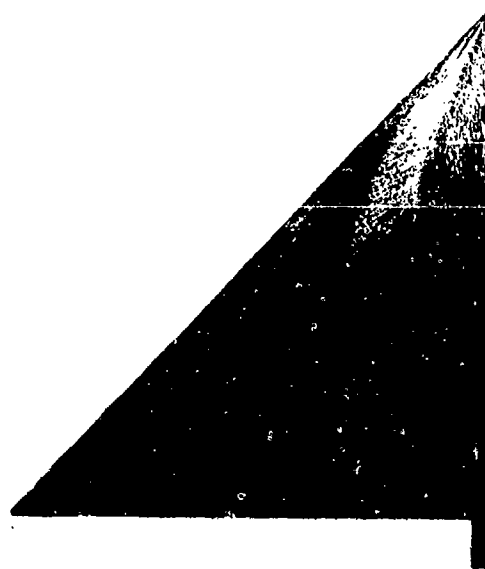


Fig. I. 15 Flow 45° delta wing,  $\alpha = 20^\circ$ , lampblack-kerosene

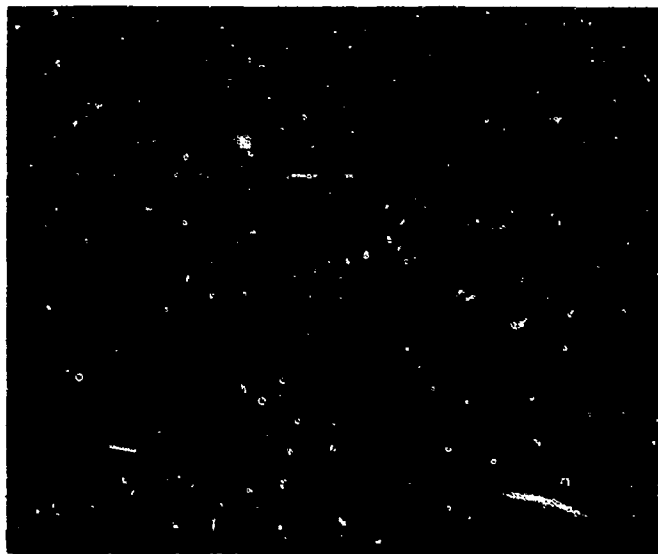


Fig. I. 16 Transition wedges shown by T10, - kerosene mixture

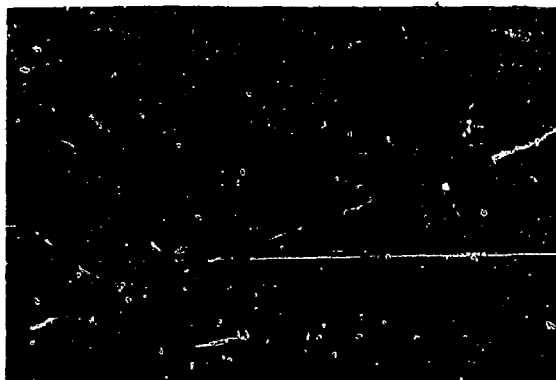
 $\alpha = 2^\circ$  $\alpha = 6^\circ$  $\alpha = 10^\circ$ 

Fig. I.17 Surface flow on portion of 25° swept wing. ('Dayglo' in U-V light)



(a)  $\alpha = 8^\circ$ : part span vortex



(b)  $\alpha = 10^\circ$ : full span leading edge vortex and trailing edge vortex near tip

Fig.1.18 Surface flow pattern on  $53^\circ$  swept wing. (Anthracene-kerosene; U-V light)

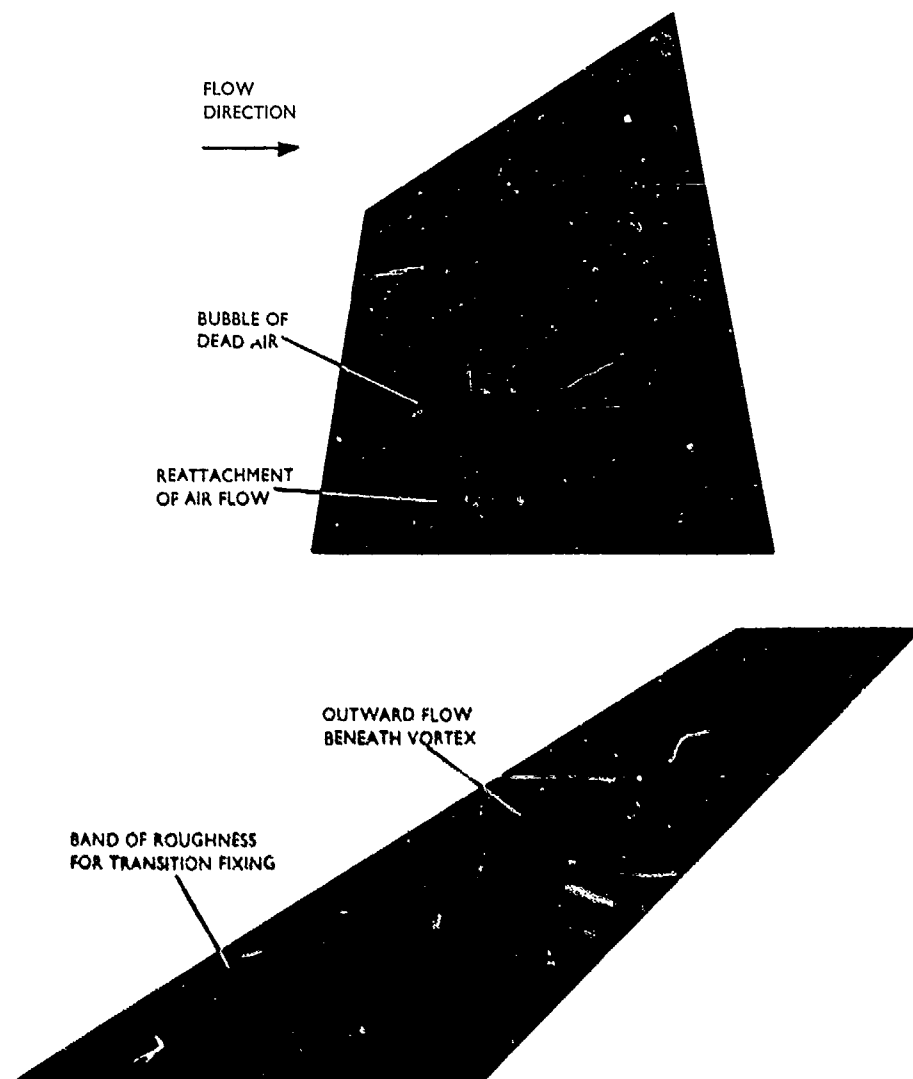


Fig. I.19(a) Examples of oil flow patterns

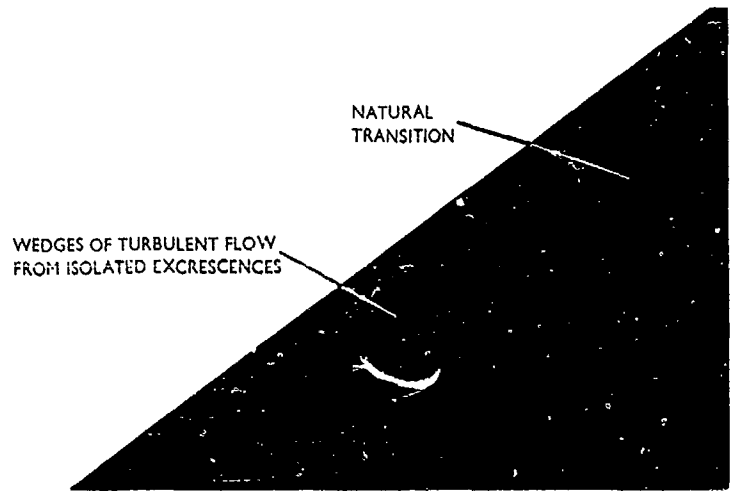


Fig. I.19(a) Examples of oil flow patterns (continued)

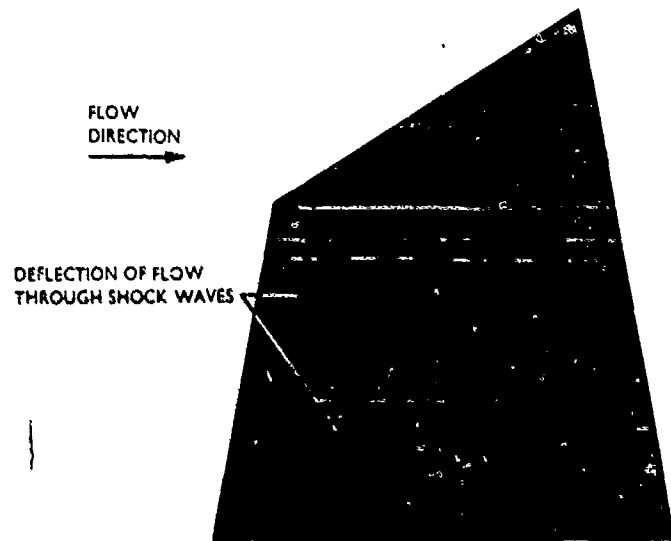


Fig. I.19(b) Examples of oil flow patterns

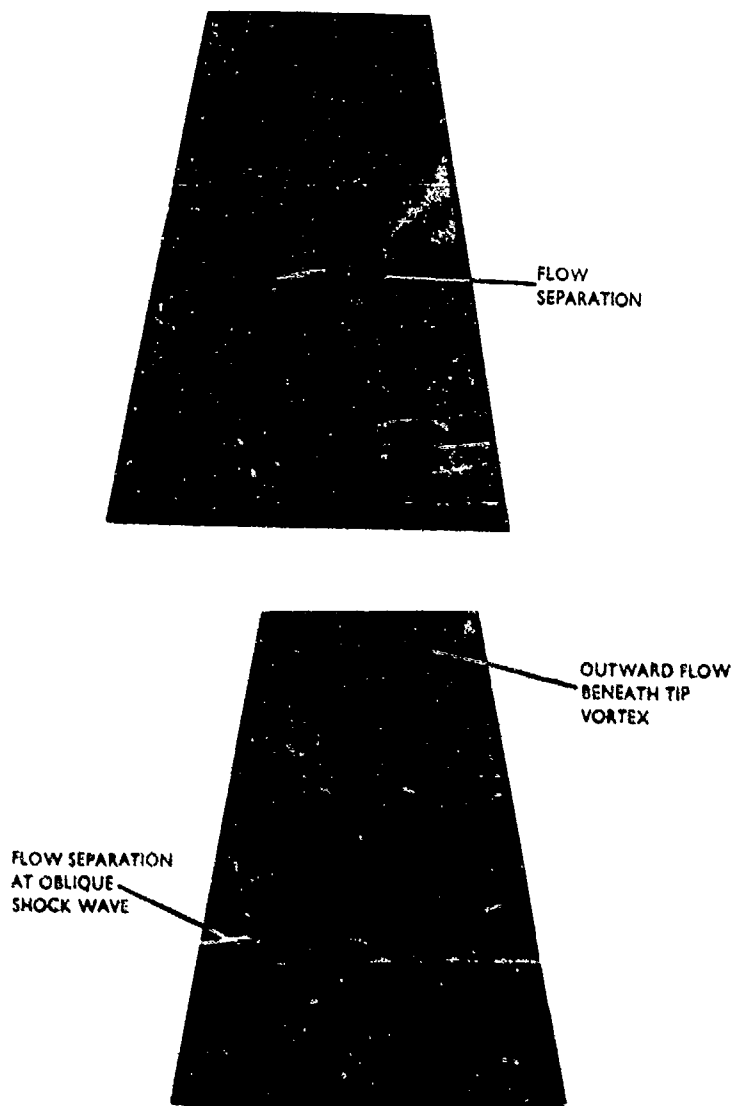


Fig. I.19(b) Examples of oil flow patterns (continued)

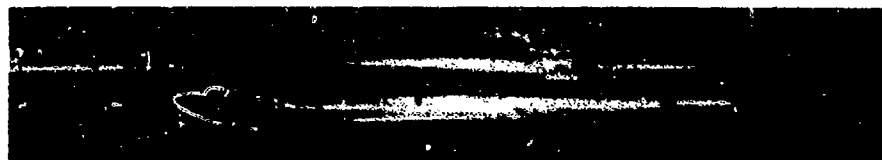
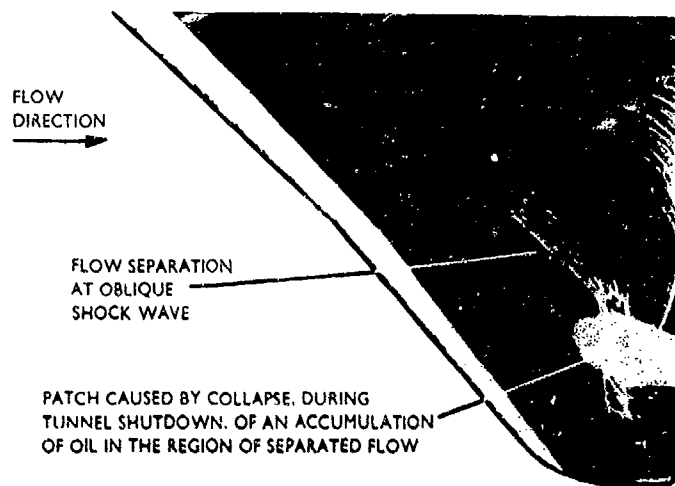


FIG. I. 19(c) Example of oil flow patterns

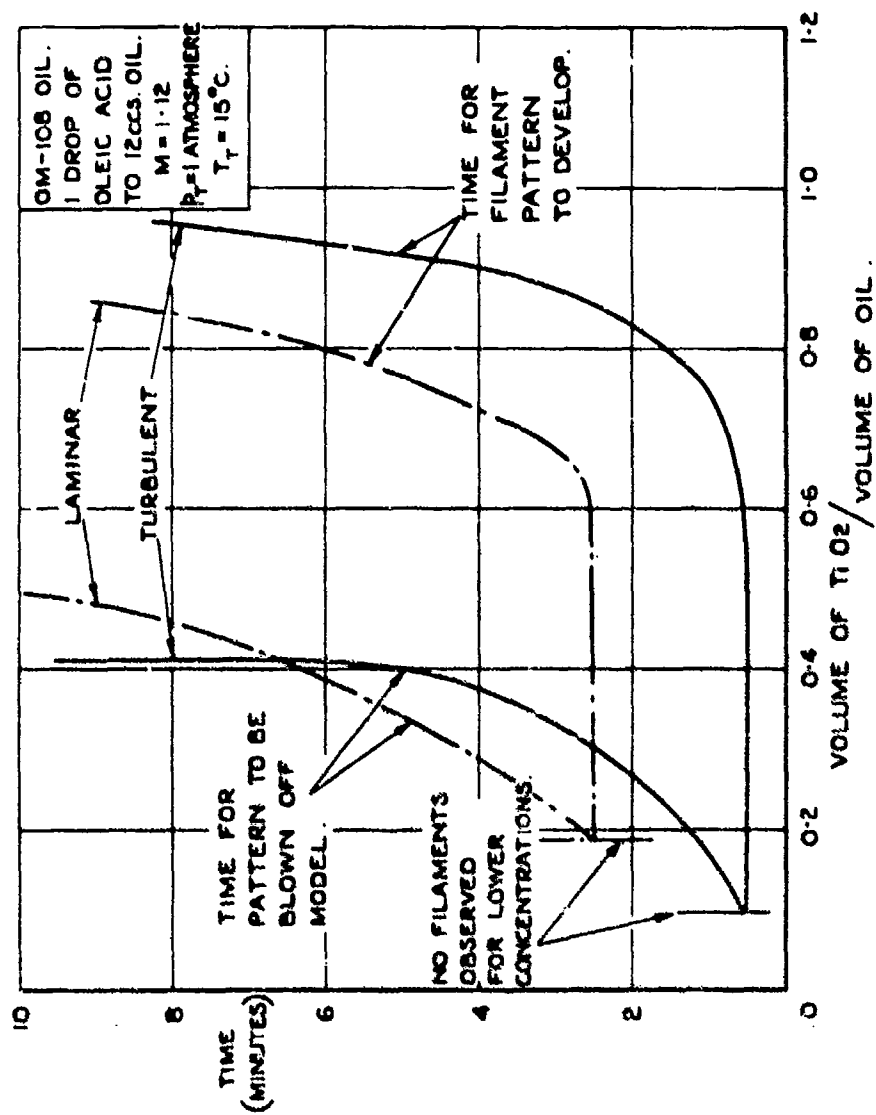


Fig. 1.20 Typical effects of varying the amount of TiO<sub>2</sub> on the development of a pattern

OIL MIXTURE USED:  
3 c.cs. OM-108; 2 c.cs. TiO<sub>2</sub>; 1 DROP OF OLEIC ACID.

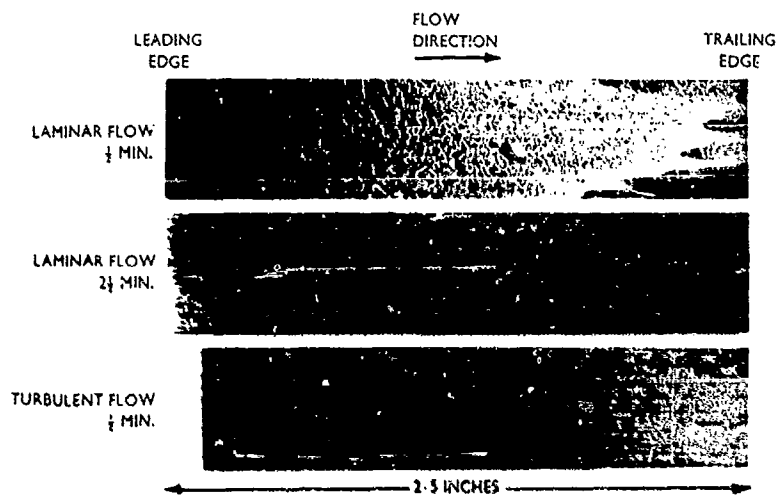


Fig. I. 21 Typical oil flow patterns on a 15° wedge

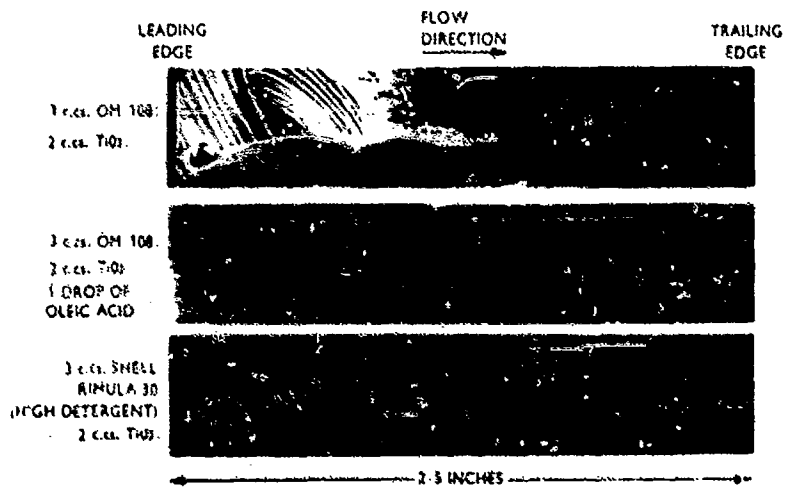


Fig. I. 22 Patterns obtained with different degrees of dispersion

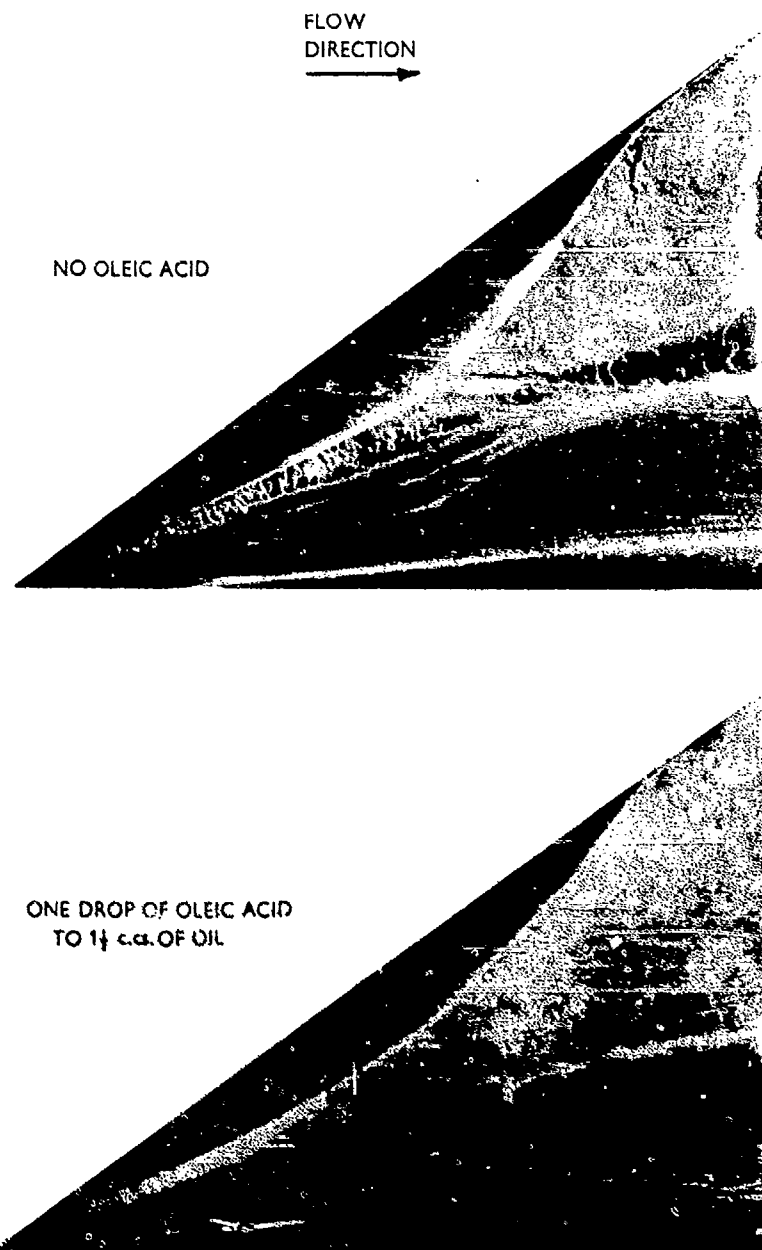


FIG. 1.73 Flow patterns obtained with and without oleic acid in the oil mixture

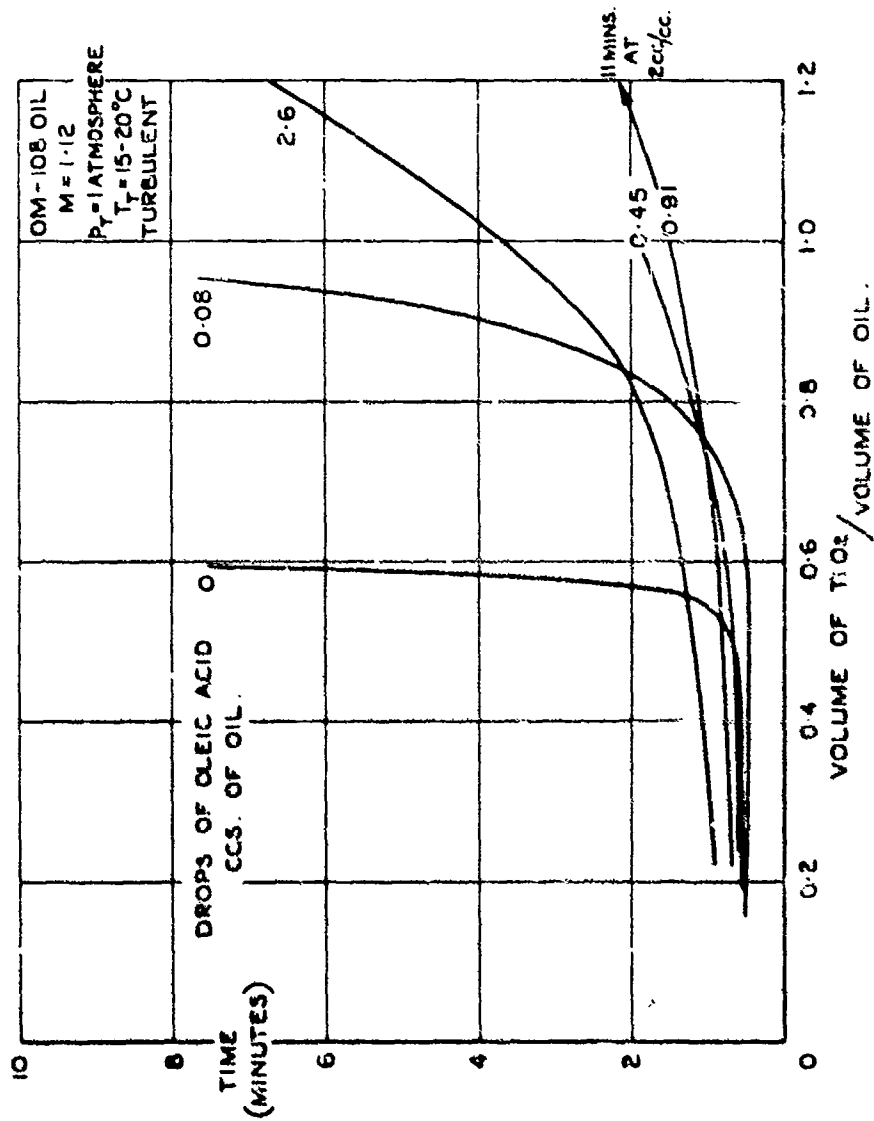


Fig. 1.24 Effect of the proportions of the mixture on the time taken to form a pattern

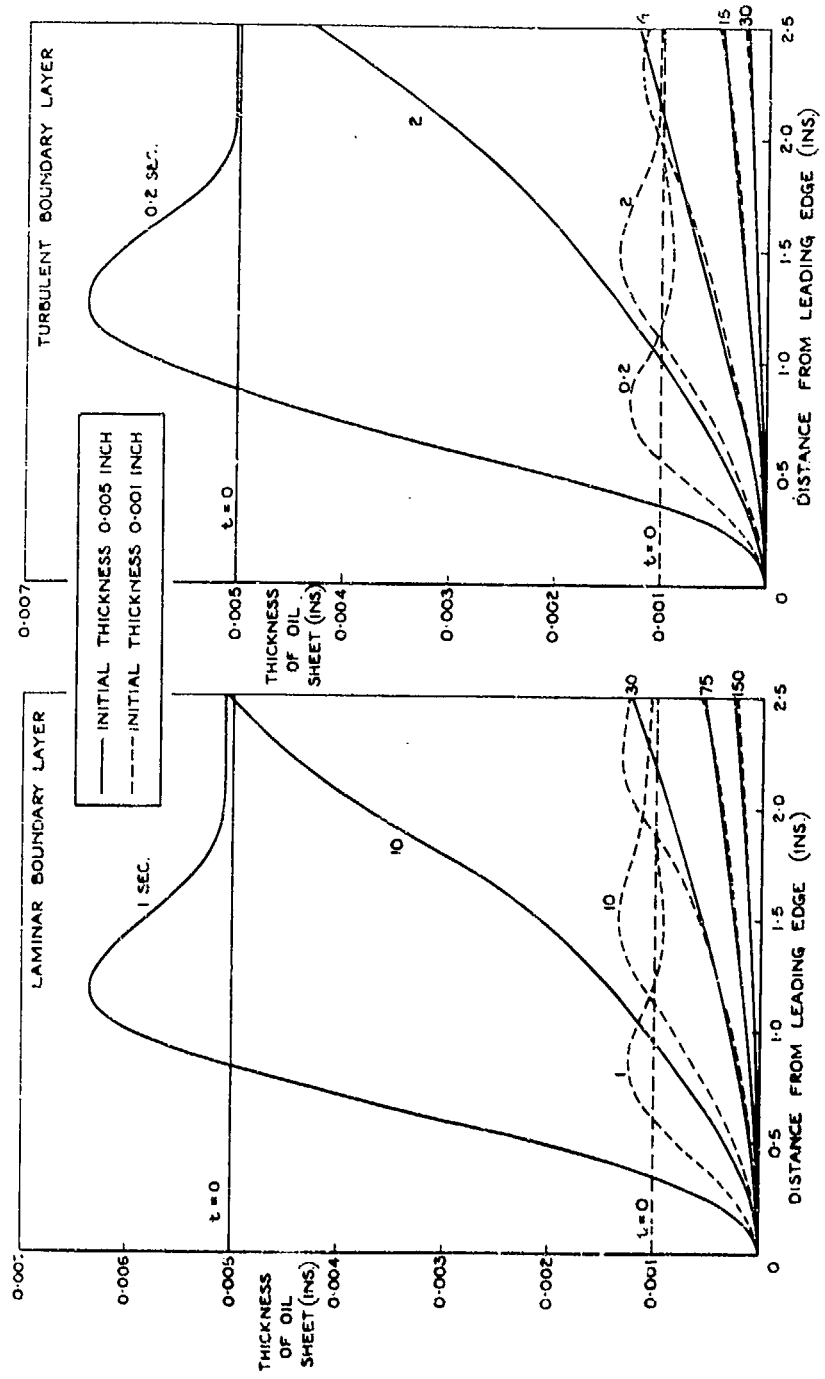


Fig. I.25 Theoretical variation of oil sheet thickness with time

○ LAMINAR BOUNDARY LAYER.  
 ▲ TURBULENT BOUNDARY LAYER.  
 FILLED SYMBOLS REPRESENT RESULTS FROM  
 INVESTIGATION IN THE 3 INCH TUNNEL.

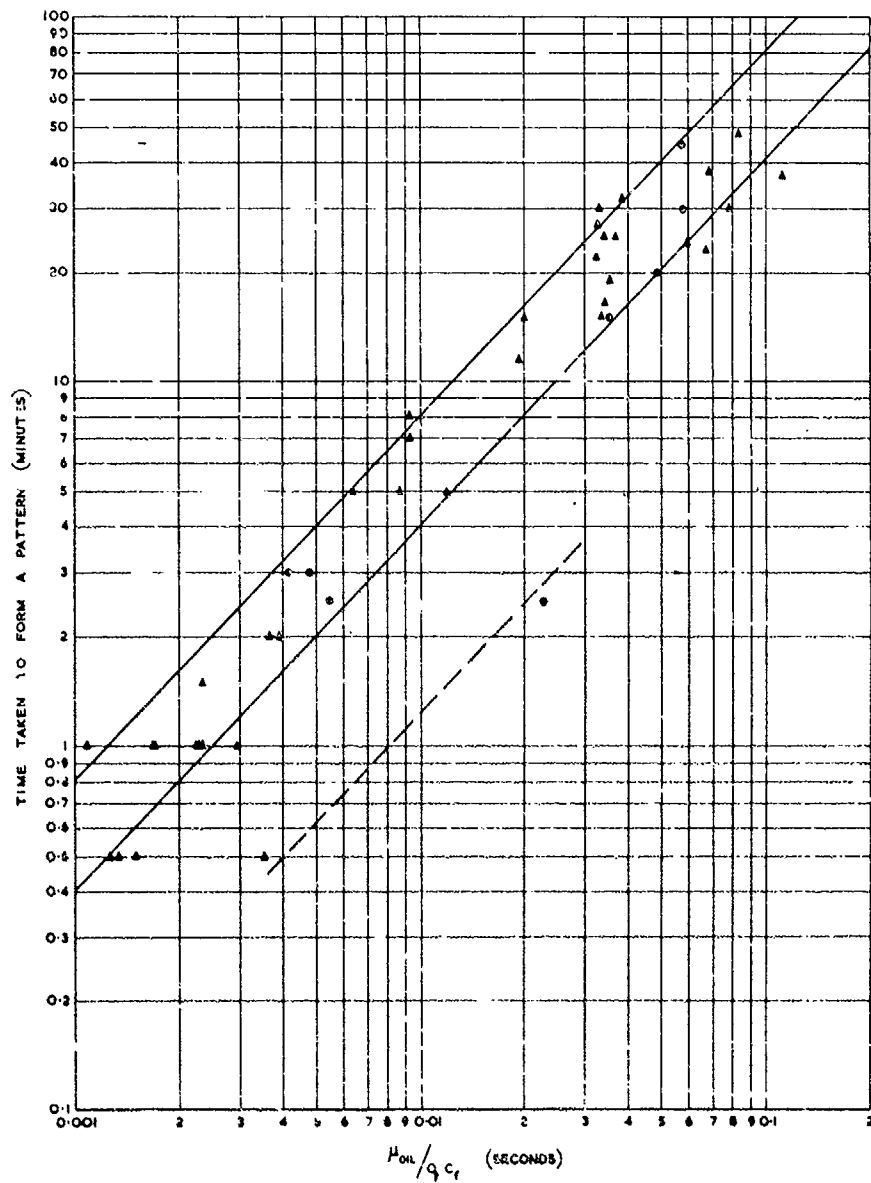


Fig. I.26 Correlation of time taken to form an oil flow pattern in various tunnels

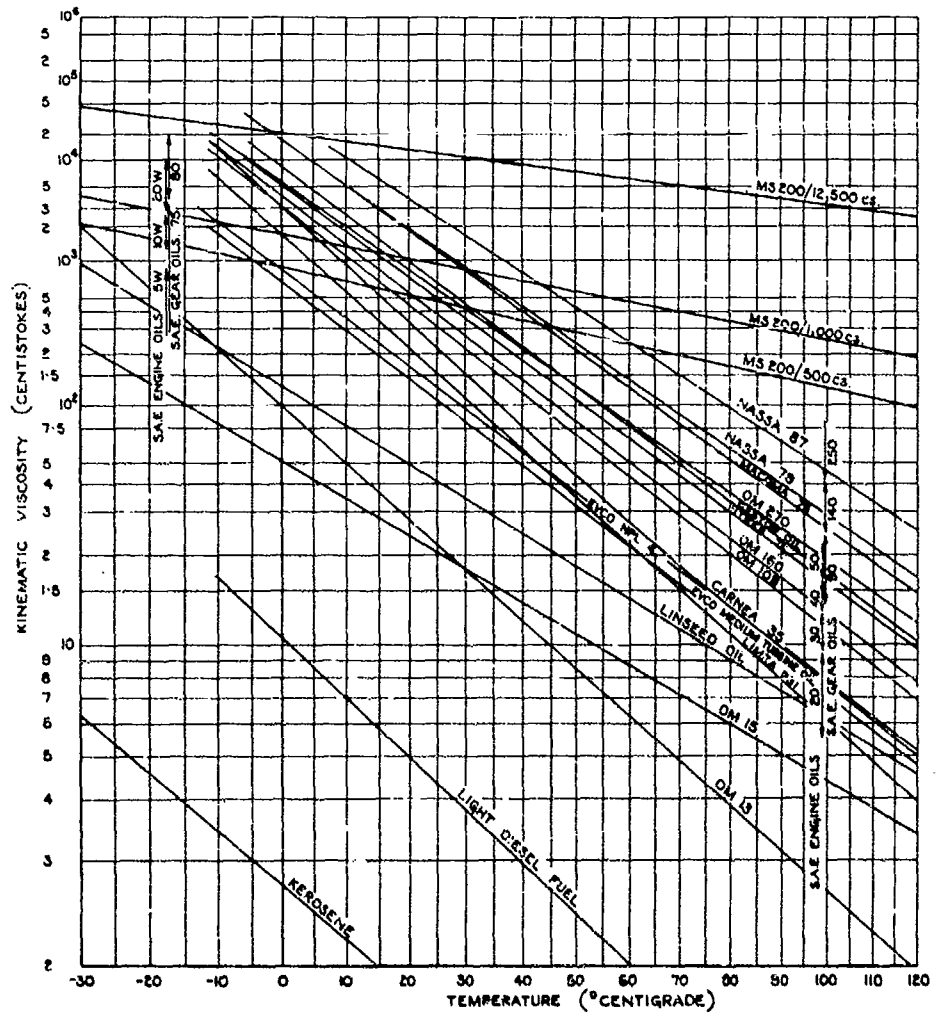


Fig. I. 27 Viscosity/temperature relationship for various oils in use

PART II

TECHNIQUES FOR LOCATING BOUNDARY LAYER TRANSITION

## CONTENTS

	Page
LIST OF FIGURES	77
TECHNIQUES FOR LOCATING BOUNDARY LAYER TRANSITION	79
REFERENCES	81
FIGURE	82

## LIST OF FIGURES

Page

Fig. II.28 Transition indicated by china clay technique (NPL)

82

## PART II. TECHNIQUES FOR LOCATING BOUNDARY LAYER TRANSITION

Apart from the methods described under the sections dealing with smoke techniques and surface oil flow techniques, several methods have been devised for locating the position of boundary layer transition by chemical and evaporative means. Descriptions of a number of these methods are given in Reference II.1 and attention is drawn to lists given there and in Reference II.2 of various toxic materials which had previously been suggested for use as indicators.

In current low speed practice only the 'china clay' and the 'liquid film' methods are in common use.

The 'china clay' method is described in detail in References II.1 and II.3. Briefly, the model is coated with a deposit of china clay (kaolin) which appears white when dry. When sprayed with a volatile liquid of about the same refractive index (such as methyl salicylate\*) the coating appears transparent. The liquid on the part of the model subjected to a turbulent boundary layer is evaporated more quickly and the white appearance is restored behind the transition line (Fig. II.28).

This method is particularly useful when many successive indications with a high degree of clarity are required on the same model but for occasional measurements the preparation of the surface is too lengthy. For rough indications a paste composed of china clay and kerosene spread on the surface of the model with the fingers has given excellent results although the comparatively uneven surface which results sometimes gives rise to transition wedges.

The liquid film technique is frequently employed when a quick indication of transition is required in the course of a wind tunnel test. A volatile oil is wiped onto the surface of the model with a swab so that it is covered with a thin film. The film evaporates more quickly in the turbulent region and the transition line can readily be seen in the reflections from the surface. The indication is clearer on a matt black surface and the contrast can be increased by dusting the unevaporated area with a white powder such as french chalk.

It is convenient to hold in the laboratory a stock of kerosene distillation fractions so that a suitable oil can be chosen for the test conditions, the heavier fractions being suited to higher speeds. Indication of the position of the transition line is sometimes made clearer if a transition wedge is created artificially by a small protrusion placed in the laminar regions for this purpose.

In high speed wind tunnels the evaporation technique has now been almost completely discarded in favour of sublimation methods (Ref. II.4) where a solution of a suitable solid in a highly volatile liquid is sprayed onto the model. Indication of the state of the boundary layer is then shown by the different rates of sublimation of the solid deposit in different flow regimes.

---

\* In practice kerosene works well, and this gives the advantage that various distillation fractions can be used as required.

Azobenzene has been generally used in continuous supersonic tunnels and more rapid indicators like acenaphthene and hexachlorethane have been used in transonic and intermittent tunnels. Acetone or petroleum ether are suitable solvents.

These sublimating solids as well as some others like diphenyl are toxic substances and precautions must be taken during application to avoid ingestion and contact with the skin.

A list of alternative materials is given in Reference II.5.

## LIST OF REFERENCES IN PART II

- II.1. Pankhurst, R.C.  
Holder, D.W. *Wind Tunnel Technique; An Account of Experimental Methods in Low and High Speed Wind Tunnels.*  
Pitman, London, 1952.
- II.2. Merewether, E.R.A.  
et alii *A Note on the Toxic Effects of Some Chemicals Previously Recommended for Use in Wind Tunnel Technique and on Vapour and Gas Explosion Risks in Wind Tunnels.*  
A.R.C. R. & M. 2198, 1946.
- II.3. Richards, E.J.  
Birstall, F.H. *The China Clay Method of Indicating Transition.*  
A.R.C. R. & M. 2126, 1945.
- II.4. Winter, K.G.  
et alii *Methods of Determination and of Fixing Boundary Layer Transition on Wind Tunnel Models at Supersonic Speeds.*  
A.R.C. C.P. 212. AGARD AG 17/P7, 1954.
- II.5. Main-Smith, J.D. *Chemical Solids as Diffusible Coating Films for Visual Indication of Boundary Layer Transition in Air and Water.* A.R.C. R. & M. 2755, 1950.



Fig. II.23 Transition indicated by china clay technique (NPL)

PART III

SMOKE TECHNIQUES FOR USE IN LOW SPEED WIND TUNNELS

## CONTENTS

	Page
LIST OF FIGURES	85
III.1 INTRODUCTION	87
III.2 OIL SMOKE	87
III.3 $\alpha$ - BROMONAPHTHALENE MIST	88
III.4 TITANIUM TETRACHLORIDE	88
III.5 WATER VAPOUR	89
III.6 SOAP BUBBLES	89
III.7 VAPORIZED RESIN SMOKE	90
III.8 SMOKE FROM CELLULOSE MATERIALS	90
III.9 SMOKE VISUALIZATION OF VORTEX TYPE EDGE SEPARATIONS	91
III.9.1 The Smoke Tube Method	91
III.9.2 The 'Smoke Screen' Technique	93
REFERENCES	96
FIGURES	97

## LIST OF FIGURES

	Page
Fig. III. 29	Titanium tetrachloride smoke on slender delta wing (Harvey) 97
Fig. III. 30	Cambridge University version of Preston and Sweeting smoke generator 98
Fig. III. 31	Luminosity of vists 99
Fig. III. 32	TiCl <sub>4</sub> smoke generator 99
Fig. III. 33	Condensation in vortex cores 100
Fig. III. 34	Flow in edge vortex shown by soap bubble traces 100
Fig. III. 35	Brooks resin smoke generator 101
Fig. III. 36	Paper smoke generator 102
Fig. III. 37	The smoke tube method 103
Fig. III. 38	Vortex breakdown using the smoke tube method 103
Fig. III. 39	Arrangement for smoke screen tests 104
Fig. III. 40	Details of light source 104
Fig. III. 41	Smoke screen technique 105
Fig. III. 42	Flow pattern on flat plate. $\alpha = 25^\circ$ 106
Fig. III. 43	Smoke screen technique using linear flash tube 107
Fig. III. 44	Smoke screen technique. Vortex development on delta wing 108
Fig. III. 45	Smoke screen technique. Vortex development on delta wing 109

## PART III. SMOKE TECHNIQUES FOR USE IN LOW SPEED WIND TUNNELS

R. L. Maltby and R. F. A. Keating

### III.1 INTRODUCTION

Smoke tunnels, which are wind tunnels designed exclusively for flow visualization tests using smoke, can give unrivalled presentations of the entire flow field around a model. These wind tunnels operate at very low speeds and elaborate precautions are taken to achieve a non-turbulent flow so that the smoke streams which are introduced in front of the model remain clearly defined. Because the Reynolds number available is necessarily very low, smoke tunnels are of limited value for investigating flow separation phenomena.

Full and detailed descriptions of this specialized technique are given in References III.1, III.2 and III.3 and the present paper will deal specifically with the use of smoke in ordinary low-speed wind tunnels.

The choice of a suitable smoke is not easy, for it should be dense and white, non-toxic and non-corrosive as well as non-clogging and non-condensing. It must be safe and simple to generate and must not issue into the airstream with sufficient velocity to disturb the experimental conditions. It should be noted that many types of chemical smoke generator designed for signalling and for military purposes are corrosive and contain toxic organic dyes. Their use is not recommended in a confined space although there may be no suitable alternative when very large volumes of smoke are required. In such cases adequate protection for the observers must be provided.

All smoke techniques depend on the quality of the lighting available in the wind tunnel; in fact it is not unusual for smoke patterns which are invisible in general lighting, to reveal important details of the flow when properly lit (Fig. III.29). If the smoke pattern has to be photographed the problem of lighting becomes even more important and care must always be taken to ensure that the best illumination is available in each set of circumstances.

### III.2 OIL SMOKE

The most common method of obtaining smoke for wind tunnels is by the vaporization of a mineral oil such as kerosene. An apparatus designed to produce a substantial quantity of kerosene smoke is described in detail in References III.4 and III.5. Oil supplied from a reservoir is boiled in a glass tube which is heated electrically. The vapour issues from a small orifice at the end of the tube where it meets a stream of air entering from the sides of a mixing vessel forming a dense white smoke. The smoke is then fed to the wind tunnel working section through tubes.

The kerosene smoke is non-corrosive and non-toxic although there is some risk of fire or explosion if the generator is mishandled. The smoke tends to condense on the walls of tubes conveying it to the model and, if the generator cannot be placed close to the model, the volume of smoke emitted may be disappointing. The apparatus becomes messy to handle unless it is quite free from leaks and the smell of a large concentration of smoke is unpleasant.

A particularly compact and reliable oil smoke generator (Fig.III.30) has been developed in the Mechanical Engineering Laboratories at Cambridge University. This is a self-contained unit to supply a small smoke tunnel and it incorporates a blower from a hair dryer to provide its air supply.

Small amounts of kerosene smoke can be generated at the surface of a wing (Ref.III.6). An asbestos pad soaked in kerosene is set into the surface of the wing and is heated electrically so that smoke can be generated at the points of interest. For instance, it can be produced along a spanwise line and can be used to give an overall indication of boundary layer transition.

### III.3 $\alpha$ - BROMONAPHTHALENE MIST ( $C_{10}H_7Br$ ).

Smoke techniques are reasonably simple to operate at low wind speeds but there is always difficulty in producing sufficient smoke to be visible at higher speeds. In the course of research on axial compressors at the National Gas Turbine Establishment, a special technique was required to make the flow visible at about 500 f.p.s. (Ref.III.7). A study of the 'apparent luminosity' of mists composed of refracting droplets (Fig.III.31) showed that a tenfold improvement could be obtained over kerosene smoke if a mist with a refractive index about 1.65 can be used.

$\alpha$  - bromonaphthalene mist has a suitably high refractive index and an apparatus, similar in principle to the oil smoke generator, has been designed to produce it. The temperature of the vapour needs careful control and an elaborate boiler is required.

Satisfactory photographs have been taken at 500 f.p.s. with a high intensity argon discharge light source.

$\alpha$  - bromonaphthalene and similar compounds are toxic substances and the mist must not be inhaled.

### III.4 TITANIUM TETRACHLORIDE ( $TiCl_4$ )

Titanium tetrachloride (Titanic chloride) is a liquid which, in the presence of moist air, produces dense white fumes consisting of titanium dioxide and hydrochloric acid. The fumes are therefore highly corrosive and irritant.

Despite these serious disadvantages, titanium tetrachloride is frequently used when a smoke trace is required with the minimum of preparation. The liquid is mixed with an equal quantity of carbon tetrachloride ( $CCl_4$ ) to minimise the formation of solid deposits. It can be applied to the surfaces of models in drops or streaks by means of a glass rod dipped in the mixture. A stream of smoke issues from the droplets until they have completely evaporated leaving a solid deposit on the model. Finely detailed smoke patterns are easily obtained in suitable lighting; for example Figure III.29(a) and III.29(b) show the colling up of the vortex sheets springing from the separation at the edge of a slender delta wing. In Figure III.29(a) the vortex core is well defined but in Figure III.29(b) the model has been yawed and the flow in the vortex core breaks down.

A continuous stream of smoke can be obtained by using the simple apparatus illustrated in Figure III.32. Air is blown gently through a bottle containing a mixture of titanium tetrachloride with carbon tetrachloride and the fumes are delivered through a glass tube to the model. There is a tendency for a solid deposit to form at the nozzle which quickly blocks the flow unless it is cleared frequently.

Titanium tetrachloride smoke is only suitable for very low wind speeds of the order of 5 f.p.s.

### III.5 WATER VAPOUR

If the relative humidity of the air in a wind tunnel is high the water vapour will condense in areas where there is sufficient drop in temperature. This sometimes occurs near the cores of the vortices from the edges of a slender wing and it gives a clear indication of the vortex paths (Fig. III.33). The process can be encouraged by throwing water into the wind tunnel settling chamber before the test. The tubular appearance of the vapour in Figure III.33 is discussed in Section III.9.

Water introduced into high velocity jets issuing from a wing in an airstream will atomise into a mist which can be used to trace the paths of the jets.

### III.6 SOAP BUBBLES

Although a stream of soap bubbles can hardly be described as a smoke, it is convenient to mention the method here since it performs a similar function. The bubbles can be produced from a mixture of a liquid synthetic detergent (such as 'Teepol') and glycerine. A piece of wire bent to form a  $\frac{1}{4}$  inch diameter circle with a handle is dipped into the mixture and is then held in a slow airstream. The wind speed is carefully adjusted so that a stream of bubbles forms from the liquid film on the wire and can be made to flow over a model for a few seconds. If they are illuminated by a spotlight from further downstream and photographed with a long exposure, the paths of the bubbles will appear as white lines. Figure III.34 illustrates the flow over a sharp-edged delta wing using this method.

A soap solution can sometimes be used to locate areas of separated flow at high wind speed by feeding it through tubes leading to holes in the model used for pressure plotting. Bubbles will form on the surface and will be blown away except when they form at holes in a region of separation. In such a region they will congregate and mark the area of zero velocity.

### III.7 VAPORIZED RESIN SMOKE\*

A compact electrically fused pyrotechnic generator (Fig. III.35) which produces a dense stream of white smoke has been developed especially for use in wind tunnels up to a speed of about 50 f.p.s. The smoke is non-toxic, non-clogging, has an in-offensive odour but is slightly corrosive to bare steel. The composition of the contents of the generators has not been divulged by the manufacturers but it is believed to be based on the vaporization of a resin. Some ammonium chlorate is present, and, since this is an unstable substance, the generators must be stored away from heat.

### III.8 SMOKE FROM CELLULOSE MATERIALS

The smokes from smouldering cellulose materials such as wood, tobacco or paper have been in use for many years and they offer one of the simplest methods of producing large quantities of smoke for long periods with a simple control of volume. These smokes tend to contain large quantities of tarry matter which may be deposited on the surfaces of the model and the wind tunnel unless they are previously filtered out. Unfortunately the volume of smoke is much reduced by such filters because the visibility of the smoke relies on the presence of water droplets. Furthermore the products of combustion of cellulose materials can contain a substantial proportion of carbon monoxide and care must be taken to ensure that the atmosphere in the laboratory is not contaminated to a dangerous level.

Smouldering paper produces a very dense smoke without an excessive amount of tarry matter if the burning conditions are carefully controlled. A suitable smoke generator is illustrated in Figure III.36 with which rolls of paper towelling are used as fuel. It consists of two substantial steel cylinders 12 in. high, one of 12 in. diameter, the combustion chamber, and another of 8 in. diameter which is a separator to remove the less volatile products of combustion. Both cylinders are fitted with lids which are bolted down firmly to make a good seal.

The combustion chamber is fitted with an air supply pipe at the bottom and also a plug through which the paper is ignited. Inside the chamber, the air supply pipe is divided into three smaller pipes arranged to distribute the incoming air. The separator is connected to the combustion chamber by a large pipe which is easily accessible for cleaning. The smoke supply pipe to the tunnel is connected to the top of the separator.

It is important to keep the temperature of combustion low in order to minimize the amount of tar produced and to extend the duration of the smoke production. The correct

---

\* Vaporized resin smoke generators are marketed as 'Brooks White Smoke Generator' Ref. W35 or W120, the number in the reference indicating the time of burning in seconds. They may be obtained from:

Brooks Fireworks Co. Ltd.,  
Hemel Hempstead,  
Hertfordshire,  
England.

burning rate is achieved by making the paper slightly damp before loading. About 2½ lb. of paper packed loosely into the combustion chamber can be made to provide a dense smoke for 40 mins.

To assess the risk from carbon monoxide poisoning from this smoke the following measurements have been made in the 13 x 9 ft Low Speed Tunnel at R.A.E. Bedford. This tunnel has the unusually large internal volume of 700,000 cu. ft and concentrations in smaller tunnels might be expected to be correspondingly greater.

CO content of smoke issuing from generator	2.5%
CO content of air in working section after burning 6 lb. paper	0.01%
CO content of air in working section after burning 10 lb. paper	0.02%
CO concentration locally in control room at the same time	0.02%
CO concentrations, locally for short times, in working section	up to 0.06%

The toxic effect is based on the great affinity of haemoglobin in the blood for carbon monoxide. Very low concentrations in the atmosphere will markedly reduce the oxygen dissociation rate and the capacity of the blood to carry oxygen. The carbon monoxide can only be displaced slowly by oxygen in a pure atmosphere, so that the effects of breathing a contaminated atmosphere for infrequent short periods over several days are cumulative. The following table gives an indication of the effects of various concentrations:

0.01%	No appreciable effect after prolonged exposure
0.02%	Slight discomfort (e.g. headache) after a few hours exposure
0.15%	Dangerous after 1 hour exposure
0.4%	Fatal after less than 1 hour exposure.

It is clear, therefore, that it is necessary to provide good ventilation in the rooms surrounding the wind tunnel and to maintain a constant circulation of air in the tunnel when attending to the model since there is reason to believe that low chronic toxicity should be avoided as well as the obvious acute poisoning hazard.

The carbon monoxide contamination of the atmosphere can be measured with a simple commercial instrument based on the discoloration effect on Potassium Pallado-Sulphite.

### III.8 SMOKE VISUALIZATION OF VORTEX TYPE EDGE SEPARATIONS

#### III.8.1 The Smoke Tube Method

Experience has shown that the vortex type separations from highly swept edges can be investigated by smoke visualization techniques up to unexpectedly high speeds (Ref.III.8). The marked inward radial component of velocity in the region of the vortex core concentrates smoke from the field into a small area so that it is not

quickly diffused as it would be in other types of flow. Figure III.37 illustrates the characteristic tubular smoke pattern in the path of a vortex above an  $A = 1$  delta wing at a wind speed of 180 f.p.s. using paper smoke.

A simple theory for the form of the 'smoke tube' can be derived from Hall's theory for the structure of the outercore of the vortex given in Reference III.9. Consider the forces in the cross-flow plane acting on a single smoke particle when it is in the neighbourhood of the vortex core. Since it is in a rotating flow it will experience a force away from the centre which will be opposed by a drag force arising from the radial velocity of the air and the radial component of the velocity of the particle relative to the vortex core. Forces due to the radial pressure gradient and the radial acceleration of the particle will also occur but these are negligibly small for the microscopic particles considered. An equilibrium will be reached at a radius from the vortex core where the resultant force in the plane is zero.

Hall gives the following expressions for the relationship between three components of velocity in the outercore:

$$\frac{V^2}{U_0^2} = K_1 \left( \frac{U}{U_0} - \frac{W}{U_0} \frac{x}{r} \right)$$

$$W \cdot \frac{x}{r} = \text{constant.}$$

where  $U_0$  is the free stream velocity  
 $U$ ,  $V$  and  $W$  are the axial, circumferential, and radial components of velocity  
 $x$  is the distance from the wing apex  
 $r$  is the radius from the centre of the core  
 $K_1$  is a constant.

The centrifugal force on a smoke particle is given by

$$F_c = \frac{4}{3} \pi r_p^3 \rho_p \frac{V^2}{r}$$

and, assuming that Stoke's Law applies, the drag force is given by

$$F_D = 6 \pi r_p \left[ U \frac{dr}{dx} - W \right] \mu$$

where  $r_p$  is the radius of a smoke particle  
 $\rho_p$  is the density of a smoke particle  
and  $\mu$  is the viscosity of the air.

For equilibrium, when  $r$  becomes the radius of the smoke tube,

$$F_c = F_D :$$

thus, if  $x$  is not too small,

$$r^2 = \frac{4}{9} r_s^2 \frac{\rho_s}{\rho_0} R_x K_1 \left\{ \frac{1 - \frac{Wx}{Ur}}{1 - 2 \frac{Wx}{Ur}} \right\} + Cx^2 \frac{Wx}{U^2} \quad (\text{III.1})$$

where  $C$  is a constant of integration

$R_x$  is the Reynolds Number based on distance from the apex  
and  $\rho_0$  is the density of the air.

In order to check this result some tests were made with paper smoke on an  $A = 1$  delta wing for which values for  $K_1$  and  $\left(\frac{W}{U} \cdot \frac{x}{r}\right)$  had previously been measured. The smoke tube radius was measured over a range of conditions and, assuming the smoke particles had the same density as water, the radius of the smoke particles was calculated. The resulting value for  $r_s$  of  $1.2 \times 10^{-5}$  in. compared reasonably well with values from electron microscope measurements which range from  $1.5$  to  $4 \times 10^{-5}$  in. (The electron microscope gave similar values for Brock's Rosin Smoke.)

In the conditions of these tests  $\left(\frac{W}{U} \cdot \frac{x}{r}\right)$  was negligibly small at the equilibrium radius and Equation (III.1) could be written

$$r^2 = \frac{4}{9} r_s^2 \frac{\rho_s}{\rho_0} R_x K_1 + C.$$

This implies that the inflow velocity of the air,  $W$ , is small compared with the outflow velocity of the particles near the centre of the core. Further out, however, the force due to the inflow velocity dominates the centrifugal effects and smoke particles originating over a wide area are drawn towards the centre. There is an intermediate region where the net inward force is small and a particle will approach the equilibrium position slowly along a spiral path. Figure III.29(a) shows that particle paths make several turns of a spiral before approaching closely to a tubular asymptote, covering an appreciable proportion of the chord in the process.

It is important to note that these particle paths are not streamlines since there is always an appreciable relative velocity between the air and the particles in the cross-flow plane.

The effect of the flow field in concentrating the smoke into a small area allows instantaneous photographs to be taken of the transient behaviour of the vortex core at reasonably high Reynolds Numbers. Figure III.30, for instance, is a milli-second flash photograph illustrating the spiral nature of vortex breakdown at  $R_x = 4 \times 10^4$ .

### III.9.2 The 'Smoke Screen' Technique

The other smoke technique to be developed for investigating the structure of vortex type separations (Ref. III.10) is known as the smoke screen technique because of its superficial similarity to the vapour screen technique (see Part IV) used in supersonic tunnels for the same purpose.

Smoke from a vaporised resin generator or other large volume device is introduced at the front of the wind tunnel working section in line with the model (Fig. III.39) so that a broad, diffused stream of smoke is allowed to flow over the model. One or more light sources with vertical slits are arranged so that planes of light normal to the air stream illuminate cross-sections of the stream of smoke.

If the position of the smoke stream is carefully adjusted in relation to the model, it will be drawn into the coiling vortex sheets and reveal their position and general shape (Fig. III.41).

Figure III.42 illustrates the use of two light sources to show the development of vortex flow over a narrow rectangular plate set at a large angle of incidence and three angles of yaw. The photographs are taken obliquely from behind (Fig. III.39) and the details of the vortex structure can be seen in both light planes.

A simple and effective light source for use in this technique is shown in Figure III.40. A 400W mercury vapour lamp of a type commonly used in street lighting is mounted vertically in a box containing a cylindrical reflector and three cylindrical Perspex (Plexiglass) lenses. An adjustable slit is provided at the front of the box and a small amount of cooling air is directed at the lamp and the adjacent lens.

The lamps are intended to operate in conjunction with a choke which limits the current to about 2 amps and gives a continuous output of 13,600 lumens. It has been found, however, that they will operate satisfactorily for periods of about 5 seconds with a current of 20 amps.\* This gives a large but somewhat variable increase in light output which facilitates photography.

This must be done with caution since failure of the lamp causes the glass envelope to explode with sufficient force to scatter hot glass fragments around the laboratory. Furthermore, in the overrun state, the lamp is said to produce a high intensity of ultra-violet light which can damage the eyes.

A similar arrangement using a linear flash tube can be used when very short exposure times are needed. Figure III.43 is a flash photograph of the flow in a plane behind the trailing edge of a model with a highly swept wing. It will be noted that, although the pair of counter-rotating vortices from the wing tips are clearly visible, there is also a confusing texture in the smoke caused by the disturbances originating at the generator. The other photographs are from exposures of the order of 1/10th second and at this speed the random movements of the smoke are not visible.

In interpreting the patterns it must be remembered that the outer boundaries of the smoke are determined by the size of the smoke stream and its placing relative to the model. The flow structure must be deduced from the distribution of the masses of smoke, their sense of rotation and the situations within them. For example, in Figure III.42, the structure of the coils and the positions of the centres of rotation can be discerned, but the overall sizes of the masses of smoke are not necessarily

---

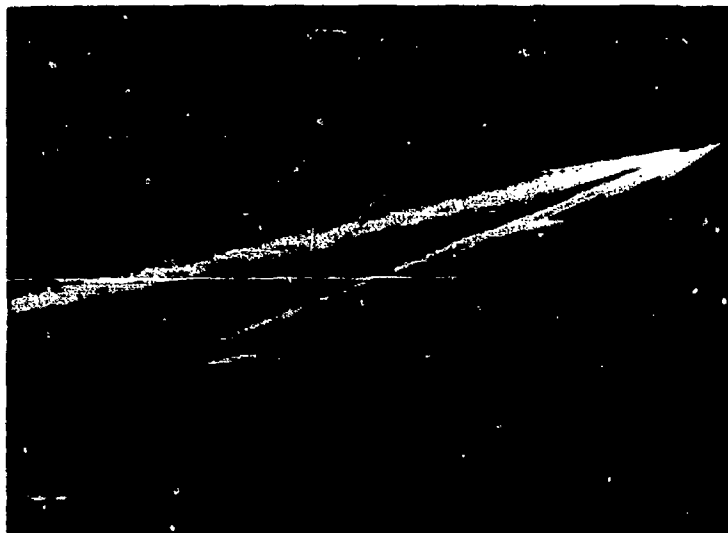
\* If the choke is replaced by a series resistance of about 35 ohms (for a 240V supply) the lamp will operate normally with a consumption of 2 amps. The overload current can be attained by shorting out an appropriate proportion of the resistance.

significant. This difficulty is resolved by observing the patterns during the test or by making cine records. As pointed out in Section III.9.1, the coiled structure of the smoke indicates the surfaces formed by the coiling particle paths rather than the stream surfaces.

Figures III.44 and III.45 give examples of the use of the technique in studying the flow over a slender wing. The development of the vortex system is traced from a plane near the apex of the wing to one several chords downstream.

## LIST OF REFERENCES IN PART III

- III. 1. Hazen, D.C.  
Finley, H.B. *Operating Characteristics of the Princeton University 14 x 2 in. Smoke Tunnel.* Princeton University, Dept. of Aero. Engineering Report No. 225.
- III. 2. Hazen, D.C.  
Lehnert, R.F. *Smoke Flow Studies Conducted at Princeton University.* Princeton University, Dept. of Aero. Engineering Report No. 290.
- III. 3. Hazen, D.C.  
Lehnert, R.F. *Operating Characteristics of the Princeton University 2 x 36 in. Smoke Tunnel.* Princeton University, Dept. of Aero. Engineering Report No. 299.
- III. 4. Pankhurst, R.C.  
Holder, D.W. *Wind Tunnel Technique: An Account of Experimental Methods in Low and High Speed Wind Tunnels.* London, Pitman, 1952.
- III. 5. O'Neill, P.G.G. *A Generator Constructed in Metal for Producing Small Quantities of Paraffin Smoke.* D.S.I.R. N.P.L./Aero/340, 1957.
- III. 6. Bergh, H.  
Bergh, B. van den *On the Visualization of Laminar Boundary Layer Oscillations and the Transition to Turbulent Flow.* Z. Angew. Math. Phys. 9b(1958) 5/6 (March 25th), pp. 97 - 104.
- III. 7. Davidson, I.M.  
et alii *An Improved Method of Flow Visualization by 'Reflected Light'.* Unpublished M.O.A. Report ARC. 12371.
- III. 8. Maltby, R.L.  
et alii *Some Measurements of Leading Edge Vortex Positions on a Delta Wing Oscillating in Heave.* Unpublished M.O.A. Report.
- III. 9. Hall, M.G. *A Theory for the Core of a Leading Edge Vortex.* Unpublished M.O.A. Report ARC. 22860.
- III. 10. Maltby, R.L.  
Peckham, D.H. *Low Speed Flow Studies of the Vortex Patterns Above Inclined Slender Bodies Using a New Smoke Technique.* ARC. 19541, 1956. Unpublished M.O.A. Report.

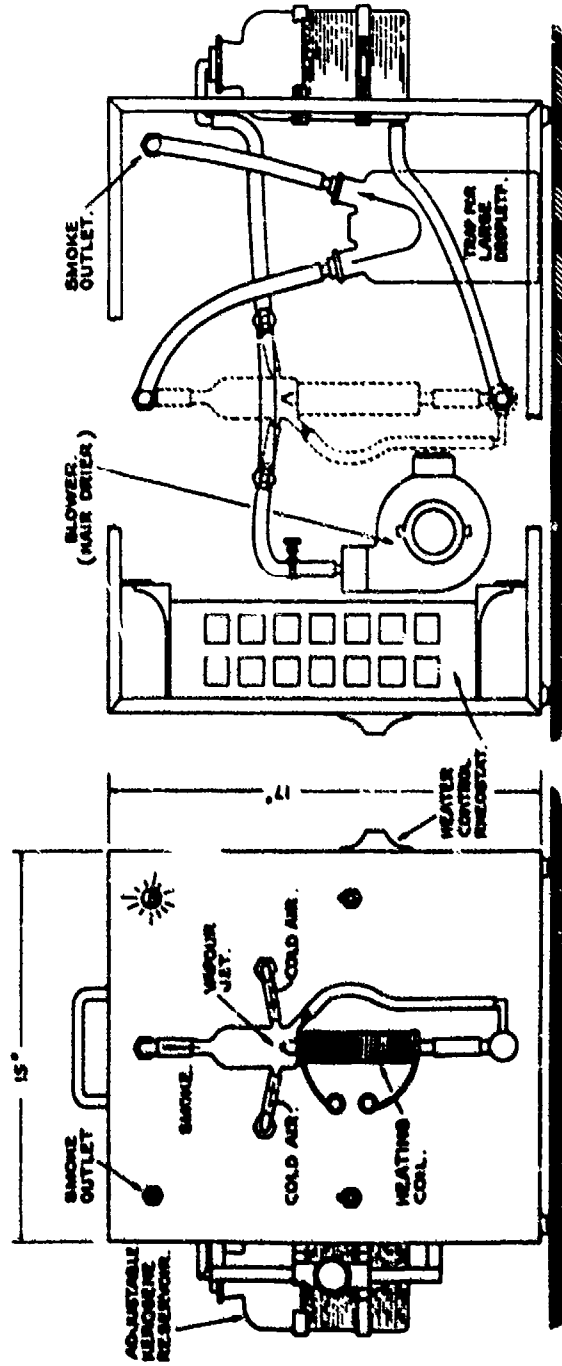


(a) Edge vortex at zero yaw



(b) Vortex breakdown on yawed wing

Fig. III.29 Titanium tetrachloride smoke on slender delta wing (Harvey)



DIAGRAMMATIC EXPLODED REAR VIEW.

FRONT VIEW.

FIG. 111.30 Cambridge University version of Preston and Sreeting smoke generator

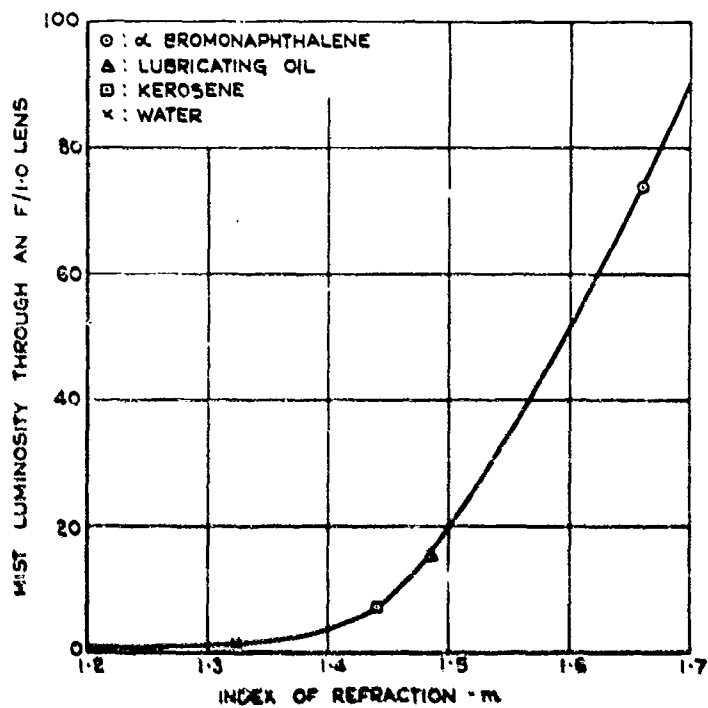
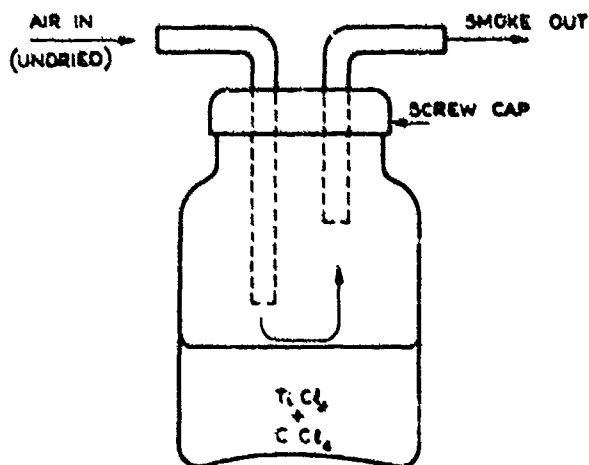


Fig. III.31 Luminosity of mists

Fig. III.32  $TiCl_4$  smoke generator

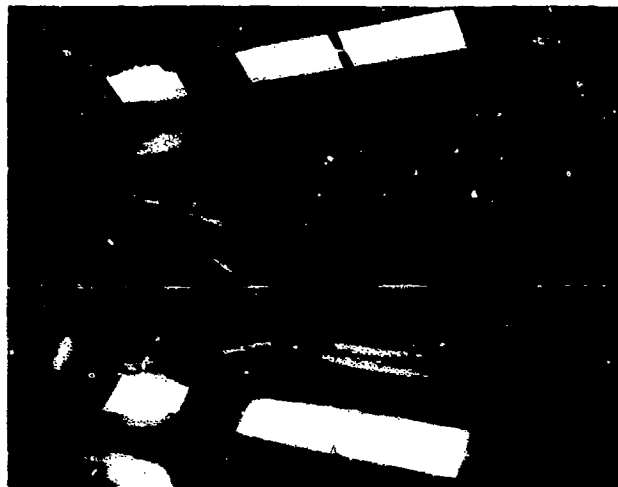


Fig.III.33 Condensation in vortex cores



Fig.III.34 Flow in edge vortex shown by soap bubble traces



Fig. III.15 Erochs resin socku generator

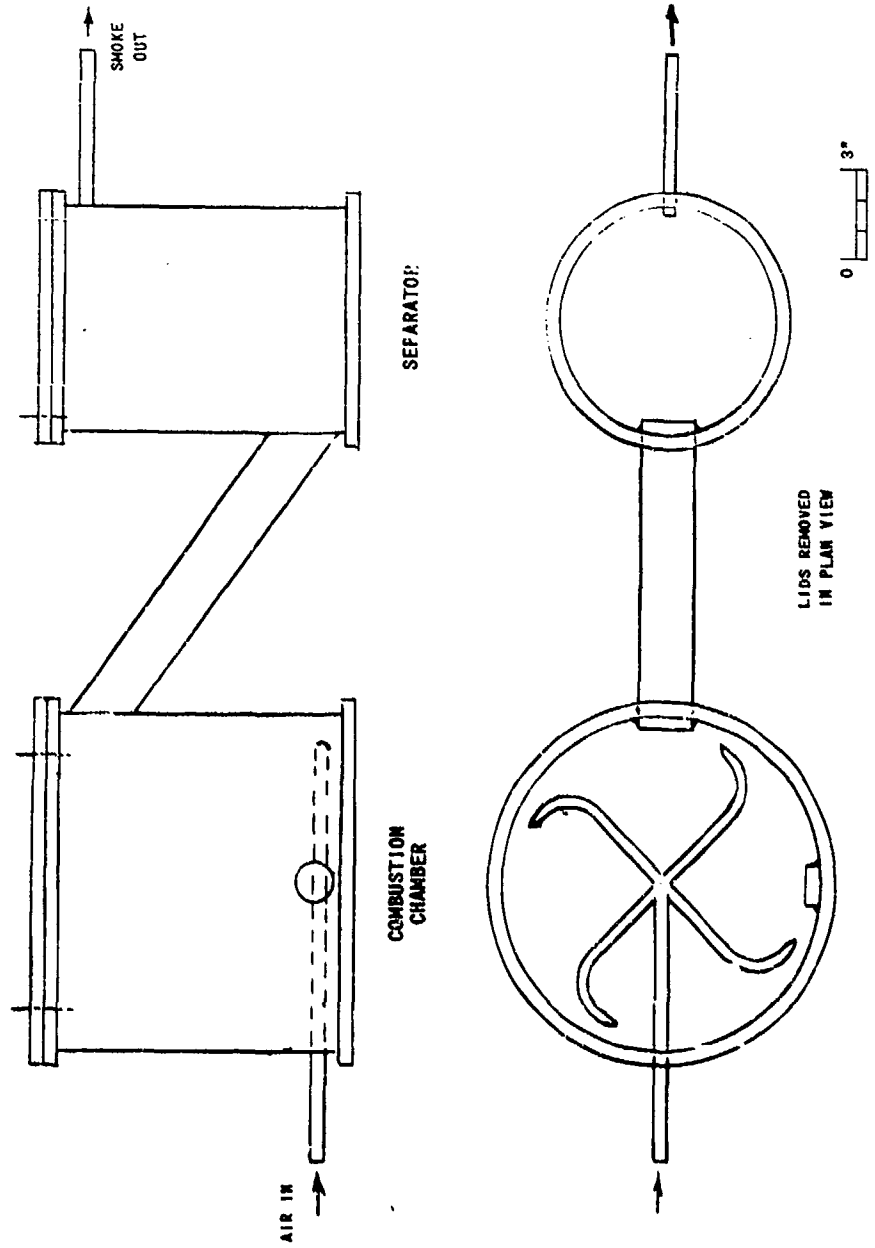


Fig. III.36 Paper smoke generator



Fig. III.37 The smoke tube method



Fig. III.38 Vortex breakdown using the smoke tube method

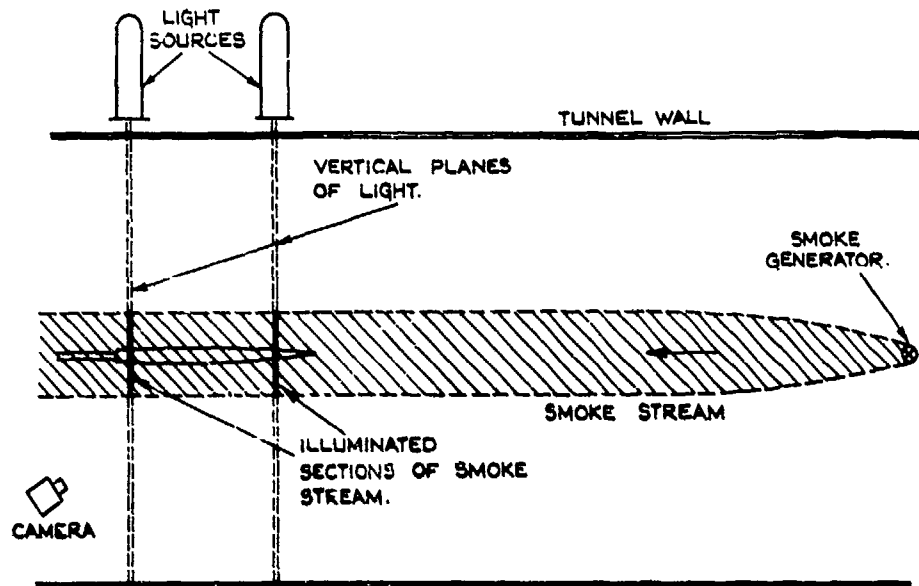
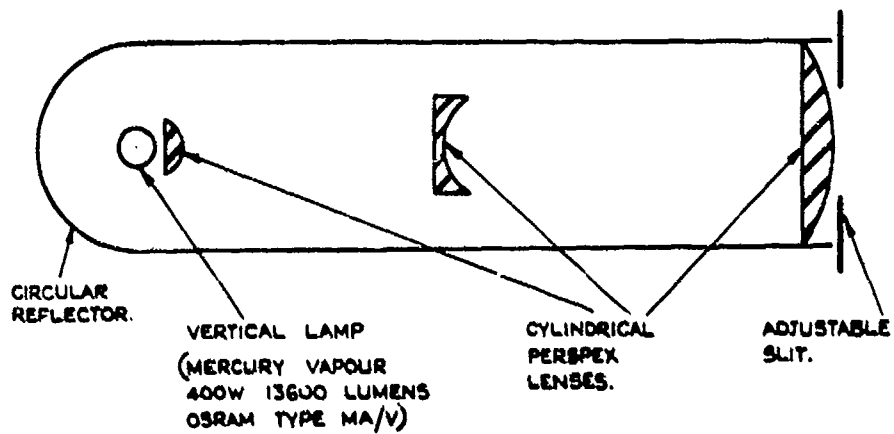


Fig.III.39 Arrangement for smoke screen tests



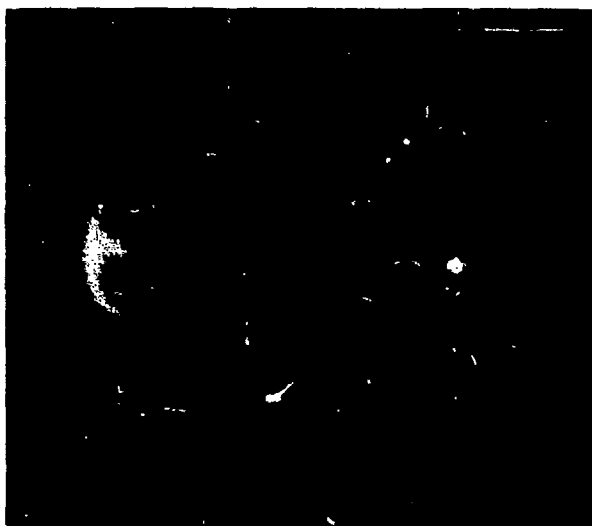
SCALE  
0 3 6 INS.

Fig.III.40 Details of light source



(a) Flow over yawed rectangular plate

$$\Lambda = \frac{1}{12}, \quad \alpha = 20^\circ, \quad \beta = 15^\circ$$



(b) Vortex pattern behind delta wing

Fig. III.41 Smoke screen technique

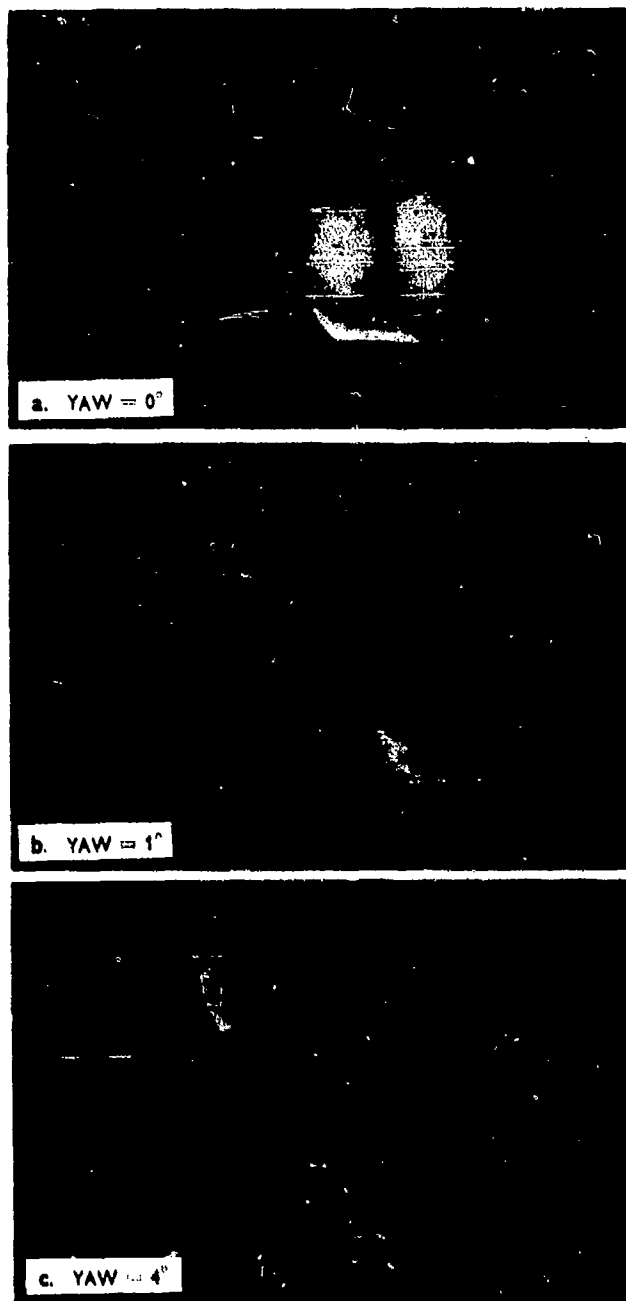


Fig. III.42 Flow pattern on flat plate.  $\alpha = 25^\circ$



Fig.III.43 Sacke screen technique using linear flash tube

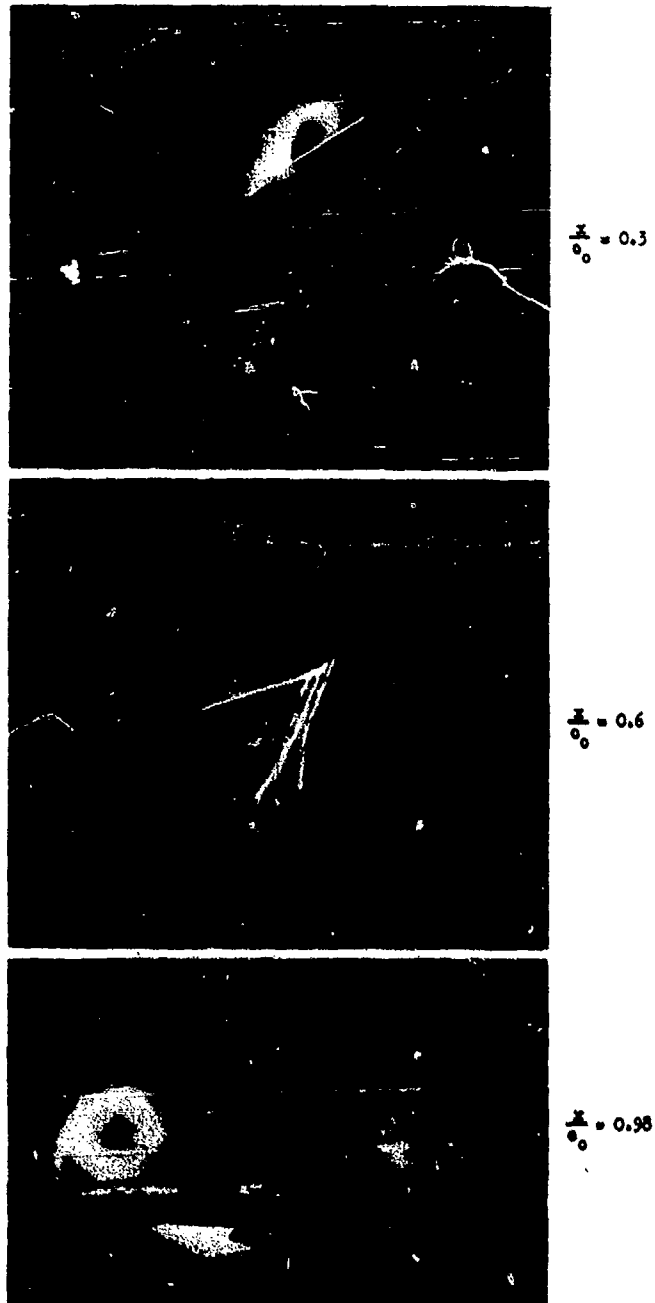


Fig. III.44 Smoke screen technique. Vortex development on delta wing

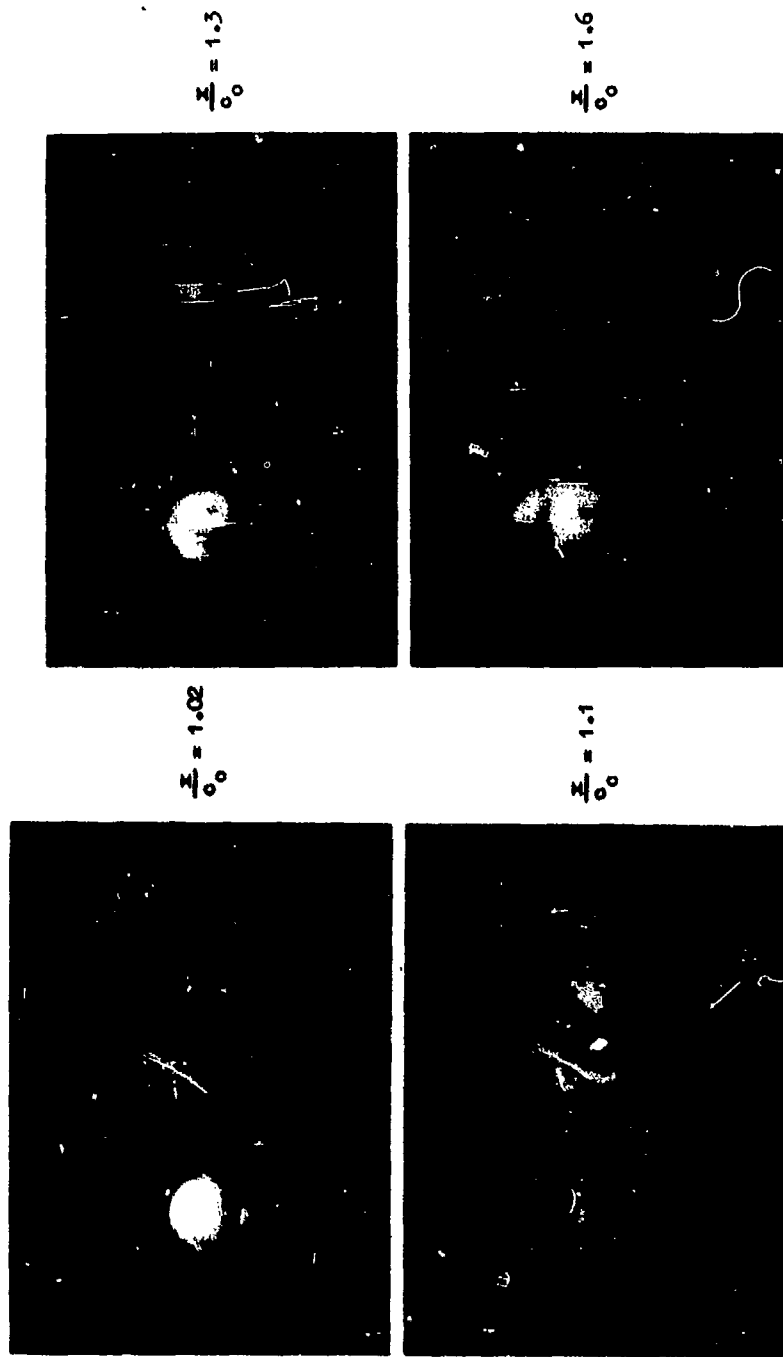


Fig. III.45 Smoke screen technique. Vortex development on delta wing

PART IV

DEVELOPMENT OF THE VAPOUR SCREEN METHOD  
OF FLOW VISUALIZATION IN  
A 3 FT x 3 FT SUPERSONIC TUNNEL

## CONTENTS

	Page
LIST OF FIGURES	113
IV.1 INTRODUCTION	115
IV.2 EXPERIMENTAL EQUIPMENT	115
IV.2.1 The Wind Tunnel	115
IV.2.2 Optical System	116
IV.2.3 Photographic Equipment	116
IV.3 EXPERIMENTAL TECHNIQUE	117
IV.3.1 Humidity Control	117
IV.3.2 Temperature Control - Effect of the Aftercooler	117
IV.3.3 Photographic Details - Determination of the 'Optimum Fog Density'	118
IV.4 EXPERIMENTAL RESULTS AND DISCUSSION	118
IV.4.1 Scope of Tests	118
IV.4.2 Presentation of Humidity Results	119
IV.4.3 Quantity of Water Required to Produce a Satisfactory Vapour Screen	119
IV.4.4 Physical Appearance and Characteristics of the Vapour Screen	121
IV.4.5 The Mechanism of Condensation	124
IV.4.6 Effect of Humidity on Working Section Static Pressure and Mach Number	125
IV.5 SOME TYPICAL VAPOUR SCREEN PHOTOGRAPHS	126
IV.5.1 Flow Behind a Cambered Wing at Two Different Mach Numbers	126
IV.5.2 Flow Over the Upper Surface of a Plane Wing at $M = 1.75$	126
IV.5.3 Comparison of Surface Oil-Flow and Vapour Screen Techniques on Two Wings at $M = 1.51$	128
IV.5.4 An Interesting Phenomenon at $M = 1.32$	129
IV.6 THE FORMATION OF THE VAPOUR SCREEN PICTURE	130
IV.7 THE VAPOUR SCREEN AT SUBSONIC SPEEDS	132
IV.8 USE OF LIQUIDS OTHER THAN WATER FOR VAPOUR SCREEN PRODUCTION	133
IV.9 CONCLUSIONS	135
APPENDIX IV.1	137
APPENDIX IV.2	141
REFERENCES	143
FIGURES	145

## LIST OF FIGURES

	Page
Fig. IV. 46	145
Fig. IV. 47	146
Fig. IV. 48	146
Fig. IV. 49	147
Fig. IV. 50	148
Fig. IV. 51	149
Fig. IV. 52	150
Fig. IV. 53	151
Fig. IV. 54	152
Fig. IV. 55	153
Fig. IV. 56	154
Fig. IV. 57	155
Fig. IV. 58	156
Fig. IV. 59	157
Fig. IV. 60	158

	Page
Fig. IV.61 Vapour screen photographs taken at $M = 1.32$ showing the 'blue line' phenomenon	159
Fig. IV.52 Vapour screen photographs of the flow behind a delta wing at $M = 0.85$ , $\alpha = 4^\circ$	160
Fig. IV.63 Vapour screen photographs of the flow behind a delta wing at $M = 0.85$ , $\alpha = 8^\circ$	161
Fig. IV.64 Saturated vapour density of some organic liquids suitable for vapour screen experiments	162
Fig. IV.65 Vapour screen photographs of the flow just behind a delta wing, using carbon tetrachloride vapour. $M = 1.96$	163
Fig. IV.66 Vapour screen photographs of the flow just behind a delta wing, using water vapour. $M = 1.88$ ( $M_{\text{dry}} = 2.00$ )	164

PART IV. DEVELOPMENT OF THE VAPOUR SCREEN METHOD  
OF FLOW VISUALIZATION IN  
A 3 FT x 3 FT SUPERSONIC TUNNEL

I. McGregor

IV.1 INTRODUCTION

Use has occasionally been made of the so-called 'vapour screen' method of flow visualization in supersonic wind tunnels (Refs. IV.1 to IV.5 for example). The principle of the method is very simple. The tunnel is run with moist air, and as the air expands through the supersonic nozzle into the working section it cools, and the moisture condenses out to form a fog. This is then illuminated by a narrow beam of light perpendicular to the axis of the tunnel. Any disturbance in the cross-flow plane, such as that caused by a model at incidence, disturbs the uniform distribution of fog particles in the plane of the vapour screen, and hence the amount of light scattered by the fog. In particular, wakes and vortices from wings and bodies appear as dark 'holes' in the screen. However, very little information has hitherto been available concerning such aspects of technique as the humidity required to produce a satisfactory screen at different Mach numbers and how this is influenced by such factors as tunnel pressure and temperature, or of the effects of the condensing vapour on the flow in the working section.

This paper describes an investigation made in the 3 ft x 3 ft supersonic tunnel at the Royal Aircraft Establishment, Bedford, to examine the suitability of the method for providing information concerning the structure of separated flow areas near wind tunnel models. The investigation included the development of a technique which provided an improved resolution of detail over a range of Mach numbers.

IV.2 EXPERIMENTAL EQUIPMENT

IV.2.1 The Wind Tunnel

The 3 ft x 3 ft tunnel is described in Reference IV.6, but a brief description is given here since certain aspects of its design are important in connection with the vapour screen technique. The tunnel is continuous running, with a working section 3 ft square, and supersonic Mach numbers between 1.3 and 2.0 are generated by a series of interchangeable blocks that form a single-sided nozzle upstream of the working section. The tunnel is driven by two centrifugal compressors in series. The total pressure can be varied between 3 in. and 60 in. of Hg by means of a compressor-evacuator set. Cooling arrangements consist of (a) an intercooler between the two compressor stages, and (b) an aftercooler, with a rather greater capacity than the intercooler, situated in the maximum section of the tunnel immediately before the contraction. The flow of water through the intercooler is continuously variable, but only coarse control of the aftercooler is possible. Drying of the air in the tunnel is effected by by-passing a fraction of the air through driers charged with silica-gel which are connected across the second stage of the compressor. The quantity of air passing through the driers is controlled by a motorized flap valve, and with the driers in reasonably good condition a humidity corresponding to a frost-point of about  $-40^{\circ}\text{C}$

is obtained after 10 to 15 minutes running. The total volume of the tunnel is approximately 45,000 ft<sup>3</sup>, and this humidity represents about 0.3 lb of water vapour remaining in the tunnel circuit.

#### IV.2.2 Optical System

It was considered that to produce a good vapour screen picture the illumination system should provide a beam of light that was (a) as intense as possible, (b) narrow, with little variation in width across the working section, and (c) sharp-edged, with a minimum of stray light entering the tunnel.

The light source selected was a 1000 watt high pressure mercury vapour lamp with an effective length of 7.5 in. and an external diameter of approximately 0.5 in. The problem was to produce a beam of light that would satisfy the above requirements. The simplest arrangement - a slit with the lamp behind it - was rejected on the grounds that to produce a suitable beam would have entailed placing the lamp at least 2 ft behind the slit, and this would cause an excessive loss of illumination. A system using cylindrical lenses was next examined, but it was considered that the intensity of illumination would not be materially better than that given by a simple slit when the beam was satisfactory in other respects.

The arrangement finally adopted made use of one of the mirrors from the tunnel Schlieren system, and proved to be very effective. It is shown in Figure IV.46. The 32 in. diameter concave mirror with a focal length of 4 metres was used to produce an image of the light source in the centre of the working section. To reduce the width and lateral spread of the beam, a slit 0.1 in. wide was placed just in front of the lamp and the sides of the mirror masked, leaving an effective area of mirror 32 in. x 10 in. This arrangement produced a sharp-edged beam of light approximately 0.15 in. wide by 9 in. high in the centre of the working section. Both the height and width of the beam increased slightly away from the centre line, but even at the windows the width of the beam was only about 0.5 in. No measurement of the beam intensity in absolute terms was attempted, but a simple comparative test with a photographic exposure meter indicated that at the centre of the tunnel the intensity of illumination was comparable with that of direct sunlight.

It was not feasible to move the mirror backwards and forwards to track the beam of light along the working section; this was accomplished by rotating the mirror about its vertical axis. As a result, the beam was perpendicular to the centre line of the tunnel in only one position, but the maximum deviation of the beam from the perpendicular did not exceed 2°.

#### IV.2.3 Photographic Equipment

The easiest way to photograph the vapour screen is obviously from the side of the tunnel. However, whilst this is adequate for some purposes, the screen is inevitably viewed at an appreciable angle, and it is difficult to locate the position of any vortices that may be present relative to the model. It is also unsuitable if the flow over the surface of a wing is being studied. For these reasons it was decided to photograph the screen from directly downstream (Refs. IV.4 and IV.5). A remotely controlled camera was used, mounted at the root of the model sting support. The camera, which was driven by clockwork, gave negatives approximately

1 in. square on standard 35 mm film. The shutter was operated by a solenoid mounted alongside the camera, but it was not possible to alter the focus from outside the tunnel.

The wing of a model remote from the light source is in a shadow cast by the sting or body, so that in general it is necessary for the field of view of the camera to contain only the body and the wing panel nearer the light source. The camera was therefore fitted with a telephoto lens of 7.5 cm focal length, which gave a field of view approximately 10 in. square at a position corresponding to the trailing edge of a typical 3 ft tunnel model, and the camera was mounted at a small angle to the centre line of the sting to enable the wing tip of the largest model to be included in the picture.

The camera and its operating solenoid were housed in a cowl constructed from brass sheet, with a plate glass window 0.25 in. thick to protect the lens. However, this cowling caused considerable blockage and it proved impossible to start the tunnel at  $M = 1.3$ , but no trouble was experienced at higher Mach numbers.

### IV.3 EXPERIMENTAL TECHNIQUE

#### IV.3.1 Humidity Control

In Reference IV.3, condensation in the working section was brought about by running the tunnel with atmospheric air without any drying. The quantity of water contained in such air can vary very considerably from day to day, and it is necessary to be able to exercise careful control of the humidity if optimum results are to be obtained. The procedure evolved for the present tests consisted of running the tunnel at the desired total pressure with the driers in circuit for a period of about 15 minutes. The driers were then switched out, and a measured quantity of water injected into the tunnel. In all the work so far undertaken the tunnel has been run at a total pressure below atmospheric, and the water was simply sucked in through pressure tappings in the tunnel wall. In early experiments, water was admitted to the maximum section of the tunnel just before the contraction, but this proved unsatisfactory, as, in air having a low velocity there, water tended to collect on the floor of the tunnel and evaporate only slowly. For all subsequent tests water was admitted into the diffuser, where vaporisation was almost instantaneous.

#### IV.3.2 Temperature Control - Effect of the Aftercooler

For the first few tests the tunnel was run in the normal manner with both the intercooler and aftercooler in operation. However, it was found that the fog produced in the working section was extremely patchy and irregular, some parts being practically devoid of any condensation, while in others there were streamers of thick fog. This suggested that the temperature distribution across the working section was uneven, so a total temperature probe was constructed to measure the distribution. The probe, which is shown in Figure IV.47, consisted of a tube mounted across the centre of the working section with a number of thermocouples arranged along its leading edge. The result of a typical survey is given in Figure IV.48, which shows a temperature difference of some  $20^{\circ}\text{C}$  between the 'hotspot' near the centre of the tunnel and the colder air at the sides. Overhaul of the aftercooler effected some improvement in

the temperature distribution, but only a slight improvement in the distribution of fog resulted, and it was considered to be still far too uneven to be acceptable.

The effect of switching off the aftercooler was then examined. This meant that, apart from heat losses from the tunnel shell, the intercooler alone was responsible for cooling, which limited the power input if overheating was to be avoided. As a result the tunnel could only be run at 30 to 50% of the maximum total pressure. The overheating problem was most serious at the top end of the Mach number range, when the mass flow of air around the tunnel circuit was low, but the pressure ratio across the compressors high. However, it was found that this arrangement gave a perfectly uniform fog in the working section, although it was first necessary to wait until the tunnel total temperature attained a reasonably steady value. For the first run of the day this warming-up period was of the order of an hour, but for subsequent runs 10 to 15 minutes sufficed. The only disadvantage was that, as the intercooler was always operating at or very near maximum capacity, it was not possible to investigate the effect of total temperature on fog formation.

#### IV.3.3 Photographic Details - Determination of the 'Optimum Fog Density'

From the photographic point of view, the optimum fog density is a compromise between two conflicting requirements. If the fog is too thin, a long exposure time is needed and there is a risk of light reflection from the model and the walls of the tunnel obscuring the low-contrast vapour screen picture. On the other hand, if the fog is too thick, there is excessive scattering of light by the fog between the plane of the vapour screen and the camera lens which results in a very 'grainy' picture with blurred detail.

A series of tests was therefore carried out with fogs of different densities, photographing the vapour screen picture produced by a model at incidence over a range of exposure times from 5 to 80 secs. The camera was set an aperture of  $f/4$  and FP 3 film used. Best results were obtained with what appeared to be a quite thin fog as viewed from the side of the tunnel. The corresponding exposure time was 20 secs.

Light reflection from the model was reduced by painting it with camera black and stray light entering the working section was kept to a minimum by masking the side windows, leaving only a slit wide enough for the main light beam to enter.

The combination of long focal length lens (7.5 cm) and wide aperture setting ( $f/4$ ) resulted in a depth of focus of only 10.8 in. at the range normally used (3 to 4 ft). However, it proved possible to take photographs with no detectable loss of clarity 3 in. from the nominal focal point, so the screen could be photographed at axial positions up to 4 in. apart without the need for refocusing.

### IV.4 EXPERIMENTAL RESULTS AND DISCUSSION

#### IV.4.1 Scope of Tests

Tests were made to determine the quantity of water required to produce a photographically suitable vapour screen at Mach numbers between 1.3 and 2.0. The effects of humidity on the flow in the working section were also investigated and measurements made of the static pressure and Mach number.

#### IV.4.2 Presentation of Humidity Results

The accepted practice is to present experimental results for tunnel humidity in a non-dimensional form, but in this case care is necessary if the results are not to be misleading. For example, although stagnation pressure was found to have some effect, the degree of condensation, and therefore of fog density, depends essentially on the amount of water present in the tunnel and not on the water/air ratio. It is therefore not relevant to express the humidity in terms of lb of water/lb of air ('absolute humidity'), as is normally done when condensation effects in wind tunnels are being discussed and the amount of heat given up to the air by the vapour as it condenses is of prime importance. The stagnation relative humidity (the ratio of the actual vapour density to the density of saturated vapour at the same temperature) is independent of stagnation pressure, but is a function of stagnation temperature, so this is also unsuitable. A parameter which avoids these defects is the frost-point, which defines a unique relation between the quantity of water vapour and the volume of the tunnel which is independent of stagnation conditions. A curve showing the frost-point as a function of the quantity of water added to the nominally 'dry' tunnel is presented in Figure IV.49. This was derived from data given on p.2304 of Reference IV.7, a mean frost-point for the 'dry' tunnel of  $-41^{\circ}\text{C}$  having been assumed. A few experimental measurements are included and these show quite good agreement with the theoretical curve. However, the quantity of water-frost-point relationship is logarithmic in character and whilst very sensitive at low humidities, in the range of interest of these tests the sensitivity is only of the order of  $2^{\circ}\text{C}$  change in frost-point per pint of water added. In view of this fact, and of the difficulty of making reliable frost-point measurements, it was decided that the most straightforward way to describe the humidity was directly in terms of quantity of water added to the 'dry' tunnel, but scales showing the frost-point or absolute humidity (when the effects of condensation on static pressure and Mach number are being considered) have been added to the figures where appropriate.

#### IV.4.3 Quantity of Water Required to Produce a Satisfactory Vapour Screen

As described in Section IV.3.3, the optimum fog density was found by injecting measured quantities of water into the tunnel and photographing the resulting vapour screen. Examination of the photographs then gave an optimum range of humidity. This detailed determination was only carried out at two Mach numbers, 1.51 and 1.81, and for other Mach numbers the range of humidity over which a satisfactory screen was produced was estimated visually. The results of these tests are presented in Figure IV.50. The results for the various Mach numbers were not obtained at exactly the same total pressure and temperature, but are substantially correct for a value of  $p_t = 12$  in. Hg and  $T_t = 45^{\circ}\text{C}$ . (The effects of pressure and temperature are discussed below.) It must be mentioned here that the Mach number quoted is that developed by the nozzle with dry air: above about  $M = 1.0$  there is a marked humidity effect on the flow and the actual Mach number when a vapour screen is present is considerably less than with dry air.

Several points of interest arise from this curve. The limits of the humidity range for a satisfactory vapour screen are a subjective matter not capable of precise determination, but even allowing for this, the range of humidity over which a satisfactory screen is produced is quite small; the humidity at which the fog density tends to be too thick is only some 25 to 30% greater than that where it tends to be too thin. Secondly, there is the very rapid increase in humidity required at Mach

numbers less than 1.5. The quantity of water vapour required to saturate a given volume increases very rapidly with temperature at low temperatures (Fig. IV.51), and the higher working section static temperature at the lower Mach numbers is sufficient to cause a large increase in the humidity necessary for saturated flow in the working section. It is well known that a considerable degree of supersaturation is necessary to cause condensation in a supersonic nozzle, so a curve has been added to Figure IV.50 which shows the quantity of water required to produce a fifteen-fold supersaturation in the working section at a total temperature of 45°C, the assumption being made that the working section static temperature is the same as with dry air. It is seen that this curve is very similar in shape to that denoting the quantity of water required to produce a satisfactory vapour screen. The third feature is that the humidity required reaches a minimum value at a Mach number of about 1.6 and thereafter shows a slight increase. Above  $M = 1.6$  it seems likely that virtually all the water added to the tunnel is condensed out, so that if the fog is to be of constant density then the stagnation humidity must increase to allow for the greater expansion of the flow with increasing Mach number, i.e. the quantity of water it is necessary to add will vary inversely with the density\* in the working section.

There are no theoretical reasons for supposing that the quantity of water required to produce a satisfactory vapour screen can be simply expressed in terms of known properties of the flow, but as a reasonable approximation over the experimental range it is given by

$$\left(\frac{\rho}{\rho_t}\right) \frac{W}{V} = 18 w_{\text{sat}} + 0.00003$$

where  $W$  = quantity of water required to produce a satisfactory vapour screen (lb)  
 $V$  = total volume of the tunnel (45,000 ft<sup>3</sup>)  
 $\rho_t$  = stagnation density of the air

---

\* It follows from continuity considerations that, as long as the water vapour remains uncondensed, the absolute humidity  $\phi$  is constant at all points around the tunnel circuit, so that the local density of the water vapour is proportional to the local density of the air. The flow in the tunnel may be regarded as the flow of a mixture of two gases which will have a mean value of the ratio of specific heats  $\gamma_{\text{mix}} = (1.40 + 1.33 \phi) / (1 + \phi)$ . Since  $\phi$  is always small,  $\gamma_{\text{mix}} \approx 1.40$  very nearly, and so the mixture will behave in the same manner as dry air.

If the water vapour has wholly or partially condensed, the average local density of the water/water vapour mixture will still be approximately proportional to the local density of the air in which it is contained, except in regions of large flow acceleration such as occur near a stagnation point, on passing through a shock wave, or in the central part of a vortex, the greater inertia of the water droplets preventing them from following the motion of the air. When condensation has taken place, the density of the air will not in general be the same as in condensation-free flow. However, for the purpose of estimating fog density in the working section it is probably adequate to assume a value appropriate to dry air.

$\rho$  = density of air in the working section (assuming isentropic flow)  
 $w_{sat}$  = density of saturated water vapour at working section static temperature under isentropic conditions (lb/ft<sup>3</sup>).

The variation of  $w_{sat}$  with temperature was derived from data given on pages 2304 and 2145 of Reference IV.7, and is shown in Figure IV.51. The volume of the working section is small compared with that of the settling chamber so that  $\left(\frac{\rho}{\rho_t}\right)^{\frac{w}{v}}$  is approximately equal to the density of the mixture of fog and uncondensed water vapour in the working section. The factor 18 may be considered as the degree of supersaturation necessary to cause condensation and 0.00003 lb/ft<sup>3</sup> as the mean density of the condensed fog particles in the working section, but this interpretation should not be taken too literally.

It was mentioned earlier that it was not possible to investigate the effects of total temperature on vapour screen formation, but some idea of its effect on the quantity of water required may be gained from the above equation. The critical parameter is working section static temperature,  $T_s$ . When this is less than about -60°C, the term  $18 w_{sat}$  is negligible in comparison with 0.00003, so that provided  $T_s$  continues to be less than about -60°C, changing  $T_t$  will have little effect. However, if a change in  $T_t$  causes  $T_s$  to rise appreciably above -60°C, the magnitude of the term  $18 w_{sat}$  increases very rapidly and so the humidity will have to be increased to maintain a satisfactory vapour screen.

The effects of tunnel total pressure on fog formation were investigated at a nominal Mach number of 1.41.  $p_t$  was varied between 18 and 4.5 in. Hg, and  $T_t$  held at 44°C ( $\pm 0.5^\circ\text{C}$ ). The results are presented in Figure IV.52 and show that as the total pressure was reduced, an increasing quantity of water had to be added to the tunnel to produce a satisfactory vapour screen. A possible explanation for this is as follows. When the water vapour condenses to form droplets of liquid water, the latent heat of evaporation is liberated and absorbed by the surrounding air, causing a rise in temperature. If the total pressure is reduced, the amount of heat absorbed by the air per unit mass of water vapour condensed is unchanged, but since there is a smaller mass of air the rise in temperature is greater. This rise in working section static temperature increases the saturated vapour density in the working section, so a greater initial humidity is necessary to produce the same amount of condensation.

At Mach numbers above about 1.6 it is expected that the effect of total pressure will not be so marked as at  $M = 1.41$ , since then a much greater proportion of the water vapour present is condensed out in the working section.

#### IV.4.4 Physical Appearance and Characteristics of the Vapour Screen

On the addition of a small quantity of water to the 'dry' tunnel no visible condensation could be detected, even if, as occurred at nominal Mach numbers of 1.81 and 2.00, a rise in working section static pressure indicated that a condensation shock was present. On further increasing the humidity a point was reached where the outline of the beam of light could just be discerned in the working section, giving rise to a very faint, deep blue vapour screen. The approximate humidity at which this blue haze could first be detected was noted and is plotted as a function of Mach number in

Figure IV.50 and of total pressure in Figure IV.52. In both cases it is seen to vary in a similar manner to the quantity of water required to produce a satisfactory vapour screen.

Further development of the vapour screen with humidity depended on Mach number. At Mach numbers up to and including 1.51 the screen at first became slightly denser, but it then gradually acquired an iridescent character in which wide vertical bands of violet, blue, green and yellowish-green light could be clearly seen when viewed from a suitable position. At the higher Mach numbers, the blue haze just became denser and slightly paler in colour.

The optical properties of fogs are rather complex and it is not proposed to enter into a detailed study here, but some consideration of the observed phenomena can yield interesting information concerning certain physical characteristics of the fog. Suppose a beam of light is projected through air containing a very large number of very small particles in suspension (of radius less than  $10^{-5}$  in., say), whose size is small relative even to the wavelength of visible light (wavelength  $1.6 \times 10^{-5}$  to  $2.7 \times 10^{-5}$  in.). In such circumstances a scattering of the light will take place (Tyndall effect), the scattering being much more pronounced for light of the shorter wavelengths (blue and violet) than for the long (Ref. IV.8). It is believed that such light scattering is responsible for the bluish colour of the vapour screen when the humidity was such that condensation could first be detected by eye. On increasing the humidity the fog particles increase in size. True scattering will also increase (in proportion to the increase in surface area of the particles) and will tend to occur more equally for light of all wavelengths, but effects due to diffraction of the light may also become important if the particles exceed a certain critical size. With a spherical particle the intensity of the diffracted light passes through a series of maxima and minima in directions making an angle  $\theta$  with the original direction of the beam given by

$$\sin \theta = k \cdot \frac{\lambda}{r} \quad (\text{Ref. IV.9})$$

where  $\lambda$  = wavelength of the light

$r$  = radius of the spherical particle

$k$  = a constant.

The first maximum occurs when  $k = 0$  (undeflected light), and the first minimum when  $k = 0.61$ . Further maxima occur when  $k = 0.810$  and  $1.333$ , and minima when  $k = 1.116$  and  $1.619$ . The intensity with  $k = 0.810$  is only 1.7% of the incident light and the subsequent intensity maxima are smaller still. However, it follows that for each wavelength there are certain directions relative to the direction of the incident light along which light of that particular wavelength has a maximum or minimum intensity, so the diffracted light is split up into a spectrum. In the case of the vapour screen there is a very large number of illuminated water droplets, each diffracting some of the light striking them, so that viewed at an angle from the side of the tunnel, bands of coloured light might be expected to appear across the screen in spectral order, with red nearest the observer (long wavelength and correspondingly large value of  $\theta$  for maximum intensity). This is in agreement with observation at Mach numbers between 1.3 and 1.5, with the exception that no red or orange bands were detected. A possible explanation for the absence of these colours is discussed later.

The existence of these coloured bands implies that all (or the greater part) of the water droplets forming the fog must be of nearly uniform size. If there is a variation in size, each droplet will diffract the light differently. With a large number of droplets whose size varies in a random manner, the resultant diffracted light would presumably appear white, since if a particular direction were the direction for maximum intensity for a certain wavelength from one droplet, there would be other droplets for which this direction was the direction of maximum intensity for other wavelengths, giving, in effect, a continuous spectrum.

It is possible to obtain an estimate of the size of the droplets in the fog by observation of the coloured bands in the vapour screen. A test was made at a Mach number of 1.41, with a total pressure of 12 in. Hg and a total temperature of 46°C. With 11 pints (6¼ litres) of water added to the 'dry' tunnel (the quantity necessary to produce a satisfactory vapour screen under these conditions), it was found that the first and second intensity maxima for blue light occurred at angles of 30° and 55° respectively to the direction of the original light beam. The wavelength of blue light is approximately  $1.8 \times 10^{-5}$  in., so from the first maximum we have:

$$r_1 = \frac{0.810 \times 1.8 \times 10^{-5}}{\sin 30^\circ} = 2.9 \times 10^{-5} \text{ in.}$$

and from the second: 
$$r_2 = \frac{1.333 \times 1.8 \times 10^{-5}}{\sin 55^\circ} = 2.9 \times 10^{-5} \text{ in.}$$

Such perfect agreement between the two results must be considered fortuitous, since it was not possible to measure the angles to better than about 2°, but it may be concluded fairly confidently that in this case the radius of the droplets is about  $3 \times 10^{-5}$  in. This is of the same order as the size of the droplets in an artificial fog (produced by the sudden expansion of some wet air in a flask) as measured by Stodola (Ref. IV. 10), using a light diffraction method.

It was mentioned above that no red or orange bands were observed in the vapour screen. Assuming a droplet radius of  $2.9 \times 10^{-5}$  in., the first maximum for red light should occur at an angle

$$\theta = \sin^{-1} \frac{0.810 \times 2.7 \times 10^{-5}}{2.9 \times 10^{-5}} = 49^\circ.$$

The second maximum for violet light will occur at an angle

$$\theta = \sin^{-1} \frac{1.333 \times 1.6 \times 10^{-5}}{2.9 \times 10^{-5}} = 47^\circ.$$

There is thus some overlapping of the first maximum for light of long wavelength with the second maximum for light of short wavelength. Now the spectrum of the mercury vapour lamp is rich in blue and violet light but rather deficient in red and orange, so that although the second maximum for violet is less intense than the first, it is probably still stronger than the first maximum for red or orange. This offers a plausible reason why the red and orange bands could not be detected.

With regard to the change in character of the screen between Mach numbers of 1.5 and 1.6, it seems probable that this is due to a change in the mechanism of condensation, which results in a greater number of smaller particles being formed at the higher Mach number so that dispersion of light by the fog remains a true scattering effect without diffraction. In addition to this change in size, a change in the nature of the fog particles from water droplets to ice crystals is also likely, although the two effects are not related. It is known (Ref. IV.11) that small droplets of pure water can be supercooled to approximately  $-40^{\circ}\text{C}$  before freezing takes place when cooled slowly. With droplets formed during the rapid expansion of saturated water vapour, an even greater degree of supercooling appears necessary, and Sander and Danköhler (Ref. IV.12) have shown that under such conditions a temperature of approximately  $-62^{\circ}\text{C}$  is required before ice crystals form. It may be that at these low temperatures the vapour condenses directly into ice crystals without passing through the liquid phase, but this point is uncertain. However, a temperature of  $-62^{\circ}\text{C}$  corresponds to the working section static temperature at a Mach number of 1.59 under isentropic conditions and with a total temperature of  $45^{\circ}\text{C}$ , so that at the higher Mach numbers the observed fog almost certainly consisted of ice crystals.

#### IV.4.5 The Mechanism of Condensation

A saturated or supersaturated vapour will condense only if there are 'condensation nuclei' present. These nuclei can be of two forms - minute particles of dust or other foreign matter, and nuclei which are generated spontaneously in the vapour by random molecular aggregation. Nuclei of the former type are invariably present to a greater or lesser degree, but whilst groups of molecules are continually forming in any gas or vapour, they are unstable and immediately break up again and so cannot form condensation nuclei unless the vapour is heavily supersaturated. When condensation occurs on foreign nuclei, the number of droplets formed per unit volume is limited by the number of nuclei present, and the rate at which the vapour condenses is determined by the rate at which the droplets can grow, which in turn depends on the degree of supersaturation, the rate of diffusion of vapour molecules onto the surface of the droplets and the rate of transfer of the latent heat of evaporation away from the droplets. On the other hand, with self-generated nuclei, the number of nuclei per unit volume can reach astronomical figures when the vapour is sufficiently supersaturated and condensation can take place extremely rapidly (condensation 'shock'), leading to a very large number of minute droplets. These two condensation processes and their relative importance in wind tunnels were first discussed in detail by Oawatitsch (Ref. IV.13), who concluded that in supersonic tunnels the effects of foreign nuclei could be neglected. In the present case, however, it is believed that at Mach numbers up to and including 1.51, condensation is occurring principally on foreign nuclei and that only at higher speeds do self-generated nuclei become predominant. The reasons leading to the adoption of this conclusion are discussed at some length in Appendix IV.1. It must be emphasised that this conclusion is only valid for the 3 ft tunnel for the particular conditions under which it was operated, and does not necessarily apply in general. It is shown, for instance, that a reduction in total temperature considerably decreases the importance of foreign condensation nuclei. The question of tunnel size is also considered briefly and it is concluded that in a smaller tunnel a greater stagnation humidity will be necessary to produce the same density of fog in the working section at the same total pressure and Mach number.

#### IV.4.6 Effect of Humidity on Working Section Static Pressure and Mach Number

Measurements were made of the variation of working section static pressure with quantity of water added to the tunnel at several Mach numbers, and the results, expressed as the ratio of the actual static pressure to the pressure with dry air,  $p/p_{dry}$ , are presented for nominal Mach numbers of 1.51, 1.81 and 2.00 in Figures IV.53 and IV.54. The actual Mach number in the working section was measured at nominal Mach numbers of 1.51 and 2.00 by sticking strips of cellulose tape approximately 0.003 in. thick on the top and bottom walls of the tunnel just ahead of the windows. These generated very weak shock waves (effectively Mach waves), which were photographed using the tunnel Schlieren system. The included angle between the two waves (equal to twice the Mach angle) was measured from photographic enlargements and the actual Mach number obtained. The variation of actual Mach number with humidity is shown in Figure IV.54. Some Schlieren pictures obtained at a nominal Mach number of 2.00 are shown in Figure IV.55.

At Mach numbers less than 1.51 it is possible to obtain sufficient condensation to produce a satisfactory vapour screen without affecting either the working section static pressure or Mach number. In this Mach number range it is believed that condensation is occurring progressively on foreign condensation nuclei without a condensation shock. At the higher Mach numbers a condensation shock is clearly present, and at a certain humidity the static pressure suddenly starts to increase and the working section Mach number to decrease. The humidity at which the static pressure diverges by 1% from the 'dry' value is a convenient indication of the onset of the condensation shock, and this humidity is shown as a function of Mach number in Figure IV.50 for a stagnation pressure of 12 in. Hg.

It will be noted from Figure IV.50 that at  $M = 1.81$  and  $2.00$  a condensation shock occurs at a lower humidity than that at which fog is first visible in the working section, whilst at Mach numbers less than 1.6 there may be visible condensation without a condensation shock. Thus, as has been previously pointed out by Oswatitch (Ref. IV.13), the appearance or disappearance of fog in the working section is not a reliable guide to the presence or absence of condensation effects.

Once a condensation shock is established, the working section static pressure does not necessarily increase steadily with increasing humidity. At both  $M = 1.81$  and  $2.00$  (Figures IV.53 and IV.54) there is a range of humidity soon after the condensation shock forms over which the static pressure is constant, and at  $M = 1.51$  and  $1.81$  at the maximum humidity investigated the rate of increase of pressure with humidity is again nearly zero. The reason for this is uncertain, but it may be associated with the passage of a reflection of the condensation shock across the static pressure tapings, which are located in the sidewalls of the tunnel just ahead of the windows. These shock reflections can be clearly seen in the Schlieren photographs, Figure IV.55. At a nominal Mach number of 2.0 the actual Mach number in the centre of the working section decreases monotonically with increasing humidity and does not show any discontinuities. The rate of decrease of Mach number with humidity is greatest immediately after the condensation shock forms.

Making the assumption that the flow is one-dimensional and isentropic before and after the condensation shock, Monaghan (Ref. IV.14) has derived the following

approximate relations for the working section static pressure and Mach number when a condensation shock is present in the nozzle:

$$\frac{p}{p_{\text{dry}}} \approx 1 + \frac{1}{2} \left[ \frac{\gamma M_{\text{dry}}^2}{M_{\text{dry}}^2 - 1} (1 + \gamma M_1^2) - \gamma M_1^2 \right] \frac{q}{c_p \cdot T_t}$$

$$\frac{M}{M_{\text{dry}}} \approx 1 - \frac{1}{2} \cdot \frac{(1 + \gamma M_1^2) \left( 1 + \frac{\gamma - 1}{2} M_{\text{dry}}^2 \right)}{M_{\text{dry}}^2 - 1} \cdot \frac{q}{c_p \cdot T_t}$$

where  $M_1$  = Mach number just ahead of the condensation shock

$q$  = heat input per unit mass of gas (C.H.U./lb)

$c_p$  = specific heat of air at constant pressure (0.24 C.H.U./lb °C)

$T_t$  = total temperature of the air ahead of the shock (°K).

These theoretical values have been compared with the experimental results at a nominal Mach number of 2.00. Details of the calculations are given in Appendix IV.2, and the resulting values of  $M$  and  $p/p_{\text{dry}}$  have been added to Figure IV.54.

The calculated Mach number compares well with experiment at the lower humidities, but the theory overestimates the effect on Mach number as the humidity is increased. The 'step' in the experimental value of  $p/p_{\text{dry}}$  is not predicted, of course, but the mean rate of increase of static pressure with humidity is approximately correct.

#### IV.5 SOME TYPICAL VAPOUR SCREEN PHOTOGRAPHS

The object of this section is to introduce a selection of typical vapour screen photographs obtained with a series of wing-body combinations and to point out features of particular interest. It is not proposed here to relate details of the flow revealed by these photographs to the general aerodynamic characteristics of the wings; for such a discussion the reader is referred to Reference IV.15. A brief comparison is made, however, between some results obtained with the vapour screen technique and the corresponding surface oil-flow patterns.

All the models mentioned in this Note consisted of various delta wings mounted on the cylindrical part of an ogive-cylinder body. With the exception of that used in section IV.5.4, all the wings had a leading edge sweep of 65° and a thickness/chord ratio of 0.04. The extreme tips of the wings were removed, giving a taper ratio of 0.05, based on the root chord  $c_0$  of the exposed wing. In all cases free boundary layer transition was permitted.

##### IV.5.1 Flow Behind a Cambered Wing at Two Different Mach Numbers

A series of vapour screen photographs showing the flow behind a cambered wing at a distance of 0.05  $c_0$  behind the trailing edge of a cambered wing at two different incidences at a Mach number of 2.00 are presented in Figures IV.56 and IV.57. The wing is a 101 section and cambered conically with respect to

the apex of the gross wing to give an approximately elliptic spanwise loading at a lift coefficient of 0.15 at  $M = 1.57$ . The photographs have been reproduced to about three-quarters full model scale, and from the point of view of technique the most remarkable feature is the wealth of fine detail shown at low incidences, particularly at the higher Mach number. For example, at incidences of  $3^\circ$  and  $4^\circ$  a tiny vortex about  $1/16$  in. diameter can be clearly seen behind the extreme tip of the wing. With increase of incidence this vortex grows in size and retains its roughly circular form, but at incidences less than  $3^\circ$  it becomes merged with a more complex flow originating on the under surface of the wing in the tip region. At  $M = 1.88$  the flow near the tip at zero incidence is particularly intriguing.

Considerable differences in the flow over the upper surface of the wing may be observed between the two Mach numbers. At  $M = 1.51$  the flow appears to be completely attached to the wing surface up to  $4^\circ$  incidence, but at  $M = 1.88$  the photographs suggest that the flow is separating at incidences greater than about  $1^\circ$ . The design lift coefficient for the camber corresponds to an incidence of approximately  $4^\circ$ , so it appears that the camber is successful in delaying leading edge separation at Mach numbers near the design value. In general, the inboard end of the vortex region is more clearly defined at  $M = 1.88$ , a rather thick wake from the inner half of the wing tending to obscure it at the lower Mach number. Also, the shape of the vortex region is more irregular at  $M = 1.88$ , and there is a sudden increase in its spanwise extent between  $6^\circ$  and  $8^\circ$  incidence. This is probably due to the presence of a shock wave above the vortex, which can be seen in the photograph at  $10^\circ$  incidence. The shock is rendered visible by the change in density which occurs across it. At this Mach number condensation is virtually complete, and in the absence of extraneous forces on the fog particles the number of particles per unit volume (and hence the amount of light scattered) will be directly proportional to the local air density. On passing through a shock wave the air undergoes a very rapid deceleration which the fog particles cannot follow owing to their much greater inertia. A relative velocity therefore exists between the air and the fog particles, but a simple calculation shows that this will be quickly reduced to zero by the action of viscosity and a short distance after passing through the shock steady state conditions will be re-established and the fog density will again be proportional to the local air density. The expansion over the leading edge causes a reduction in density and the screen darkens progressively from the leading edge towards the terminal shock. At the shock there is a sudden increase in density and the screen appears lighter due to the greater concentration of fog particles. The position of the shock therefore corresponds with the boundary between the darker and lighter regions, and some idea of the shock strength may be gained from the change in shade between the two regions. These effects are shown up much more clearly in Figure IV.58 than in the present example.

\* The relative velocity  $\dot{c}u$  at time  $t$  after passing through the shock wave is given approximately by

$$\dot{c}u = \dot{c}u_0 \exp \left[ - \frac{18\mu}{d^2} \cdot \frac{t}{\rho_1} \right]$$

where  $d$  is the diameter of the particle (assumed to be spherical),  $\rho_1$  its density (slug/ft<sup>3</sup>) and  $\mu$  the viscosity of the air (lb sec/ft<sup>2</sup>). For a spherical particle of radius  $10^{-5}$  in. the relative velocity will be reduced to 1% of its initial value in a time of approximately  $5 \times 10^{-6}$  sec., i.e. in a distance of less than 0.1 in. after passing through the shock wave.

A row of small black patches about 1/8 in. diameter is visible behind the inner part of the wing at  $M = 1.88$  and  $1^\circ$  incidence (Fig. IV.57). It is believed that these are due to streamwise vortices in the boundary layer, caused by an instability of the three-dimensional shear flow in the region of the swept leading edge, the continuous transverse shear breaking down into a number of discrete vortices (Ref. IV.15). They are probably also present at  $M = 1.51$ , the wake behind the wing at  $1^\circ$  and  $2^\circ$  incidence having a rather jagged appearance, but are not nearly so distinct as at the higher Mach number.

White streaks or patches can be seen in all but one of the photographs at  $M = 1.51$ , below the wing at negative incidences and above it at positive incidences. Originally these were thought to be of no account and due merely to light reflection from the body. However, it now seems certain that they are caused by additional condensation in regions of local flow expansion around the model. The matter is considered further in Section 5.4. No condensation streaks were ever encountered at Mach numbers above 1.51.

#### IV.5.2 Flow Over the Upper Surface of a Plane Wing at $M = 1.75$

Some photographs of the flow over the upper surface of a plane delta wing at an actual Mach number of 1.75 ( $M_{dry} = 1.81$ ) are shown in Figure IV.58. The wing was of the same section (R.A.E. 101, 4% thick) as before, but uncambered. The plane of the vapour screen was located approximately  $0.28 c_o$  ahead of the trailing edge.

As mentioned previously, a shock wave is clearly visible above the wing vortex in this case, its strength increasing quite sharply with incidence above  $10^\circ$ .

An interesting change in the flow pattern occurs at an incidence of about  $10^\circ$ . ~~Below this angle the flow separates from the~~ leading edge, but later re-attaches, leaving a closed bubble containing a vortex on the wing surface. At higher incidences, however, a sheet of vorticity can be seen springing from the leading edge and rolling up into a vortex some distance above the surface. This vortex induces an outflow near the wing surface, but the outflow itself appears to separate and form a secondary vortex underneath the main vortex sheet.

Two further vortices close to the body at  $15^\circ$  and  $18^\circ$  incidence can be identified. The upper is one of a pair of body vortices caused by separation of the cross-flow over the forward part of the body at high incidence (Ref. IV.1). The lower appears to be a wing-body junction vortex of the type described by Stanbrook (Ref. IV.18), which is caused by the interaction of the body boundary layer with the leading edge of the wing. A vortex sheet can be seen separating from the body at an angular position approximately  $40^\circ$  above the plane of the wing and rolling up to form this vortex.

#### IV.5.3 Comparison of Surface Oil-Flow and Vapour Screen Techniques on Two Wings at $M = 1.51$

Figures IV.59 and IV.60 have been prepared so that details of the flow shown by the vapour screens may be easily compared with those given by surface oil-flow patterns. Both of these figures show vapour screen photographs obtained just behind the trailing edge and at three stations on a wing at  $5^\circ$  incidence at a Mach number of 1.51, together with a photograph of the oil-flow pattern (obtained using a mixture of heavy

oil and titanium dioxide with a trace of oleic acid as anti-coagulant) at the same conditions. The two wings used were the plane and cambered 4% thick delta wings referred to above, Figure IV.59 showing the results for the plane wing.

The only significant differences shown by the oil-flow patterns are that on the cambered wing separation occurs slightly further aft of the leading edge, and the re-attachment line is slightly curved. However, the vapour screen pictures show that the height and area of the vortex region and the angle at which the flow separates from the wing surface are appreciably greater in the case of the plane wing. The vapour screen photographs on the cambered wing also show what appear to be three small vortices in the boundary layer inboard of the main leading edge vortex. There is no indication of these vortices in the oil-flow pattern, and their origin is obscure. They may also be seen in the photograph at  $0^\circ$  incidence in Figure IV.56, but there is no similar effect on the plane wing.

The position of re-attachment may be obtained with considerable accuracy from the oil flow patterns, and this point has been marked on the vapour screen photographs for the three stations on the wing. Close examination of the vapour screen photograph at the  $0.85 c_x$  station on the plane wing reveals that the flow immediately above the wing may be divided into three parts - a black region over the outer part of the wing shaped roughly like a segment of a circle and which appears to be devoid of fog particles, a grey region which extends as a narrow band above the wing surface from the inboard end of the black region to the body, and a thin bright line running from the body to the leading edge of the wing which forms an upper boundary to both the grey and black regions. It appears that the point of re-attachment coincides with the inboard end of the black region, so it is not unreasonable to suppose that the size and shape of this region correspond fairly closely with those of the actual leading edge vortex. At the other vapour screen stations, and on the cambered wing, it is virtually impossible to distinguish between these two regions and they appear as a single dark region, but in general re-attachment occurs at a spanwise position near the point of inflection of the bright line surrounding the dark region. This line, and the dark region over the inner part of the wing where the flow is attached, are characteristic of results obtained at Mach numbers up to 1.51. Above this speed, as shown in Figures IV.57 and IV.58, the inboard end of what is assumed to be the leading edge vortex is quite sharply defined and there is no contiguous dark band over the inner part of the wing. In Section IV.6 it is suggested that this difference is due to the smaller size of the fog particles at the higher Mach numbers.

#### IV.3.4 An interesting phenomenon at $M = 1.32$

At an early stage of the present investigation, when fog formation at different Mach numbers was being studied, a test was being performed at a Mach number of 1.32. As usual during these tests, a model was mounted in the tunnel so that the quality of the vapour screen picture could be judged. As the beam of light was being moved further aft behind the model a most interesting phenomenon occurred. In addition to the normal black patches on the screen caused by vortices from the wing, a symmetrical pattern of bright blue lines developed, which appeared to emanate from the centre of the screen and become entrained with the wing vortices. It is not possible in a black and white reproduction to fully recapture the striking nature of this effect - a pattern in blue and black on an iridescent background half green, half violet - but the photographs in Figure IV.61, which were originally taken on colour film, give a

good impression of the phenomenon. The model used was similar to those described previously, but fitted with a  $55^\circ$  leading edge sweep delta wing of R.A.E. 101 section, 6% thick. The plane of the vapour screen was located approximately 9.5 in. (1.2 wing root chords) behind the trailing edge of the wing. The blue lines were present even at zero incidence, when they formed a roughly triangular shape behind each wing panel, with the apex towards the body. With application of incidence, their shape changed, the upper side of the triangle becoming curved and the lower side swinging round as if to unite with the wing vortex.

The lines from the body became rather diffuse by about  $7^\circ$  incidence, but two blue lobe-like shapes appeared in the screen on top of the sting on which the model was mounted. With further increase of incidence the vertical height of the lobes increased and their tips assumed a whitish tinge. It was found that on moving the light beam towards the model the main pattern of blue lines became fainter, and they disappeared completely when the beam was about 6 in. from the trailing edge of the wing. The blue lobes above the body at high incidence persisted, however, until the beam was ahead of the trailing edge.

At the time, the origin of the blue line was the subject of much speculation. No quite similar effect could be found at other Mach numbers, although at  $M = 1.41$  and  $1.51$  blue lobes could be seen at high incidence when the light beam was behind the wing trailing edge. The matter was finally resolved when a long, slender body of revolution was being tested at a Mach number of  $1.41$ . The light beam was located towards the rear of the body and the model happened to be at a considerable incidence while water was being added to the tunnel. It was discovered that two faint blue lobes could be seen above the body in the path of the light beam before the humidity was sufficient to produce a visible vapour screen. It was therefore concluded that the blue coloration was due to local condensation, caused by flow expansion in the immediate vicinity of the model.

This explanation further confirms the mechanism of condensation proposed in Section IV.4.5. No blue lines were detected under any conditions at a Mach number greater than  $1.51$ . However, condensation occurs at a condensation shock above this Mach number and the flow is not supersaturated after the shock. It is therefore not possible for additional condensation to occur at the model. At Mach numbers up to and including  $1.51$  it is believed that the primary condensation occurs on foreign nuclei and only a fraction of the water vapour present in the working section is condensed out. The flow is still well supersaturated and secondary condensation may occur in any region where expansion of the flow is sufficient to raise the local level of supersaturation above the critical value. In view of the comparatively small size of the regions causing additional condensation, it is probable that such condensation occurs on self-generated nuclei. This implies that there may be condensation shocks in the vicinity of the model, but it is considered that the influence of these shocks on the overall flow around the model is likely to be very small.

#### IV.6 THE FORMATION OF THE VAPOUR SCREEN PICTURE

The mechanism by which a shock wave is rendered visible by the vapour screen has already been discussed in Section IV.5.1. We will now consider briefly other ways in which the uniform distribution of fog particles may be disturbed sufficiently to produce noticeable changes in the amount of light scattered by the fog.

A priori, two causes would appear to be responsible - heating, so that the fog particles tend to evaporate, and failure of the fog particles to follow the motion of the air in regions of flow curvature or acceleration due to their much greater inertia.

Heating due to compression will only occur to a significant extent near a stagnation point or through a strong shock wave, but in these circumstances effects due to droplet inertia will be much more important. Other regions in which the temperature may be considerably above the stream temperature are the boundary layer and regions of low mean velocity after boundary layer separation. However, Crane (Ref. IV. 17) has deduced from measurements of recovery temperature that in a laminar boundary layer no re-evaporation occurs and that with a turbulent boundary layer re-evaporation is only partial. It therefore appears that localised temperature effects are not important in the formation of the vapour screen picture, except possibly in the case of wakes behind wings or bodies at low incidence.

Effects due to droplet inertia occur in two distinct regions - the region near the leading edge of a wing or the front stagnation point of a body, and regions of vortical flow. The behaviour of water droplets in the neighbourhood of the leading edge has long been of interest in connection with the problem of icing (Ref. IV. 18). Unfortunately the equations governing the motion of the droplets cannot be solved in closed form, but numerical solutions have been obtained for a number of different aerofoils at subsonic speeds, and the effects of wing sweep have been examined (Ref. IV. 19). The behaviour of the droplets depends on the dimensionless inertia parameter  $k$ , defined as

$$k = \frac{2}{9} \frac{w_L \cdot r^2 U}{\mu \cdot c}$$

where  $w_L$  is the density of the droplet of radius  $r$ ,  $\mu$  the viscosity of the air,  $U$  the free stream velocity and  $c$  the chord of the aerofoil. For a particular aerofoil at a given incidence there is a critical value of  $k$ . If  $k$  is less than the critical value, no droplets strike the aerofoil, but if  $k$  exceeds the critical value, all the droplets in a certain stream tube an infinite distance ahead of the leading edge strike the aerofoil. Both the width of this stream tube and the area of impingement increase with  $k$ . This effect may explain the dark bands over the inner parts of the wings shown in the vapour screen photographs at  $M = 1.51$  (Fig. IV. 59 and IV. 60) and mentioned in Section IV. 5.3. At  $M = 1.51$ , when the radius of the fog particles is about  $3 \times 10^{-5}$  in.,  $k$  is of order 0.1. The radius is not known with any degree of certainty at higher Mach numbers, but it is probably not greater than  $10^{-5}$  in., so that  $k$  is of order 0.01. Thus at  $M = 1.51$  droplets are likely to impinge on the nose of the aerofoil (where they presumably evaporate) and so the air immediately above the surface is devoid of fog particles, but at higher Mach numbers the lower value of  $k$  greatly reduces this tendency, and may even eliminate it completely.

There is little doubt that all the above mentioned effects are of quite minor importance in the formation of the vapour screen picture compared with the influence of vortices. The radial acceleration produced by circulatory flow exerts a powerful centrifuging action on the fog particles and they are rapidly swept from the centre of the vortex. A point of great interest, but one which cannot be definitely resolved

from the present tests, is the relationship between the size and shape of a region clear of fog with those of the vortex causing it. The boundary of such regions is invariably well-defined, but can a vortex possess such a boundary? This difficulty is removed if it is remembered that the vortices under consideration here are quite different from the classical concept of an irrotational vortex in an inviscid fluid. They are essentially three-dimensional, rotational and viscous, produced by the accumulation of vorticity shed from lines of boundary layer separation near the leading edge of the wing or from the body. From examination of large numbers of photographs, it is suggested that the black regions shown on the vapour screen are caused by these rotational vortex cores, and the boundary of the region is a fairly close approximation to the boundary between the core and the outer irrotational flow field, but a detailed survey of flow conditions is necessary before this can be definitely established.

#### IV.7 THE VAPOUR SCREEN AT SUBSONIC SPEEDS

All previous applications of the vapour screen technique have been restricted to supersonic speeds, but there are no fundamental reasons why the method should not be employed at the higher subsonic and transonic speeds provided a sufficiently large drop in temperature between the settling chamber and working section can be achieved. Some tests were therefore made to examine vapour screen production under these conditions.

Ideally, the use of a slotted or porous wall working section is necessary for such an investigation, but this was impossible in the present instance since the transonic working section of the 3 ft tunnel does not possess any apertures suitable for the passage of the light beam. As an alternative, a flat top liner was used in the supersonic working section, converting it, in effect, to a subsonic tunnel. This presented no serious disadvantage since the main purpose of these tests was to determine the lowest subsonic Mach number at which the vapour screen technique could be usefully employed.

The first test was made at  $M = 0.80$  (based on the value of  $p/p_0$  and uncorrected for constraint effects) with a total pressure of 20 in. Hg and a total temperature of approximately  $40^\circ\text{C}$ . The same procedure was followed as in previous tests at supersonic speeds. It was found necessary to inject some 15 gallons of water before an adequately dense vapour screen was produced, but the screen tended to thin once the flow of water into the tunnel ceased. This was because the air was saturated at stagnation conditions and condensation occurred on the tunnel walls and in other cool parts of the circuit. The trouble was cured by injecting water continuously into the tunnel at a rate sufficient to make up for this condensation. However, in spite of the screen appearing reasonably satisfactory when viewed from the side of the tunnel, attempts to photograph it from downstream were unsuccessful, the picture being almost completely obscured by dense white patches caused by local condensation around the model. An impression was gained that the droplets forming the fog were considerably larger than those at higher speeds, and globules of water could frequently be seen streaming over the surface of the model and collecting at the trailing edge of the wing and the base of the body.

A second test at  $M = 0.85$  with the same total temperature and pressure as before proved much more successful. About 10 gallons of water were required to produce an

adequate vapour screen, which had the same iridescent character as at the lower supersonic Mach numbers. Some typical results are presented in Figures IV.62 and IV.63, which show the rolling-up of the vortex sheet at various distances behind a  $65^\circ$  leading edge sweep delta wing at incidences of  $4^\circ$  and  $8^\circ$ . At  $4^\circ$  incidence the results are quite normal and the edges of the vortex sheet are clearly defined, but at  $8^\circ$  it is possible that the higher velocities inside the vortex region caused a drop in temperature sufficient to cause condensation to occur at a greater rate than the fog particles could be swept from the core of the vortex. At the most rearward station there is a complete 'image reversal' effect, the vortex sheet appearing white on a relatively dark background.

The conclusion drawn from these tests is that the lowest Mach number at which the vapour screen technique is practicable is approximately 0.85, but this may be rather too low if the shape of the model or the range of incidence over which it is to be examined is such that flow expansion around the model causes excessive local condensation.

#### IV.8 USE OF LIQUIDS OTHER THAN WATER FOR VAPOUR SCREEN PRODUCTION

An undesirable feature of the vapour screen technique is that at Mach numbers greater than about 1.6 a condensation shock occurs upstream of the working section at a humidity less than that necessary to produce a satisfactory vapour screen. This shock reduces the actual Mach number below the nominal for the nozzle, increases the static pressure and may produce flow disturbances in the working section.

The condensation shock is caused by the sudden liberation of the latent heat of evaporation when vapour condenses into liquid, and to first order the strength of the shock and its effect on the flow are directly proportional to the amount of heat added per unit mass of air. It is possible to reduce the strength of the shock for a given degree of condensation by increasing the total pressure, but the improvement available is strictly limited by the design of the tunnel. A more fundamental approach lies in the use of liquids which have a lower latent heat of evaporation than water. Now the latent heat  $h$  and molecular weight  $m$  are related by  $h \times m = C \times T_b$  (Trouton's Rule), where  $T_b$  is the boiling temperature and  $C$  is a constant which has the value 21 for substances which are unassociated in both the liquid and vapour states. It therefore follows that a liquid of high molecular weight will have a low latent heat of evaporation. The advantage that could be gained from liquids having a lower boiling point is negligible in comparison with that available from the high values of molecular weight that are physically attainable.

The properties desirable in a liquid whose use is contemplated for vapour screen production can be summarised as follows. It must be (a) chemically stable, (b) of high molecular weight, (c) of low toxicity, (d) non-corrosive, (e) non-inflammable, (f) preferably readily available commercially, and (g) have a saturated vapour density such that (i) a sufficient quantity can be introduced before reaching saturation under stagnation conditions, (ii) an excessive quantity is not required to produce saturation at the working section static temperature. The number of liquids satisfying all these conditions is quite small and the most promising appear to be a group of organic

chlorine compounds, carbon tetrachloride\*,  $\text{CCl}_4$ , tetrachlorethylene,  $\text{C}_2\text{Cl}_4$ , tetrachloroethane,  $\text{C}_2\text{H}_2\text{Cl}_4$ , and pentachloroethane,  $\text{C}_2\text{HCl}_5$ . n-Octane,  $\text{C}_8\text{H}_{18}$ , and turpentine,  $\text{C}_{10}\text{H}_{16}$ , are also attractive in that, due to their low specific gravity, their latent heats per unit volume are some 30% less than any of those listed above, but the fire risk obviously renders their use impracticable. Data pertaining to all these compounds are given in Reference IV.7, and the density of their saturated vapours as a function of temperature has been estimated from the values of saturated vapour pressure quoted therein: the results are plotted in Figure IV.64.

It was decided to carry out a test using carbon tetrachloride as bulk supplies were immediately available. The relevant physical properties of carbon tetrachloride and water are compared in the Table below:

	$\text{CCl}_4$	Water
Specific gravity at $0^\circ\text{C}$	1.63	1.00
Boiling point at 760 mm Hg, $^\circ\text{C}$	76.8	100
Freezing point, $^\circ\text{C}$	-23	0
Molecular weight	154	18
Latent heat of evaporation (C.H.U./lb)	46.4 at $76.8^\circ\text{C}$	595 at $0^\circ\text{C}$
Latent heat of fusion (C.H.U./lb)	4.16	79.7
Specific heat of liquid (C.H.U./lb $^\circ\text{C}$ )	0.20	1.00
Surface tension at $20^\circ\text{C}$ (dynes/cm)	27	72.7

The test was made at a nominal Mach number of 2.00, with a total pressure of 9.00 in. Hg, and a total temperature of approximately  $47^\circ\text{C}$ . The air was dried as thoroughly as possible before admitting any carbon tetrachloride. The liquid was injected into the diffuser one pint (0.57 litre) at a time and the working section static pressure measured. Condensation could first be detected visually after 4 pints (2.3 litres) had been added, and by the time 8 pints (4.6 litres) were added the vapour screen was adjudged to be sufficiently dense to permit satisfactory photographs to be taken. The screen appeared a deep bluish-violet colour viewed from the side of the tunnel.

The increase in static pressure,  $p/p_{\text{dry}}$ , with quantity of carbon tetrachloride in the tunnel is shown in Figure IV.54. Between 2 and 6 pints (1.1 to 3.4 litres) the mean slope is approximately one-seventh that when using water, which is roughly the ratio predicted by simple theory. With 8 pints in the tunnel,  $p/p_{\text{dry}} = 1.040$  and the actual Mach number = 1.96, approximately. Using 6 pints of water at the same total temperature and pressure,  $p/p_{\text{dry}} = 1.205$  and the actual Mach number = 1.88. It is thus seen that the severity of the condensation shock may be greatly reduced by the use of carbon tetrachloride in place of water.

---

\* The saturated vapour of carbon tetrachloride is over 300 times as dense as that of water at low temperatures and initially there was some doubt as to whether it would satisfy condition (ii) above, that is whether a sufficient degree of supersaturation could be obtained with a reasonable quantity of the liquid. However, results proved this fear groundless, at least at  $M = 2.0$ . All the other compounds mentioned have a considerably lower saturated vapour density than carbon tetrachloride at the same temperature.

Some photographs of the flow just behind the trailing edge of a  $65^\circ$  leading edge sweep delta wing with a 4% thick biconvex section obtained using the carbon tetrachloride screen are presented in Figure IV.65, with the corresponding photographs using water in Figure IV.66 for comparison. The general quality of the photographic is similar in the two cases, and the most noticeable difference is that with the carbon tetrachloride screen (and higher working section Mach number) the shock wave visible on top of the vortex at incidences of  $6^\circ$ ,  $8^\circ$  and  $10^\circ$  is located approximately 6% of the semi-span further inboard.

#### IV.9 CONCLUSIONS

The vapour screen technique affords a simple and practical method of flow visualization at supersonic speeds, and, with some limitations, may even be employed at Mach numbers as low as 0.85. It is capable of providing much useful information about the flow over and behind wings and bodies, such details as vortices, vortex sheets, lines of flow separation or re-attachment and shock waves being rendered clearly visible.

A high standard of temperature uniformity over the working section is essential if good results are to be obtained, and to achieve such a standard in the 3 ft tunnel entailed shutting off the aftercooler and running at reduced total pressure at a total temperature of  $40^\circ$  to  $50^\circ\text{C}$ . Close control of the humidity is also necessary, the procedure used consisting of running the tunnel with the driers in circuit to reduce the humidity to a low level (corresponding to a frost-point of about  $-40^\circ\text{C}$ ), switching off the driers, and then injecting measured quantities of water into the diffuser.

The humidity required to produce an optimum density of fog in the working section (from the point of view of obtaining the best photographs of the vapour screen picture) is fairly critical, and is affected by Mach number, total pressure and temperature. With a total pressure of 12 in. Hg and a total temperature of  $45^\circ\text{C}$  it was found that the optimum humidity reached a minimum value at about  $M = 1.6$ , increasing very rapidly below this Mach number and rather slowly above it. At Mach numbers up to and including 1.51 (with the above conditions of temperature and pressure) the screen had an iridescent appearance due to diffraction of the light beam by the fog particles. An estimate of the size of the particles based on the position of the coloured diffraction bands at  $M = 1.41$  gave the radius as approximately  $3 \times 10^{-5}$  in., corresponding to a particle density of about  $10^7$  per cubic in. In this Mach number range it was possible to obtain sufficient condensation to form a satisfactory vapour screen without affecting either the working section static pressure or Mach number and it is suggested that condensation occurred on foreign condensation nuclei.

At higher Mach numbers the vapour screen was pale blue in colour and the fog probably consisted of ice crystals rather than water droplets. Condensation occurred at a condensation shock in the nozzle upstream of the working section, which increased the static pressure and decreased the Mach number in the working section. Tests at a nominal Mach number of 2.00 showed that the variation of Mach number and static pressure with humidity agreed well with the first order theory of Monaghan at low humidities, but the theory was unduly pessimistic of the effect on Mach number in the range of humidity necessary to produce a satisfactory vapour screen.

The quality of the vapour screen picture was generally superior at Mach numbers above 1.51, this being ascribed to the smaller size of the fog particles due to the

different mechanism of condensation. At lower speeds the flow in the working section was still supersaturated and patches of additional local condensation caused by flow expansion around the model were frequently observed. Under certain conditions, and particularly at  $M = 1.32$ , these condensation patches or streaks formed an intricate pattern superimposed on the normal vapour screen picture.

The adverse effects of the condensation shock on the flow at the higher Mach numbers may be alleviated by the use of liquids with a lower latent heat of evaporation than water. A test at a nominal Mach number of 2.00 showed that a vapour screen picture of a quality comparable with that obtained using water vapour could be produced with carbon tetrachloride vapour. The actual Mach number in the working section was 1.96, compared with a value of 1.88 when using water vapour.

## APPENDIX IV. 1

## The Mechanism of Condensation at Mach Numbers Less than 1.5

It is suggested in Section IV. 4.5 that, at Mach numbers up to and including 1.51, condensation is occurring principally on foreign nuclei rather than on nuclei generated spontaneously in the supersaturated vapour by random molecular aggregation. Since this is at variance with the commonly accepted view of the mechanism of condensation in wind tunnels at supersonic speeds, the matter will be considered in some detail.

We will first attempt to show that the size of the droplets, as estimated from observation of the coloured diffraction bands at  $M = 1.41$ , is of the same order as that predicted theoretically on the assumption that a droplet starts to form around a condensation nucleus at the point in the nozzle where the water vapour is just saturated and continues to grow on its passage down the nozzle by a process of diffusion of water vapour onto the surface of the droplet. To perform this calculation it is necessary to make an assumption concerning the variation of the density of the uncondensed water vapour along the length of the nozzle. This variation is known when there is no condensation, but is indeterminate once condensation has started unless the number of droplets is also known. Consequently, the calculated value of the droplet radius must be regarded as a rough estimate only, but its order of magnitude should be correct.

The equation governing the rate of growth of a droplet in a moving airstream is given by Oswatitsch in Reference IV. 13 as

$$r \frac{dr}{dx} = \frac{w - w_{sat}}{w_L} \cdot \frac{D}{u}$$

where  $r$  = radius of the (spherical) droplet  
 $x$  = axial coordinate  
 $w$  = density of the uncondensed vapour surrounding the droplet  
 $w_{sat}$  = density of saturated vapour at the surface of the droplet  
 $w_L$  = density of the liquid forming the droplet = 62.4 lb/ft<sup>3</sup>  
 $D$  = coefficient of diffusion of water vapour in air  
 $u$  = velocity of the airstream.

This equation may be integrated to give

$$r^2 = 2 \int_0^l \frac{w - w_{sat}}{w_L} \cdot \frac{D}{u} \cdot dx$$

where  $l$  is the distance travelled by the drop since its formation. In the case of the flow through a supersonic nozzle, all the quantities on the right hand side of this equation (with the exception of  $w_L$ ) are functions of  $x$ , but it may be shown that in the Mach number range we are concerned with here (1.0 to 1.5 approximately) the ratio  $D/u$  is very nearly constant, so that

$$r^2 = \frac{2}{w_L} \cdot \left(\frac{D}{u}\right) \cdot \int_0^l (w - w_{\text{sat}}) dx .$$

Unfortunately, the variation of  $(w - w_{\text{sat}})$  with distance along the nozzle is indeterminate, but we can obtain a rough estimate of the droplet radius by assuming a simple, plausible variation of  $(w - w_{\text{sat}})$  with  $x$ . For example, suppose we assume that  $(w - w_{\text{sat}})$  increases linearly with  $x$ . We then have for the radius

$$r = \sqrt{\left(\frac{D}{u}\right) \cdot \frac{l}{w_L} [w - w_{\text{sat}}]_l} .$$

Let us consider the case of  $M = 1.4$ , with a total pressure  $p_t$  of 12.0 in. Hg, a total temperature  $T_t$  of 45°C, and with 12 pints (6.8 litres) of water added to the tunnel. The flow becomes just saturated at a point in the nozzle where the local Mach number is 0.98, and in accordance with our initial hypothesis it will be assumed that condensation starts from this point. From Reference IV.6, the distance from this point to the centre of the working section, i.e. the distance  $l$ , is 9.5 ft. The coefficient of diffusion  $D$  is given by Oswatitsch as

$$D = 0.000225 \cdot (T/273)^{1.86} \cdot (30/p) \text{ ft}^2/\text{sec}$$

so that the mean value of  $D/u$  between  $M = 1.0$  and  $M = 1.4$  is  $0.93 \times 10^{-6}$  ft for the conditions specified above. The working section static temperature is -43°C under isentropic conditions, and from Figure IV.51 the corresponding density of saturated water vapour,  $w_{\text{sat}}$ , is  $5.1 \times 10^{-6}$  lb/ft<sup>3</sup>. If we assume that half of the water vapour has condensed at the working section, the actual density of the uncondensed vapour is

$$\frac{1}{2} \times \frac{12 \times 1.25}{45,000} \left(\frac{\rho}{\rho_{t, M=1.4}}\right) = 73 \times 10^{-6} \text{ lb/ft}^3 .$$

Inserting these values in the equation for  $r$  gives a droplet radius of  $3.8 \times 10^{-5}$  in., which is considered to be in quite reasonable agreement with the value of  $3 \times 10^{-5}$  in. estimated from observation of the coloured diffraction bands at  $M = 1.41$ .

If we again assume half of the vapour to have condensed by the time the working section is reached, and taking the droplet radius as  $3 \times 10^{-5}$  in., the number of droplets in this case works out at  $10^7$  per cu.in. Therefore if condensation is occurring on foreign condensation nuclei, there must be at least this number of nuclei present in the air in the tunnel. At first sight this may appear to be an excessive number, but in fact is less than the number that have been measured in ordinary room air, and is of the same order as that found in an urban atmosphere. We thus conclude that the size and number of the droplets are not inconsistent with the proposition that condensation is occurring on foreign nuclei.

The theory of molecular nucleus formation is based on the kinetic theory of gases, and whilst complicated in detail, the results may be expressed comparatively simply. It is found that the rate of nucleus formation per unit volume depends on two

parameters - the temperature and the ratio of the actual vapour pressure to the saturation vapour pressure, i.e. the supersaturation.

Burgess and Seashore in Reference IV.20 present a chart of the rate of nucleus formation as a function of the supersaturation and stream temperature. At a Mach number of 1.4, with a total temperature of 45°C and a static temperature of -43°C, the relation between the supersaturation  $S$  and the rate of nucleus formation  $J$  (expressed as the number of nuclei generated in 1 cu.in. of vapour while travelling a distance of 1 ft) is as follows:

$J$	$S$
1	10.0
$10^2$	11.3
$10^4$	12.9
$10^6$	15.2
$10^8$	18.2
$10^{10}$	22.2
$10^{12}$	28.7

Thus the number of self-generated nuclei becomes of the same order as the number of droplets estimated to be present when a 16-fold supersaturation is attained. Referring to Figure IV.50, it is seen that at  $M = 1.4$  condensation is first detectable in the working section at just this level of supersaturation. This might be considered excellent agreement between theory and experiment and fully justifying the assumption that in supersonic tunnels condensation is due to self-generated nuclei, but there are reasons for supposing that this agreement is fortuitous. If the supersaturation is increased by increasing the initial humidity a comparatively small amount, the rate of nucleus formation increases by several orders of magnitude, which would cause a sudden and complete collapse of the supersaturated state, i.e. a condensation shock. The experimental results do not reveal the existence of any such shock in the Mach number range under consideration until humidities rather greater than that found necessary to produce a satisfactory vapour screen. There is also the evidence (Section IV.5.4) that the flow in the working section is still well supersaturated, although this is not the case at the higher Mach numbers when condensation does occur at a condensation shock.

The molecular nucleus formation theory disregards an important factor when applied to the flow in wind tunnels. This is the effect of the temperature gradient along the nozzle (Ref.IV.21). Suppose we express the supersaturation not as the ratio of the actual pressure of the supersaturated vapour to the saturated vapour pressure, but as the 'adiabatic supercooling'. This is defined as the difference in temperature between the point in the nozzle at which the vapour is just saturated, and the actual vapour temperature. At  $M = 1.4$  and with a 16-fold supersaturation in the working section (where the static temperature is -43°C), the flow is just saturated at a point in the nozzle where the local static temperature is -12°C. Thus the adiabatic supercooling is 31°C, which is a fairly typical value of the supercooling necessary to cause condensation, as given by this theory. However, there is experimental evidence (Ref.IV.21) that even in large tunnels condensation effects are rarely

encountered with an adiabatic supercooling of less than  $40^{\circ}\text{C}$  and in a small tunnel this may rise to  $60^{\circ}$  or  $70^{\circ}\text{C}$  or more. A change in the adiabatic supercooling from  $31^{\circ}\text{C}$  to  $40^{\circ}\text{C}$  represents an increase of over 100% in the supersaturation.

It is therefore considered that at the lower supersonic speeds the weight of evidence is against the theory that condensation is due to self-generated nuclei, and it appears that foreign nuclei are primarily responsible. It must be emphasised, however, that this conclusion is only valid for the 3 ft tunnel for the particular conditions of pressure and temperature under which it was operated, and will not necessarily be true in general. For example, a reduction in total temperature while keeping the stagnation humidity constant will have little effect on the rate of growth of a droplet forming around a foreign condensation nucleus, but it will increase the adiabatic supercooling, thus greatly increasing the likelihood of self-generated nuclei dominating the condensation process. It might well be found that at a total temperature of  $15^{\circ}\text{C}$  the presence of foreign nuclei is significant only at Mach numbers less than about 1.2.

The effect of a reduction in tunnel size is interesting. The shorter distance between throat and working section is obviously unfavourable to the growth of droplets on foreign nuclei, which tends to increase the supersaturation of the uncondensed vapour, thus increasing the probability of molecular nucleus formation. However, the steeper temperature gradient in the shorter nozzle increases the adiabatic supercooling necessary to cause condensation. It is therefore difficult to predict the effect of a reduction in tunnel size on the mechanism of condensation, but it is certain that to produce, at the same Mach number and total pressure, a vapour screen of equal density in a small and in a large tunnel, then the stagnation humidity must be greater in the former case than in the latter.

## APPENDIX IV. 2

Estimation of Working Section Mach Number and Static Pressure  
when a Condensation Shock is Present in the Nozzle at  $M_{dry} = 2.0$

Monaghan (Ref. IV. 14) has derived the following approximate relations for the working section static pressure and Mach number when a condensation shock is present in the nozzle:

$$\frac{p}{p_{dry}} \approx 1 + \frac{1}{2} \left[ \frac{\gamma M_{dry}^2}{M_{dry}^2 - 1} (1 + \gamma M_1^2) - \gamma M_1^2 \right] \frac{q}{C_p T_t}$$

$$\frac{M}{M_{dry}} \approx 1 - \frac{1}{2} \frac{(1 + \gamma M_1^2) \left( 1 + \frac{\gamma - 1}{2} M_{dry}^2 \right)}{M_{dry}^2 - 1} \frac{q}{C_p T_t}$$

where  $M_1$  = Mach number just ahead of the condensation shock  
 $q$  = heat input per unit mass of gas (C.H.U./lb)  
 $C_p$  = specific heat of air at constant pressure (0.24 C.H.U./lb °C)  
 $T_t$  = total temperature of the air ahead of the shock (°K).

Before these expressions can be evaluated it is first necessary to estimate the value of  $M_1$ , and this has been done by assuming a constant adiabatic supercooling of 50°C (see Appendix IV. 1), which corresponds to condensation effects being just detectable at a frostpoint of -37°C with an initial total temperature of 47°C. It is assumed that the wet air expands isentropically through the nozzle until condensation occurs, and that the density and temperature of the small quantity of water vapour present vary directly as that of the much larger mass of air. The temperature  $T_{sat}$  at which the vapour is just saturated may then be found for any stagnation vapour density by cross-plotting on Figure IV. 51. With a total temperature  $T_t$  of 47°C and assuming an initial vapour density of  $0.7 \times 10^{-5}$  lb/ft<sup>3</sup> (corresponding to a frostpoint of -40°C) for the 'dry' tunnel, we can calculate  $M_1$  as follows.  $W$  is the quantity of water added to the tunnel,  $w_t$  the density of the water vapour in the settling chamber and  $T_1$  the temperature just ahead of the condensation shock.

$W$	$w_t$	$T_{sat}$	$T_1$	$T_1/T_t$	$M_1$
lb	lb/ft <sup>3</sup>	°C	°C		
2.5	$6.3 \times 10^{-5}$	-24	-74	0.632	1.74
5.0	$11.8 \times 10^{-5}$	-18	-68	0.641	1.67
7.5	$17.3 \times 10^{-5}$	-13	-63	0.657	1.62

In calculating  $q$  it has been assumed that all the water vapour is condensed out at the shock, and that ice crystals rather than water droplets are formed, so a total latent heat  $h$  of 690 C.H.U./lb has been used. With a total pressure of 9 in. Hg, the density  $\rho_t$  of the air in the settling chamber is 0.0218 lb/ft<sup>3</sup>. Since  $q = h w_t / \rho_t$ , we have finally:

W	M <sub>1</sub>	q/C <sub>p</sub> T <sub>t</sub>	M	p/p <sub>dry</sub>
1b				
2.5	1.74	0.026	1.92	1.07
5.0	1.67	0.049	1.86	1.13
7.5	1.62	0.072	1.80	1.18

These values of M and p/p<sub>dry</sub> have been added to Figure IV.54.

## LIST OF REFERENCES IN PART IV

- IV. 1. Allen, H.J.  
Perkins, E.W. *A Study of Effects of Viscosity on Flow Over Slender Inclined Bodies of Revolution.* NACA Report 1048, 1951.
- IV. 2. Gępcynski, J.P. *An Experimental Investigation of the Flow Phenomena Over Bodies at High Angles of Attack at  $M = 2.01$ .* NACA/TIB 4848, Oct. 1955.
- IV. 3. Hall, I.M.  
et alii *Experiments with Inclined Blunt-Nosed Bodies at  $M_c = 2.45$ .* ARC 19,479, F.M.2574, Aug. 1957.
- IV. 4. Jorgensen, L.H. *Elliptic Cones Alone and With Wings at Supersonic Speeds.* NACA Tech. Note 4045, Oct. 1957.
- IV. 5. Jorgensen, L.H. *Inclined Bodies of Various Cross-Sections at Supersonic Speeds.* NASA/TIL 6245, Nov. 1958.
- IV. 6. Morris, D.E. *Calibration of the Flow in the Working Section of the 3 ft x 3 ft Tunnel.* National Aeronautical Establishment C.P.261, Sept. 1954.
- IV. 7. Hodgman, C.D.  
(Editor) *Handbook of Chemistry and Physics.* 39th Edition, 1957-1958. Chemical Rubber Publishing Co., Cleveland.
- IV. 8. Middleton, W.E.K. *Visibility in Meteorology.* Chapter II. 2nd Edition, University of Toronto Press.
- IV. 9. Wood, R.W. *Physical Optics.* 2nd Edition, The Macmillan Co., New York, 1911.
- IV.10. Stodola, A. *Steam and Gas Turbines.* Vol.1, 6th Edition, McGraw-Hill, 1927, pp.123-4.
- IV.11. Mason, B.J. *The Physics of Clouds.* Chapter IV, Section 4.3 Clarendon Press, Oxford, 1957.
- IV.12. Sander, A.  
Danköhler, O. *Supersaturation in the Spontaneous Formation of Nuclei in Water Vapour.* NACA Tech. Memo. 1365, Nov. 1953.
- IV.13. Gwatitch, K.I. *Formation of Fog in Wind Tunnels and its Influence on the Investigation of Models.* Unpublished MOA Report. ARC 11345.
- IV.14. Monaghan, R.J. *Tests of Humidity Effects on Flow in a Wind Tunnel at Mach Numbers between 2.48 and 4.* ARC Current Paper No. 247, 1956.
- IV.15. Squire, L.C.  
et alii *An Experimental Investigation of the Characteristics of Some Plans and Cambered  $65^\circ$  Delta Wings at Mach Numbers from 0.70 to 2.0.* Unpublished MOA Report. ARC 23110.

- IV. 16. Stanbrook, A. *Experimental Observation of Vortices in Wing-Body Junctions.* ARC R & M 3114, 1959.
- IV. 17. Crane, J. F. W. *The Effect of Humidity on Laminar Recovery Temperature Measurements in Supersonic Flow of Air in Wind Tunnels.* ARC R & M 3215.
- IV. 18. Glauert, M. *A Method of Constructing the Paths of Raindrops of Different Diameters Moving in the Neighbourhood of (1) a Circular Cylinder, (2) an Aerofoil, Placed in a Uniform Stream of Air; and a Determination of the Rate of Deposit of the Drops on the Surface and the Percentage of Drops Caught.* ARC R & M 3023, Nov. 1940.
- IV. 19. Dorach, R. G.  
Brun, R. J. *A Method for Determining Cloud-Droplet Impingement on Swept Wings.* NACA Tech. Note 2031, April 1953.
- IV. 20. Burgess, W. C.  
Seashore, F. L. *Criteria for Condensation-Free Flow in Supersonic Tunnels.* NACA Tech. Note 2518, Dec. 1951.
- IV. 21. Smolderen, J. J. *Condensation Effects and Air Drying Systems for Supersonic Wind Tunnels.* AGARDograph No. 17, July 1955.

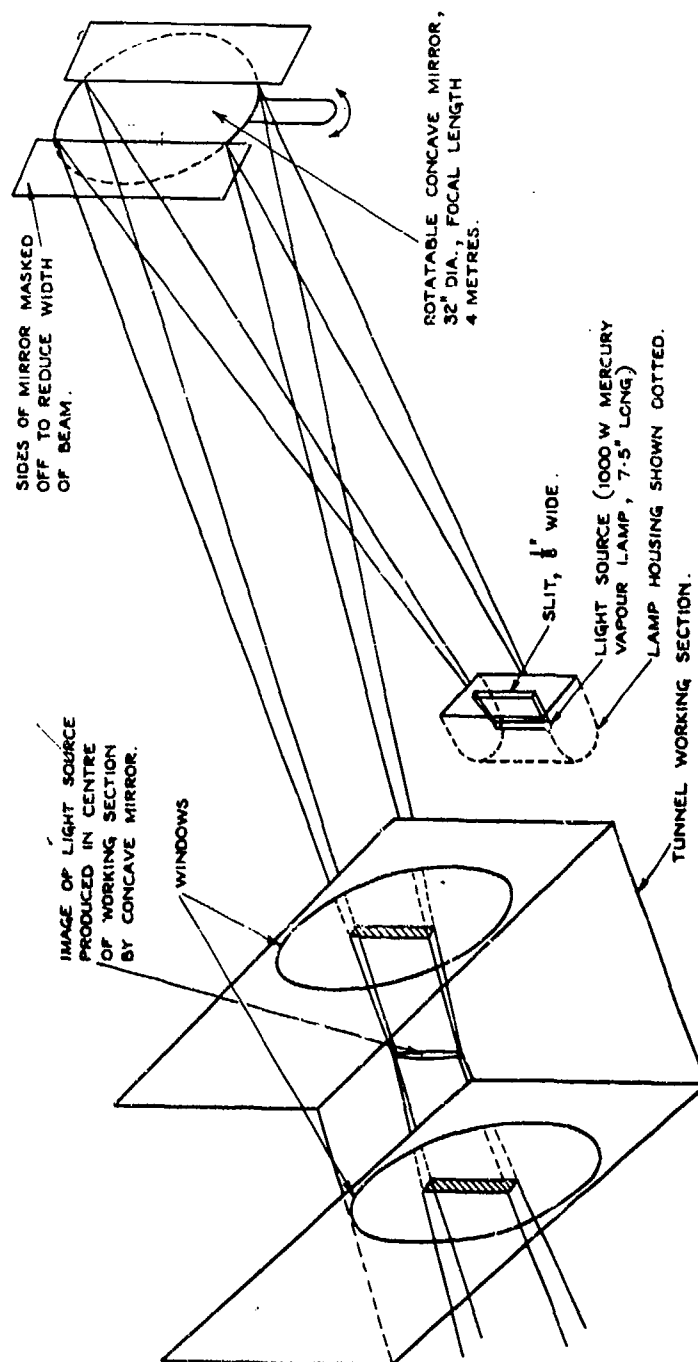


Fig. IV. 46 Illumination system for vapour screen experiments

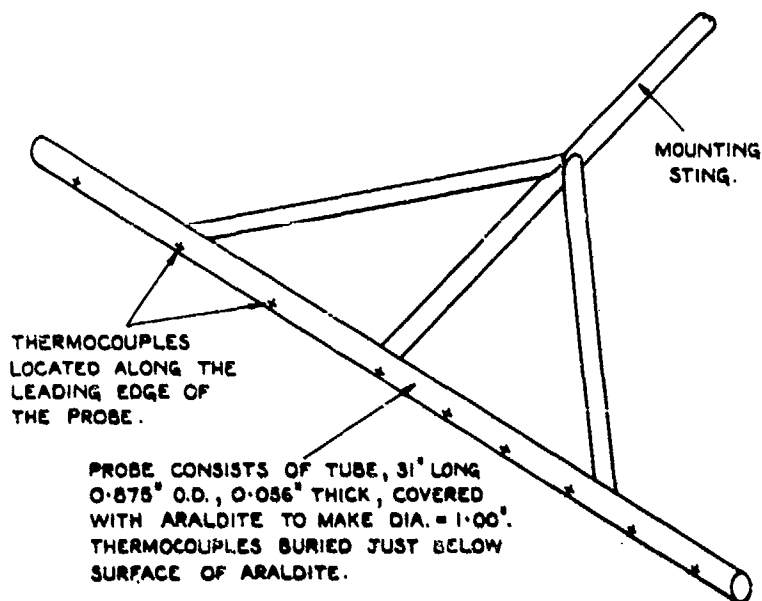


Fig. IV.47 Total temperature probe

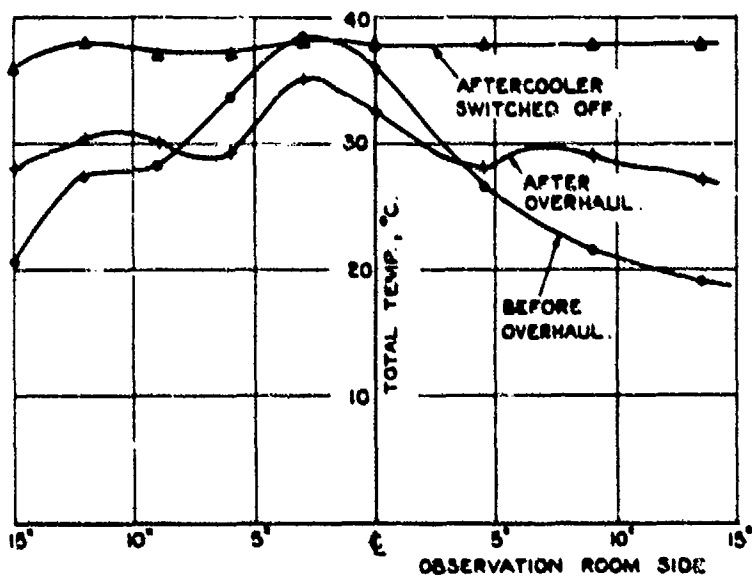


Fig. IV.48 Variation of total temperature across the working section before and after overhaul of the aftercooler

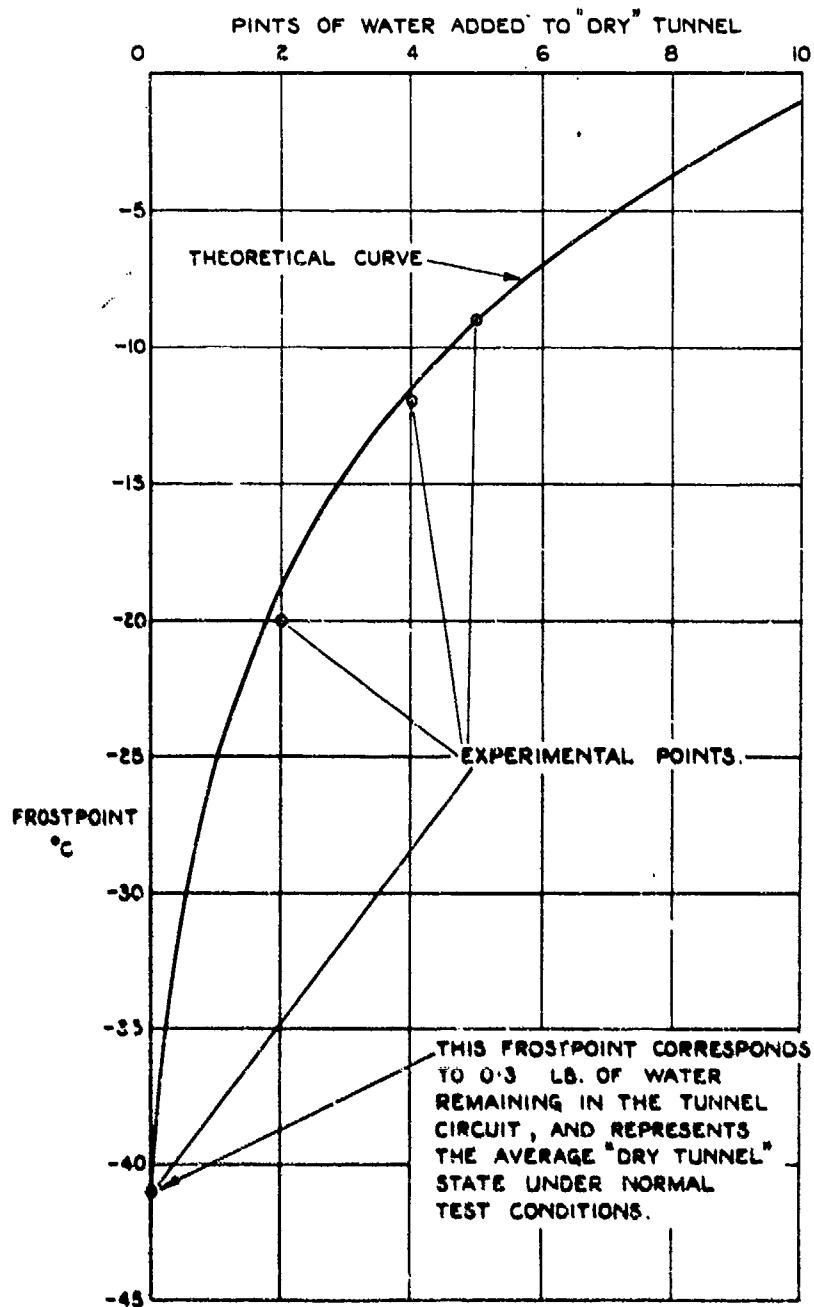


Fig. IV. 40 Relation between quantity of water added to the tunnel and the frostpoint

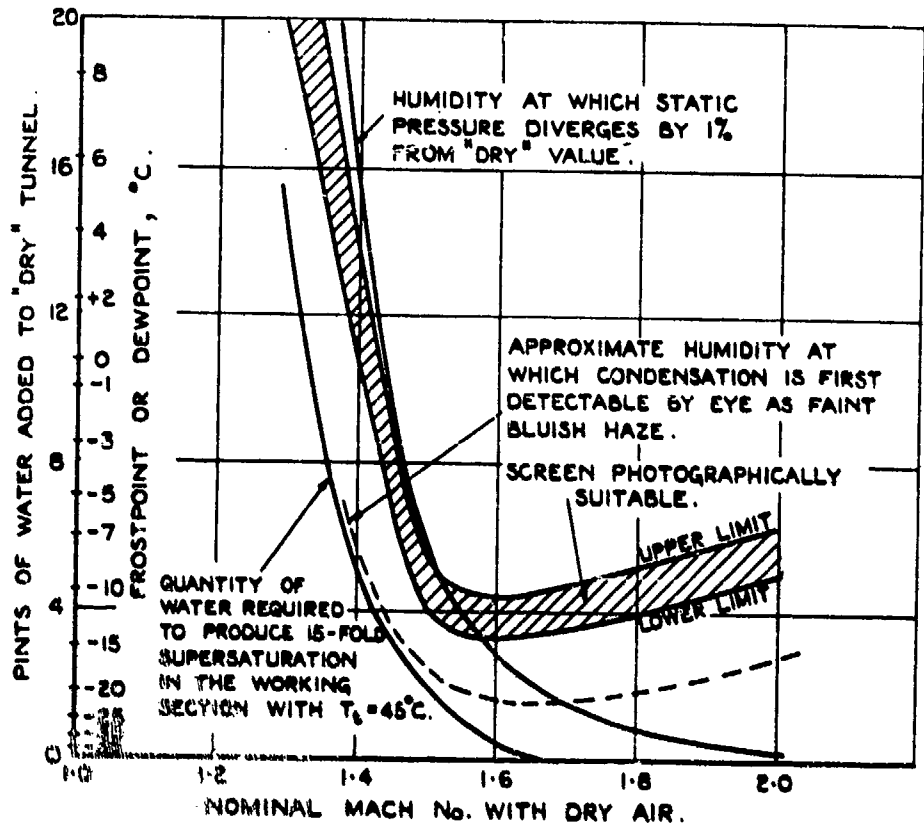


FIG. IV.51 Effect of Mach number on quantity of water required to produce a satisfactory vapour screen.  
Total pressure = 12 in. Hg. total temperature = 45°C

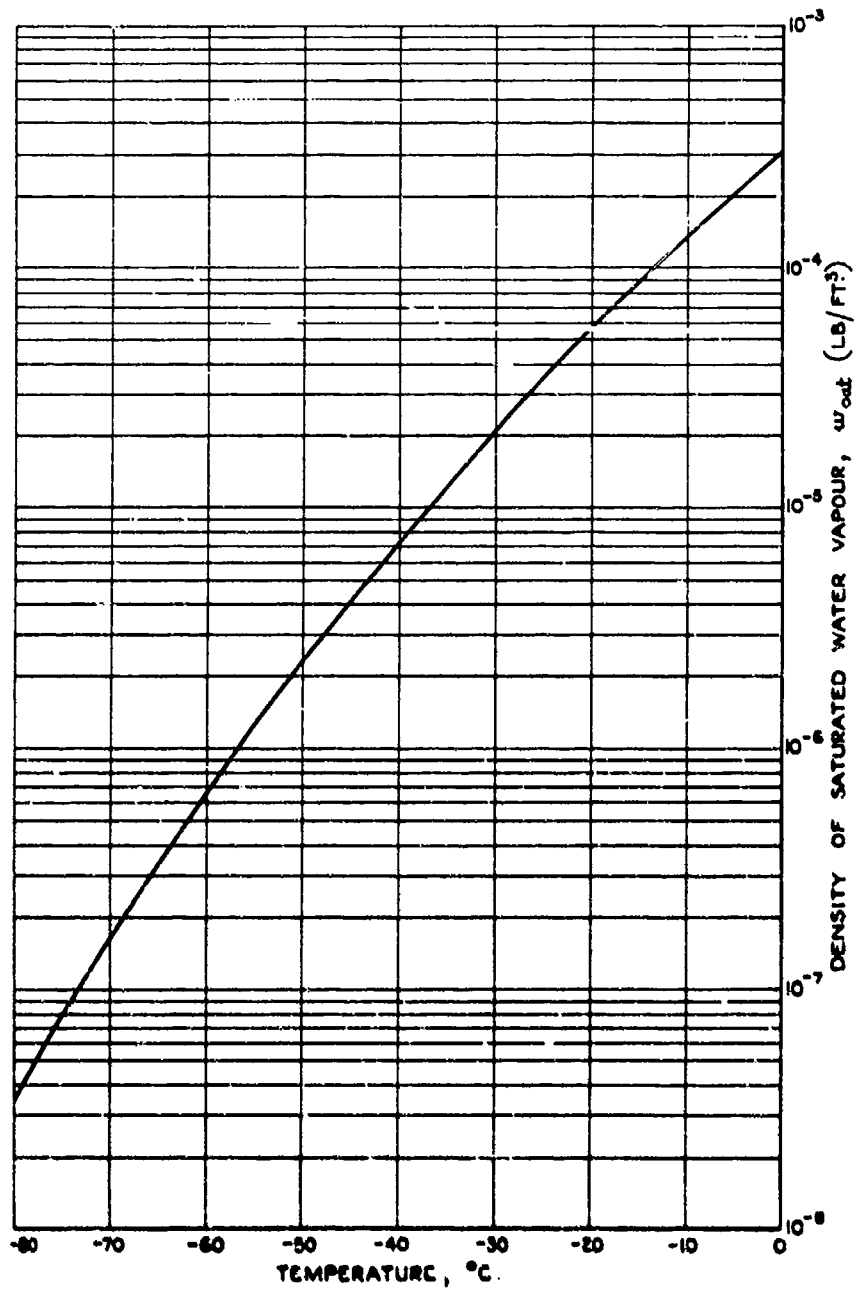


Fig. IV.51 Density of saturated water vapour as a function of temperature

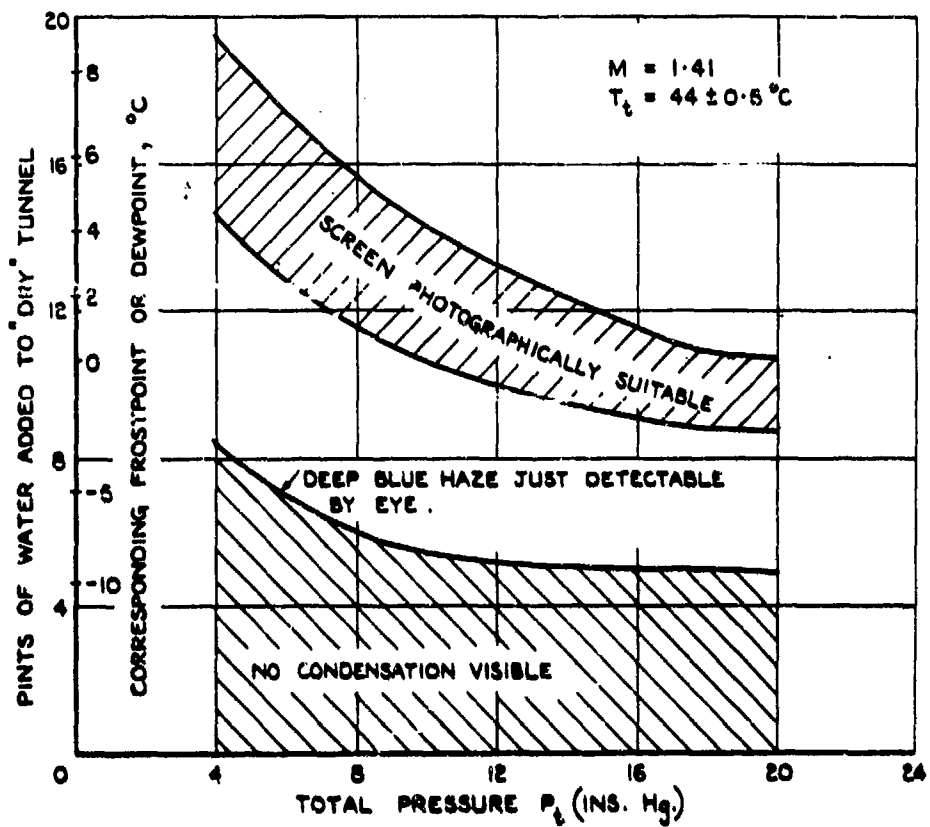
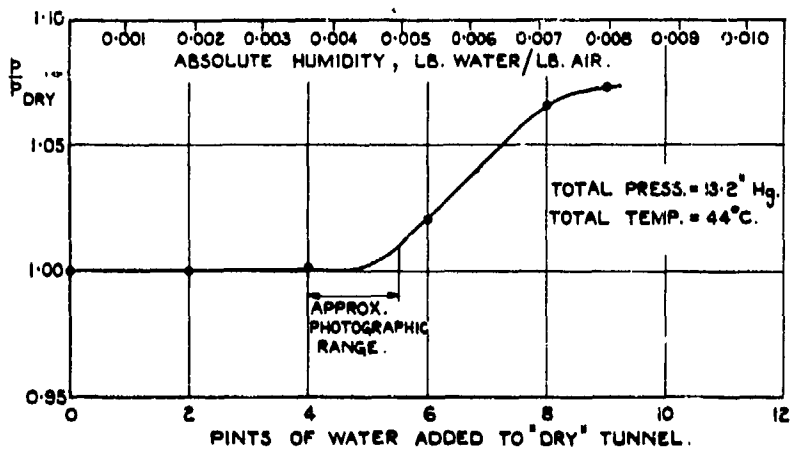
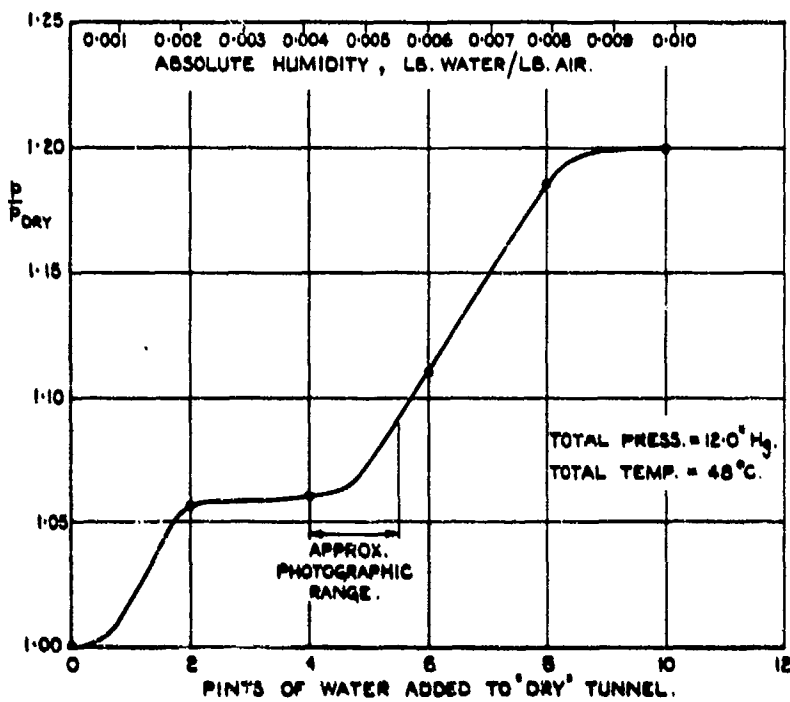


FIG. IV.52 Effect of total pressure on the quantity of water required to produce a satisfactory vapour screen at a Mach number of 1.41



$$(a) M_{DRY} = 1.51$$



$$(b) M_{DRY} = 1.81$$

Fig. IV.53 Effect of humidity on working section static pressure at nominal Mach numbers of 1.51 and 1.81

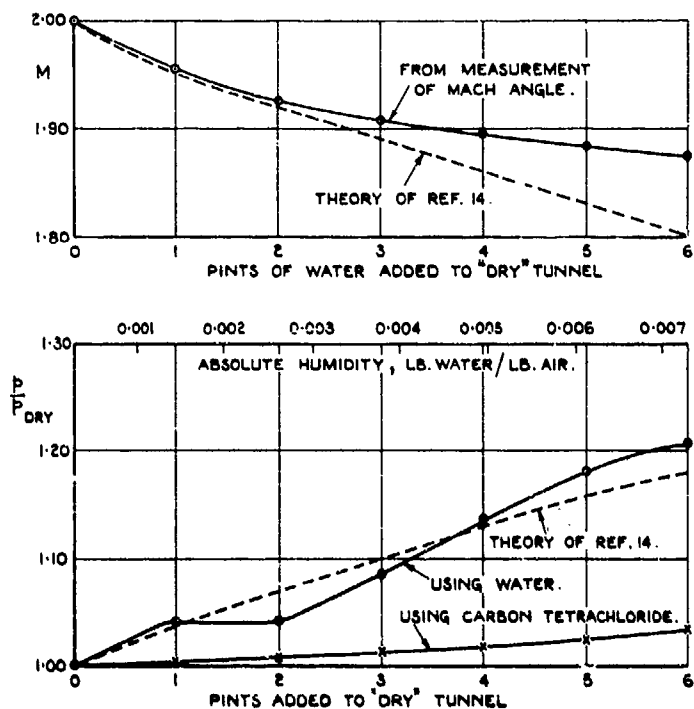
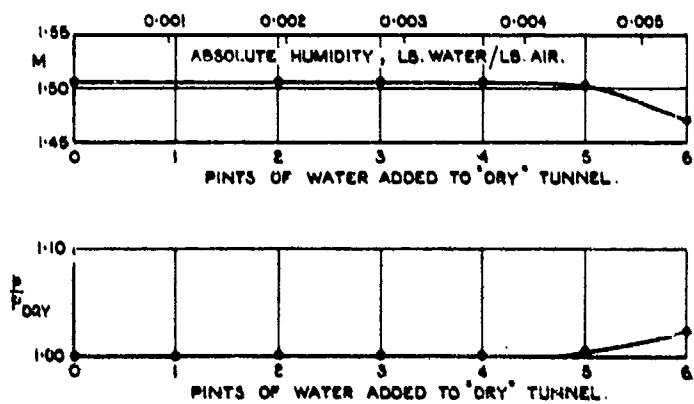
(a)  $M_{dry} = 2.00$ , Total pressure = 9.0 in. Hg., total temperature  $\approx 47^{\circ}\text{C}$ (b)  $M_{dry} = 1.51$ , Total pressure = 13.2 in. Hg., total temperature =  $42^{\circ}\text{C}$ 

Fig. IV.54 Effect of humidity on actual Mach number and static pressure in the working section at nominal Mach numbers of 2.00 and 1.51

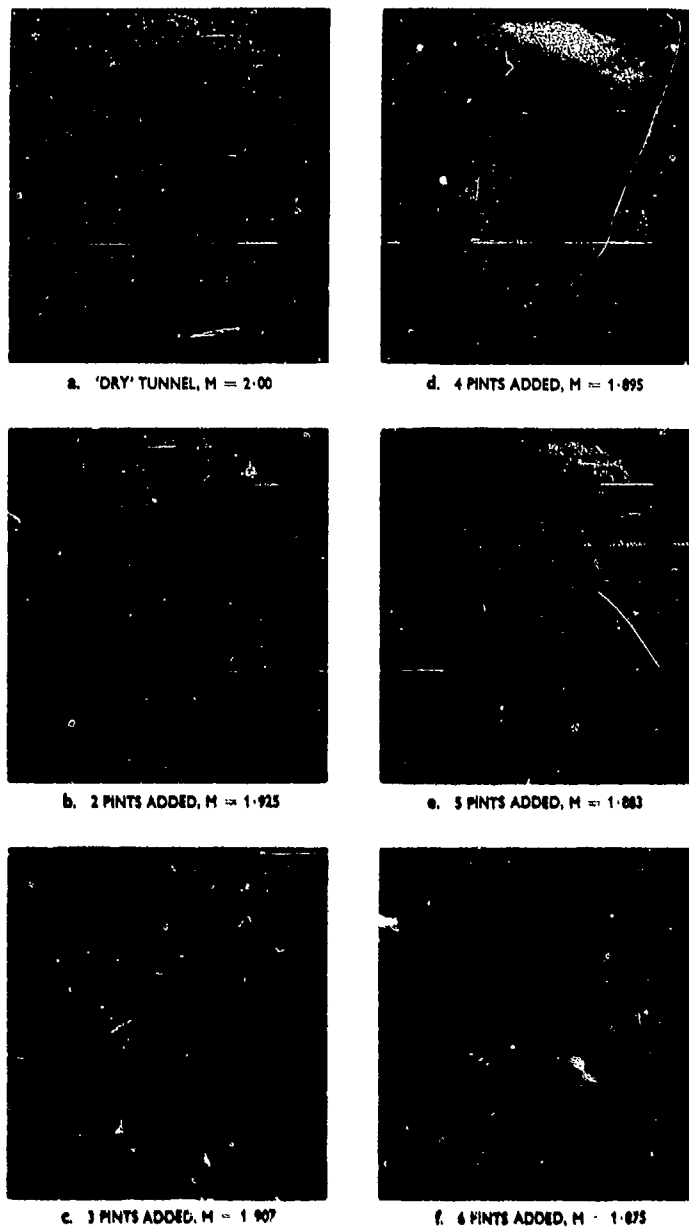


Fig. IV. 55 Schlieren photographs of Mach waves used to determine the actual Mach number in the working section

$$M_{dry} = 2.00, \quad p_t = 9.0 \text{ in. Hg.}, \quad T_t \approx 47^\circ\text{C}$$

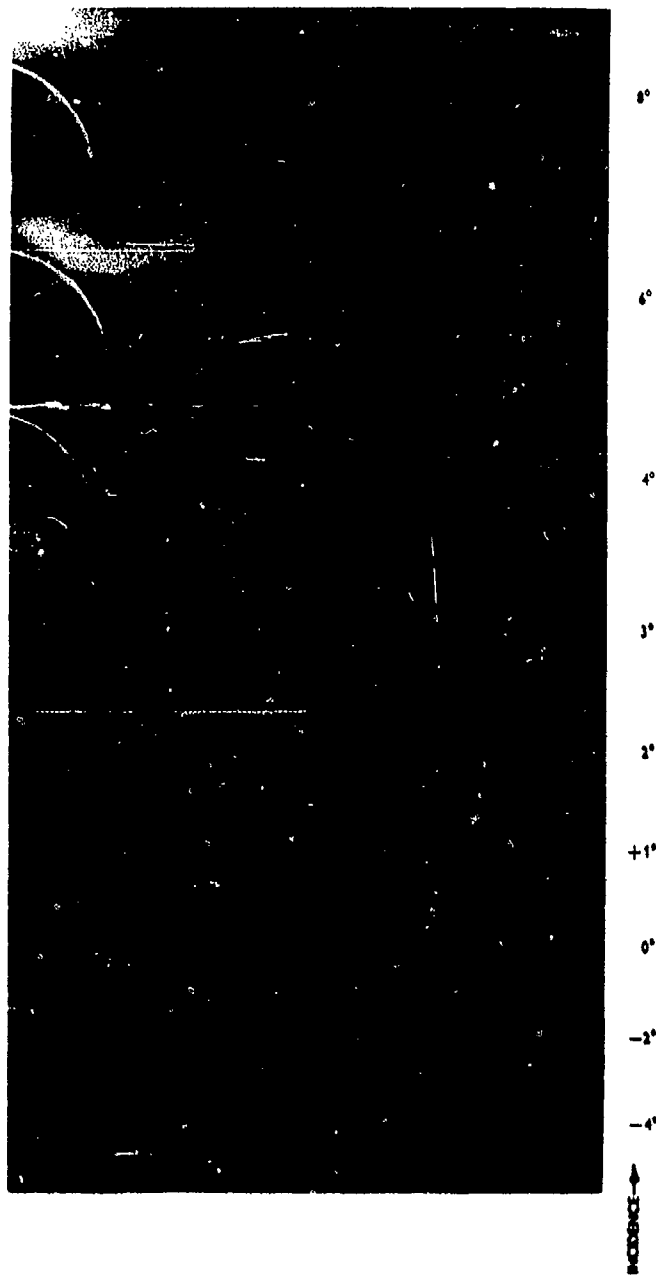


Fig. IV.56 Vapour screen photographs of the flow behind a cambered delta wing  
at  $M = 1.51$

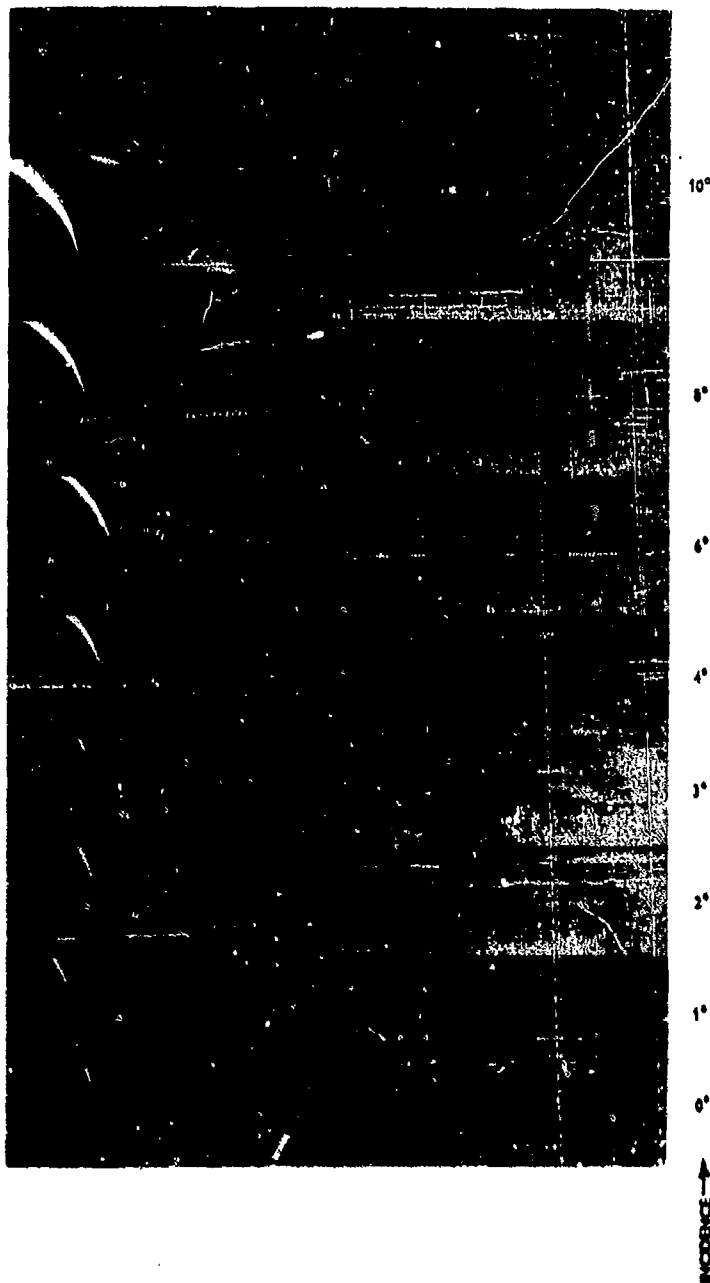


Fig. IV.67 Vapour screen photographs of the flow behind a cambered delta wing  
at  $M = 1.88$  ( $M_{dry} = 2.00$ )

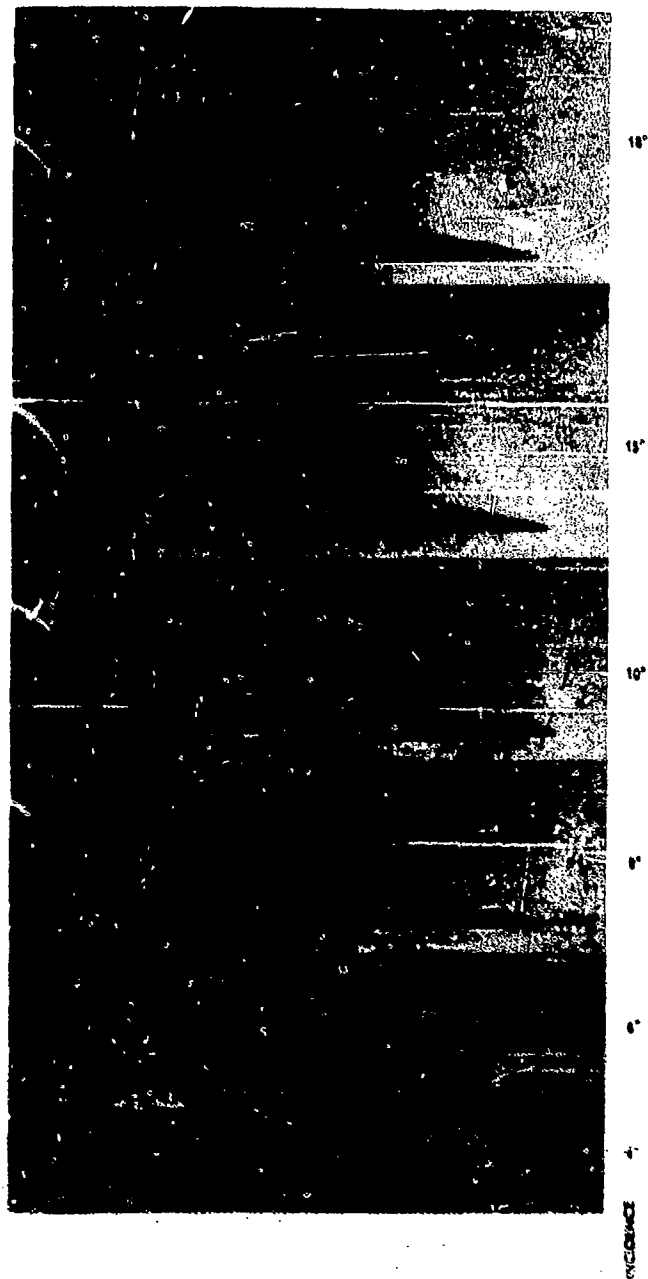


Fig. IV.38 Vapour screen photographs of the flow over the upper surface of a plane wing at  $M = 1.75$  ( $M_{dry} = 3.81$ )

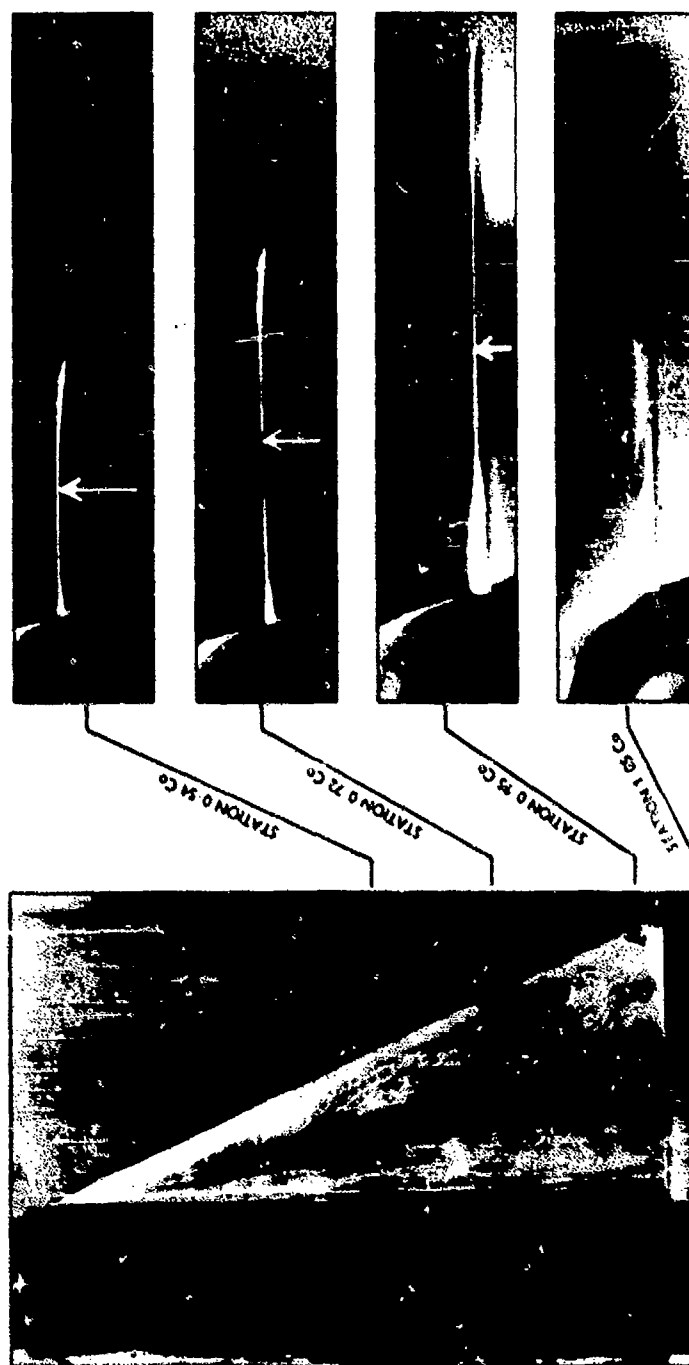


Fig. IV. 59 Comparison of surface oil-flow and vapour screen results on a plane wing at  $M = 1.51$ ,  $\alpha = 8^\circ$

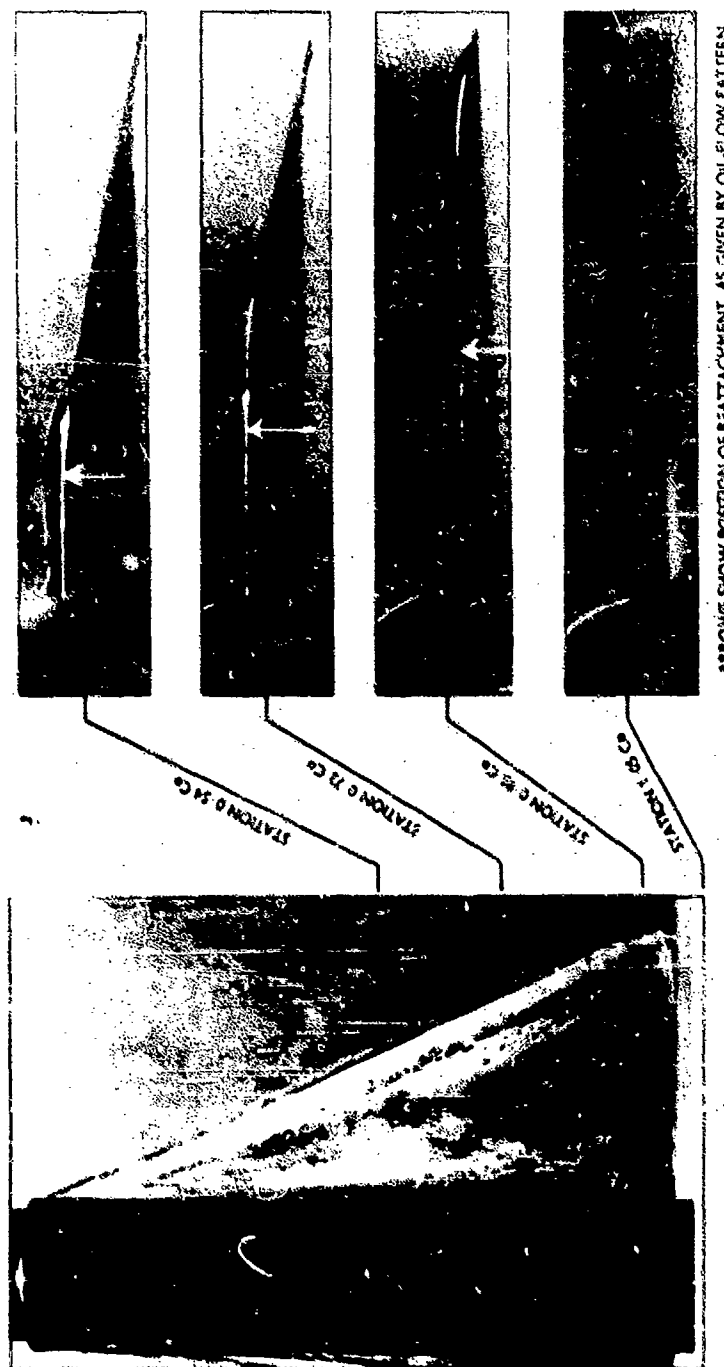


Fig. IV.60 Comparison of surface oil-flow and vapour screen results on a cambered wing at  $M = 1.51$ ,  $\alpha = 8^\circ$

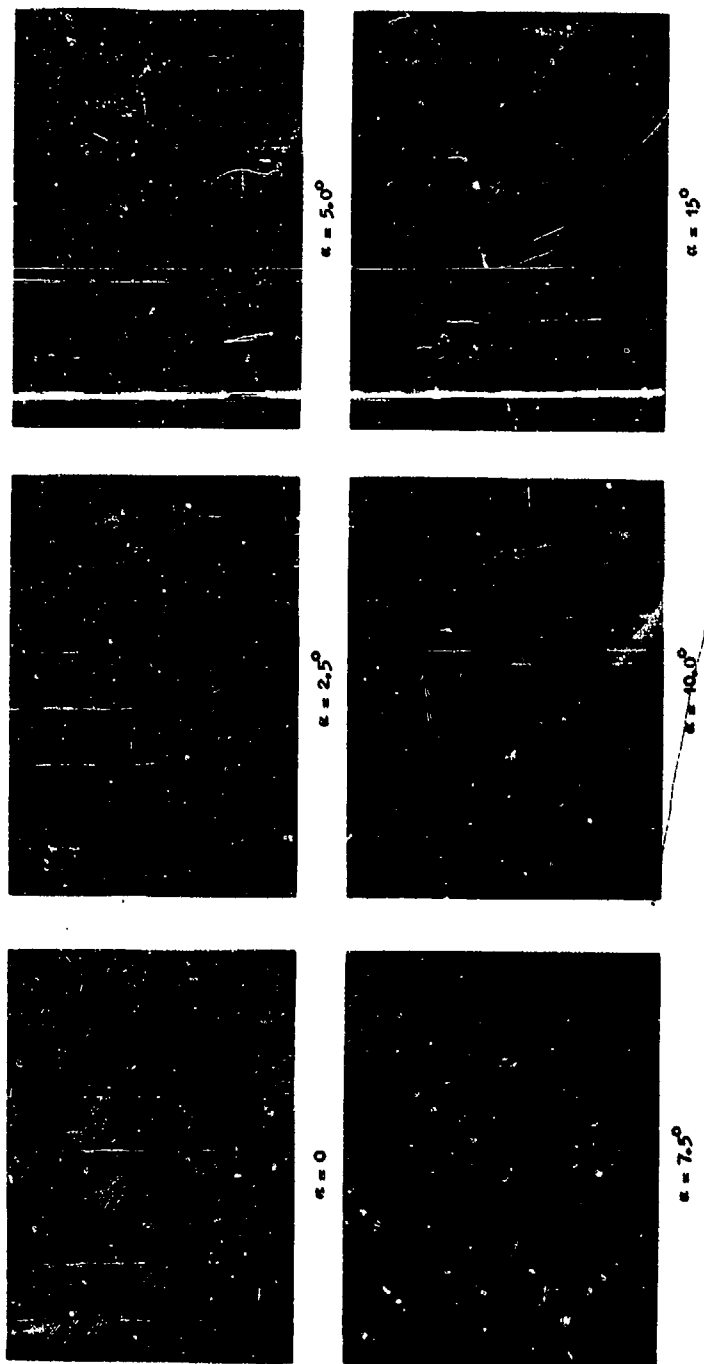


Fig. IV.61 Vapour screen photographs taken at  $M = 1.32$  showing the 'blue line' phenomenon

(i) BEAM POSITION 0.05  $C_o$  AHEAD OF TRAILING EDGE(ii) BEAM POSITION 0.05  $C_o$  AFT OF TRAILING EDGE(iii) BEAM POSITION 0.30  $C_o$  AFT OF TRAILING EDGE(iv) BEAM POSITION 0.50  $C_o$  AFT OF TRAILING EDGE

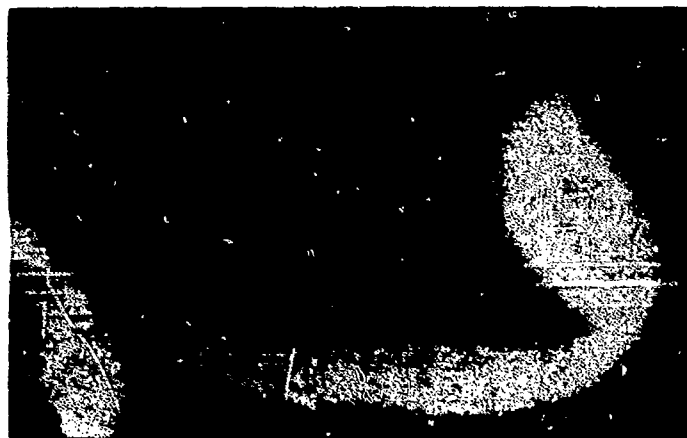
Fig. IV.62 Vapour screen photographs of the flow behind a delta wing  
at  $M = 0.85$ ,  $\alpha = 4^\circ$



(I) BEAM POSITION 0.05  $C_o$  AFT OF TRAILING EDGE



(II) BEAM POSITION 0.20  $C_o$  AFT OF TRAILING EDGE



(III) BEAM POSITION 0.50  $C_o$  AFT OF TRAILING EDGE

Fig. IV.63 Vapour screen photographs of the flow behind a delta wing  
at  $M = 0.85$ ,  $\alpha = 8^\circ$

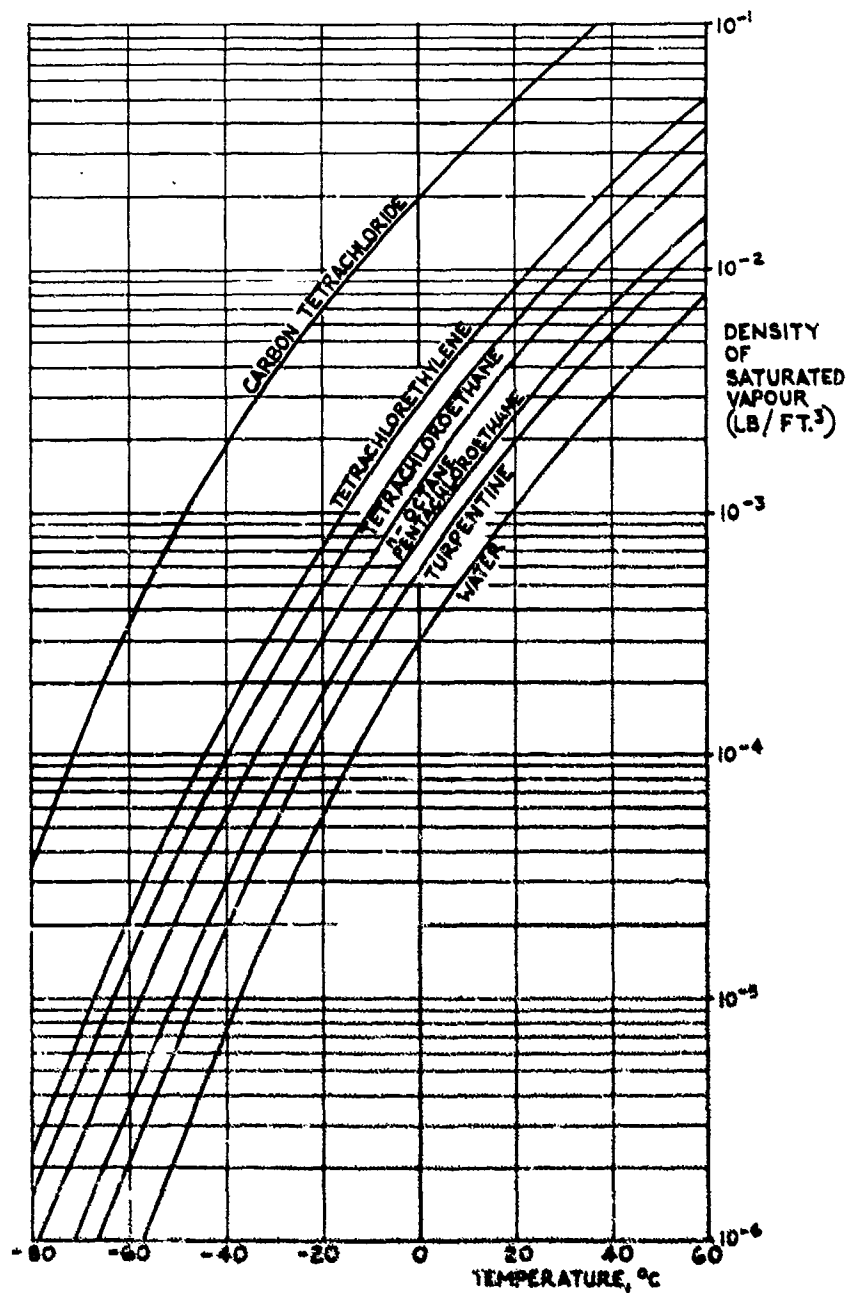


Fig. IV.64 Saturated vapour density of some organic liquids suitable for vapour screen experiments.

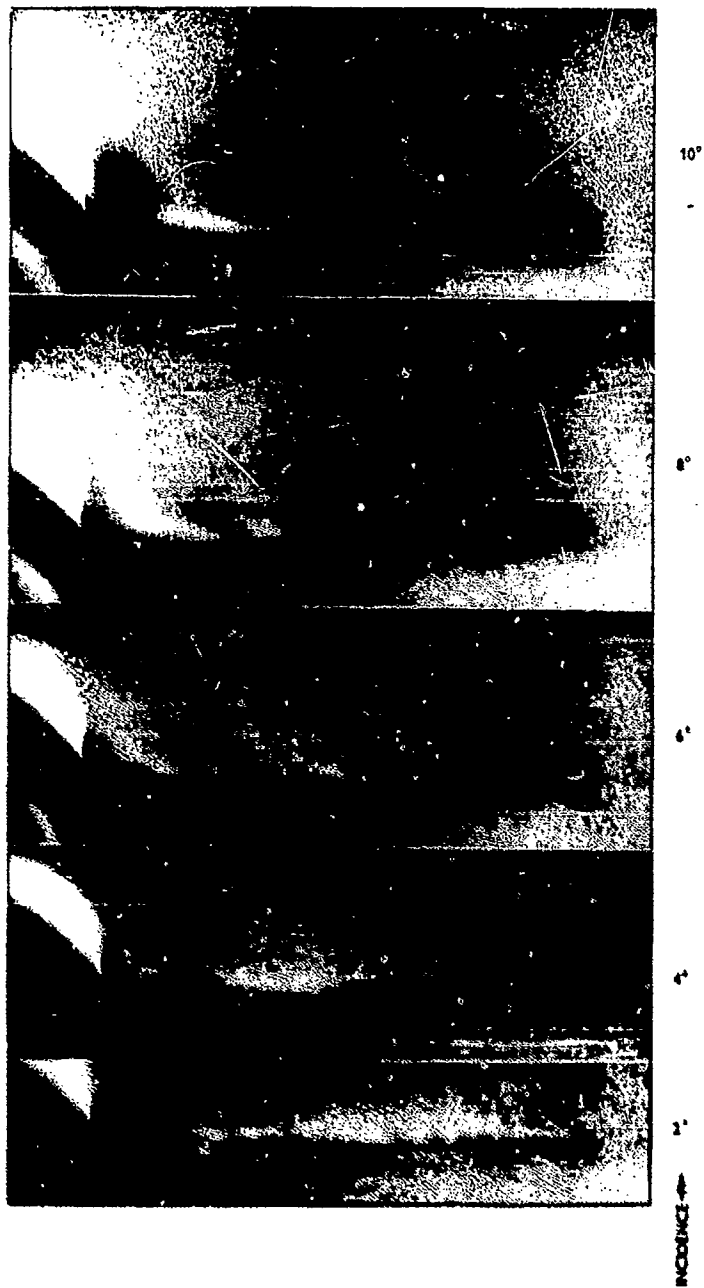


Fig. 17.65 Vapour screen photographs of the flow just behind a delta wing, using carbon tetrachloride vapour.  $M = 1.96$

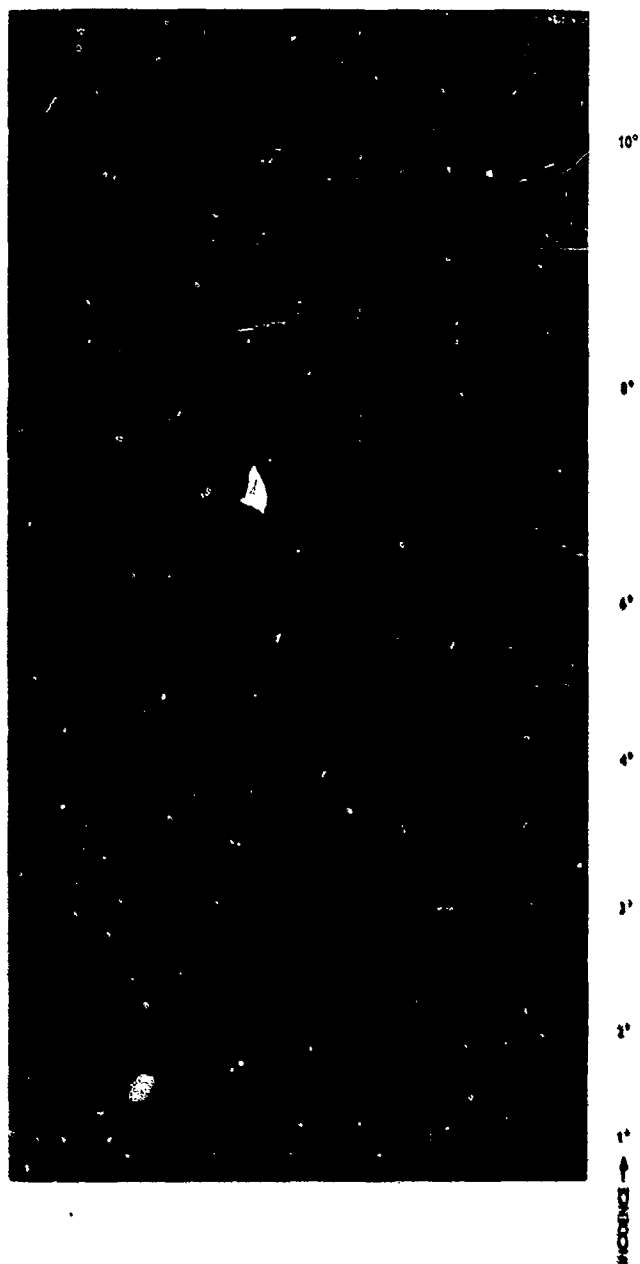


Fig. IV.66 Vapour screen photographs of the flow just behind a delta wing, using water vapour.  $M = 1.48$  ( $M_{dry} = 2.00$ )

**PART V**

**BIBLIOGRAPHY**

## CONTENTS

	Page
V.1 INTRODUCTION	167
V.2 GENERAL REFERENCES	167
V.3 METHODS USING DRY ICE	168
V.4 METHODS USING DUST AND BALSA DUST	168
V.5 METHODS USING ELECTRIC SPARKS	168
V.6 METHODS USING OIL FLOW	169
V.7 METHODS USING SMOKE	170
V.8 METHODS USING TUFTS	175
V.9 METHODS USING VAPOUR SCREEN	175
V.10 TRANSITION MEASUREMENT	176

## PART V. BIBLIOGRAPHY

## V.1 INTRODUCTION

In Parts I to IV of this AGARDograph references are made to papers which bear directly on the subjects being discussed. These papers are listed at the end of each section. The list of papers given in the Bibliography is intended to give references over the whole range of indicator flow visualization techniques and particularly those techniques which are too well established to be dealt with in the text. It does not seem appropriate to attempt an exhaustive list in a paper with this title but a representative selection of papers in English has been chosen together with a few in other languages where they are known to contain additional information.

## V.2 GENERAL REFERENCES

- B. 1 July 1932  
Gough, M.N. and Johnson, E.  
*Methods of Visually Determining the Air Flow Around Airplanes.*  
NACA TN 425.  
(Streamers, lampblack and kerosene, fine powder and smoke)
- B. 2 1933  
Clark, K.W.  
*Methods of Visualising Airflow with Observations on Several Airfoils in the Wind Tunnel.*  
ARC R & M 1552.  
(Tufts, smoke, chalk, lampblack and Lockspeiser's method of absorbent paper, lead hydroxide and ammonium sulphide)
- B. 3 1938  
Goldstein, B. (Editor)  
*Modern Developments in Fluid Dynamics Vol.1, pp.280 - 288.*  
Oxford, Clarendon Press, 1938.
- B. 4 November 1946  
Preston, J.H.  
*Visualization of Boundary Layer Flows.*  
ARC R & M 2267, ARC 10,094.
- B. 5 1952  
Pankhurst, R.C. and Holder, D.W.  
*Wind Tunnel Technique: An Account of Experimental Methods in Low and High Speed Wind Tunnels.*  
Pitman, London, 1952.
- B. 6 June 1953  
Balint, E.  
*Techniques of Flow Visualization: A Discussion of the Fundamentals with Examples of Techniques Used in Research.*  
*Aircraft Engineering* 23 (1953) June, pp.161 - 167.

- B. 7 August 1955  
 Perry, C.C.  
*Visual Flow Analysis.*  
 Product Engineering August 1955, pp.154 - 161.

### V.3 METHODS USING DRY ICE

- B. 8 December 1953  
 Sellerio, A.  
*Impiego del Ghiaccio Secco nella Visualizzazione delle Correnti d'Aria.*  
*(On the Use of Dry Ice for the Visualization of Air Streams.)*  
 L'Aerotecnica 33 (1955) 6 (December), pp.398 - 400.

### V.4 METHODS USING DUST AND BALSA DUST

- B. 9 November 1950  
 Taylor, M.K.  
*A Balsa-Dust Technique for Airflow Visualization and its Application to Flow Through Model Helicopter Rotors in Static Thrust.*  
 NACA TN 2220.
- B.10 April 1955  
 Smith, A.M.O. and Murphy, J.B.  
*A Dust Method for Locating the Separation Point.*  
 Journal of the Aeronautical Sciences 22 (1955) 4 (April), pp.273, 274.

### V.5 METHODS USING ELECTRIC SPARKS

- B.11 January 1950  
 Sahaki, Y.  
*On the Measurement of Wind (Tunnel) Velocity (Distributions) by the Electric Spark Method.*  
 National Research Council, Canada, Tech. Translation No. TT-100.  
 (TIL No.P.34187)
- B.12 January 1956  
 Bomelburg, H.J.  
*A Method for the Measurement of the Flow of Air by Means of a Series of Electric Sparks.*  
 Maryland Univ. TN BN 68.  
 AFOSR TN 58-35, ASTIA AD 80549, (TIL No.P.64967).
- B.13 July 1957  
 Herzog, J. and Weske, J.R.  
*Characteristics of the Technique of Aerodynamic Investigation by Means of Electric Sparks.*  
 Maryland Univ. TN BN 105, U.S.A. AFOSR TN 57-387, ASTIA AD 132,432.

- B.14 April 1958  
Weske, J.R.  
*Application of the Electric Spark Method to the Investigation of Transonic Flow Past Airfoils and Airfoil Grids.*  
Maryland Univ. TN BN 128, U.S.A. AFOSR TN 58-304, ASTIA AD 154,214.
- B.15 January 1959  
Bomelburg, H.J., Herzog, J. and Weske, J.R.  
*The Electric Spark Method for Quantitative Measurements in Flowing Gases.*  
Maryland Univ. TN BN 157, U.S.A. AFOSR TN 59-273,  
ASTIA AD 212,707 (T.L. No.P.77300).

#### V.6 METHODS USING OIL FLOW

- B.16 October 1938  
Abbott, I.H. and Sherman, A.  
*Flow Observations with Tufts and Lampblack of the Stalling of Four Typical Airfoil Sections in the NACA Variable-Density Tunnel.*  
NACA TN 672.
- B.17 June 1950  
Moos, G.F. and Hills, R.  
*Visualization of the Flow at the Stall on Wind Tunnel Models.*  
Unpublished NDA Report ARC 13599.  
(White oil, medium gearbox oil - Duckham Q 400 is used)
- B.18 February 1953  
Manoni, L.R. and Cadwell, J.D.  
*An Oil Spray Technique Suitable for Visual Transonic Flow Observations.*  
United Aircraft Corp., U.S.A. Res. Dept. Report R-14107-11.
- B.19 September 1954  
Haines, A.B.  
*Some Notes on the Flow Patterns Observed over Various Sweptback Wings at Low Mach No. (in the R.A.E. 10 x 7 ft High Speed Tunnel).*  
ARC 17087. Unpublished NDA Report.  
(Titanium oxide technique)
- B.20 October 1954  
Johnson, H.I. and Mungall, R.O.  
*A Preliminary Flight Investigation of an Oil-Flow Technique for Air-Flow Visualization.*  
NACA/TIB/4472, NACA RM L54Q14a.
- B.21 October 1956  
Bazzocchi, E.  
*Boundary Layer Flow Visualization Tests in a Low Velocity Wind Tunnel.*  
(In Italian).  
*L'Aerodinamica* 36 (1956) 8 (October), pp.315-332.  
(Kerosene - carbon black)

- B. 22 1957  
Persoz, B. and Grenier, G.  
*Enduits de Visualisation à Base de Corps Gras.*  
La Recherche Aéronautique No.60 September - October 1957, pp.19 - 22.  
(Coating materials which melt at temperatures of 30° or 40°C.)
- B. 23 March 1958  
Ogle, J.S.  
*Memorandum on the Fluorescent Oil Flow Visualization System.*  
Southern California Co-operative Wind Tunnel Project No.K-323.
- B. 24 March 1959  
Loving, D.L. and Katzoff, S.  
*The Fluorescent-Oil Film Method and Other Techniques for Boundary-Layer Flow Visualization.*  
NASA/TIL/6310, NASA Memo. 3-17-59L, ARC 21689.
- B. 25 August 1959  
Carter, E.C.  
*Model Testing in the ARA Co-operative Wind Tunnels.*  
ARA WT Note 49.
- B. 26 February 1960  
Squire, L.C.  
*The Motion of a Thin Oil Sheet under the Boundary Layer on a Body.*  
Journ. Fluid Mech. Vol.II, 1961, Part 2, June.
- B. 27 July 1960  
Stanbrook, A.  
*An Experimental Study of the Glancing Interaction Between a Shock Wave and a Turbulent Boundary Layer.*  
ARC CP 335.
- B. 28 August 1960  
Stanbrook, A.  
*The Surface Oil Flow Technique Used in High Speed Wind Tunnels.*  
Unpublished NDA Report ARC 22385.
- B. 29 August 1960  
Maltby, R.I.  
*Flow Visualization in Low Speed Wind Tunnels: Current British Practice.*  
Unpublished NDA Report ARC 22373.

#### V.7 METHODS USING SMOKE

- B. 30 January 1925  
Bryan, L.W. and Williams, D.H.  
*Discontinuous Flow Around the Edge of a Bluff Obstacle.*  
AFC R & M 962.  
(Smoke jet of ammonium chloride used to visualize the flow.)

- B.31 February 1930  
Simmonds, L.F.G. and Dewey, N.S.  
*Wind Tunnel Experiments with Circular Disks.*  
ARC R & M 1334.
- B.32 May 1930  
Simmonds, L.F.G. and Dewey, N.S.  
*Photographic Records of Flow in the Boundary Layer.*  
ARC R & M 1335.  
(Vapour of volatile liquids, smoke formed through chemical combination of two vapours, and smoke produced by the chemical action of vapour in the presence of moist air.)
- B.33 1931  
Tanner, T.  
*Movement of Smoke in the Boundary Layer of an Aerofoil Without and With Slot.*  
ARC R & M 1352.
- B.34 1932  
Farren, W.S.  
*Air Flow; With Demonstrations on the Screen by Means of Smoke.*  
Royal Aeronautical Society Journal 23 (1932), pp.451 - 472.
- B.35 1938  
Valensi, J.  
*Application de la Méthode des Fillets de Fumée à l'Etude des Champs Aérodynamiques.*  
Publications Scientifiques et Techniques de Ministère de l'Air No.128.
- B.36 1939  
Lippisch, A.  
*Results from the Deutsche Forschungsinstitut für Segelflug Smoke Tunnel.*  
Royal Aeronautical Society Journal 43 (1939) September, pp.683 - 672.
- B.37 1943  
Preston, J.H. and Sweeting, N.E.  
*Food Smoke as a Means of Visualizing Boundary Layer Flow at High Reynolds Numbers.*  
Royal Aeronautical Society Journal 47 (1943) 37 (March), pp.93 - 102.
- B.38 October 1943  
Preston, J.H. and Sweeting, N.E.  
*An Improved Smoke Generator for use in the visualization of Airflow, particularly Boundary Layer Flow at High Reynolds Numbers.*  
ARC R & M 2023, ARC 7111.
- B.39 March 1949  
Davidson, I.M., Forbaker, G.N. and Inney, L.E.  
*An Improved Method of Flow Visualization by 'Reflected' Light.*  
Unpublished MIA Report ARC 17371.

- B. 40      September 1949  
 Brotherhood, P. and Stewart, W.  
*An Experimental Investigation of the Flow through a Helicopter Rotor in Forward Flight.*  
 ARC R & M 2734.
- B. 41      March 1950  
 Salter, C.  
*Multiple Jet White Smoke Generators.*  
 ARC 10296, 13004, ARC R & M 2657.
- B. 42      April 1951  
 Meijer Drees, J. and Hendal, W.P.  
*The Field of Flow Through a Helicopter Rotor, Obtained from Wind Tunnel Smoke Tests.*  
 NLL, Amsterdam, Report A.1205.  
 Aircraft Engineering 23 (1951) 266 (April), pp. 107 - 110.  
 (Describes apparatus used.)
- B. 43      1952  
 Brown, F.N.M.  
*An American Method of Photographing Flow Patterns.*  
 Second Midwestern Conference on Fluid Mechanics, pp. 119 - 129.  
 Aircraft Engineering 24 (1952) June, pp. 154 - 169.  
 (Using a smoke tunnel.)
- B. 44      August 1952  
 Herzig, H.Z., Hansen, A.G. and Costello, G.R.  
*A Visualization Study of Secondary Flows in Cascades.*  
 NACA Report 1163. (Formerly NACA/TIB/3111 (NACA RM E52F19) and NACA TN 2947.)  
 (Methods used are smoke traces and hydrogen sulfide gas reacting with lead carbonate in glycerin.)
- B. 45      1953  
 Hazen, D.C. and Finley, H.B.  
*Operating Characteristics of the Princeton University 14 x 2 ft Smoke Tunnel.*  
 Princeton Univ. Dept. of Aero. Eng. Report 225.
- B. 46      February 1954  
 Pascale, L.  
*Il Tunnel a Fumo dell' Istituto di Costruzioni Aeronautiche dell' Universita di Napoli.*  
 L' Aerotecnica 34 (1954) 1 (February), pp. 16 - 22.
- B. 47      1954<sup>+</sup>  
 Knowlton, M.P.  
*Theoretical Investigation on the Determination of Lift Coefficients in Two-Dimensional Smoke Tunnels.*  
 Princeton Univ. Dept. of Aero. Eng. Report 249.

- B. 48 1954?  
Hazen, D.C. and Lehnert, R.F.  
*Smoke Flow Studies Conducted at Princeton University.*  
Princeton Univ., Dept. Aero. Eng. Report 290. ASTIA AD 63022,  
(TIL No. P.83055).
- B. 49 1955  
Hazen, D.C. and Lehnert, R.F.  
*Operating Characteristics of the Princeton University 2 x 36 ft Smoke Tunnel.*  
Princeton Univ. Dept. Aero. Eng. Report 299.
- B. 50 1955  
Hazen, D.C.  
*Some Results of the Princeton University Smoke Flow Visualization Program.*  
Proceedings of the IAS-R.Ae.S. Fifth International Aeronautical Conference, Los Angeles, 1955, pp.316 - 352.  
IAS Preprint 555.
- B. 51 June 1956  
*Airflows Studied in Miniature Smoke-Jet Wind Tunnels.*  
Aero. Digest June 1956, pp.35 - 39.
- B. 52 November 1956  
Maltby, R.L. and Peckham, D.H.  
*Low Speed Flow Studies of the Vortex Patterns above Inclined Slender Bodies Using a New Smoke Technique.*  
Unpublished MJA Report ARC 19541.
- B. 53 March 1957  
Bull, G.V. and Jeffery, C.B.  
*Wake Visualization Studies in the Aeroballistics Range.*  
Ballistics Res. Lab., U.S.A., Report 1005 pt.1, pp.127 - 148.  
(Flow visualization by the interaction of hydrochloric acid and ammonia hydroxide vapours.)
- B. 54 October 1957  
O'Neill, P.G.G.  
*Generator Constructed in Metal for Producing Small Quantities of Paraffin Smoke.*  
NPL Aero 1340.
- B. 55 February 1958  
Lippisch, A.M.  
*Flow Visualization: An Amplification of the Author's Remarks made at the Fifth International Aeronautical Conference, with Prints taken from Films of his Studies.*  
Aeronautical Engineering Review 17 (1958) 2 (February), pp.24 - 32.

- B. 56 March 1958  
Bergh, H. and Berg, B. van den  
*On the Visualization of Laminar Boundary Layer Oscillations and the Transition to Turbulent Flow.*  
Z. Angew. Math. Phys. 9 (1958) 5/6 (March 25th), pp.97 - 104.  
(Smoke with a stroboscopic light source.)
- B. 57 May 1958  
*Voir le sillage.*  
Air Revue May 1958, pp.272 - 273.  
(Evaluation of smoke techniques.)
- B. 58 November/December 1958  
LeManach, J. and Robert, E.  
*Contribution of Visualisation to the Study of Low Velocity Flow in Models of Centrifugal Compressors.*  
MOA TIL/T.5088. La Recherche Aéronautique No.67, November - December, 1958, pp.21 - 34.  
(Methods of visualization include Hostafilon powder floating on the surface for the water compressors and kerosene smoke trails for the air compressor.)
- B. 59 June 1959  
Cox, A.F.  
*Measurements of the Velocity at the Vortex Centre on an A.P.1 Delta Wing by Means of Smoke Observations.*  
ARC CP 511.
- B. 60 August 1959  
Muirhead, J.C.  
*On the Inertial Lag of Tobacco Smoke Particles and the Effect of Small Orifices on Shock Tube Flows.*  
Suffield, Canada, Tech. Paper 167. (TIL No.P.84154).
- B. 61 November 1959  
Goddard, V.P., McLaughlin, J.A. and Brown, F.N.M.  
*Visual Supersonic Flow Patterns by Means of Smoke Lines.*  
Journal of the Aero/Space Sciences 26 (1959) 11 (November), pp.761 - 762.
- B. 62 August 1960  
Maltby, R.L. and Keating, R.F.A.  
*Flow Visualization in Low Speed Wind Tunnels: Current British Practice.*  
Unpublished MOA Report ARC 22373.
- B. 63 1962  
Maltby, R.L., Engler, P.B. and Keating, R.F.A.  
*Some Measurements of Leading Edge Vortex Positions on a Delta Wing Oscillating in Heave.*  
Unpublished MOA Report.
- B. 64 May 1962  
Maltby, R.L. and Whitmore, G.  
*Smoke for Flow Visualization - A Warning.*  
Journal R. Ae. Soc. Vol.68, No.617, p.326.

## V.8 METHODS USING TUFTS

- B.65 1928  
Haslam, J. A. G.  
*Wool Tufts: A Direct Method of Discriminating Between Steady and Turbulent Airflow over the Wing Surfaces of Aircraft in Flight Applied to Explore the Region of Effect of the Slot on a Bristol Fighter Wing.*  
ARC R & M 1209.
- B.66 1932  
Melvill Jones, B. and Haslam, J. A. G.  
*Airflow about Stalled and Spinning Aeroplanes shown by Cinematographic Records of the Movements of Wool-Tufts.*  
ARC R & M 1494.
- B.67 October 1938  
Abbott, I. H. and Sherman, A.  
*Flow Observations with Tufts and Lampblack of the Stalling of Four Typical Airfoil Sections in the NACA Variable-Density Tunnel.*  
NACA TN 672.
- B.68 May 1952  
Bird, J. D. and Riley, D. R.  
*Some Experiments on Visualization of Flow Fields Behind Low-Aspect-Ratio Wings by Means of a Tuft Grid.*  
NACA TN 2874.
- B.69 July 1952  
Bird, J. D.  
*Visualization of Flow Fields by Use of a Tuft Grid Technique.*  
*Journal of the Aeronautical Sciences* 19 (1952) 7 (July), pp. 481 - 485.

## V.9 METHODS USING VAPOUR SCREEN

- B.70 1951  
Allen, R. J. and Perkins, E. W.  
*A Study of Effects of Viscosity on Flow over Slender Inclined Bodies of Revolution.*  
NACA Report 1048.
- B.71 August 1957  
Hall, I. M., Rogers, E. W. E. and Davis, B. M.  
*Experiments with Inclined Blunt-Nosed Bodies at  $M = 2.45$ .*  
ARC R & M 3128 ARC 19, 479.  
(Vapour-screen techniques described in Appendix.)
- B.72 August 1960  
McGregor, I.  
*Development of the Vapour Screen Method of Flow Visualization in the 3 ft Tunnel at RAE, Bedford.*  
*Jour. Fluid Mech.*, Vol. II, 1961, Part 4, Dec.

## V. 10 TRANSITION MEASUREMENT

- B. 73 April 1940  
Richards, E.J. and Brown, T.W.  
*Note on Methods of Determining Transition on an Aerofoil in a Wind Tunnel.*  
ARC R & M 2053, ARC 4486.  
(Lycopodium powder)
- B. 74 July 1944  
Gray, W.E.  
*A Chemical Method of Indicating Transition in the Boundary Layer.*  
ARC 8034. Unpublished MOA Report.  
(Starch iodide - sodium thiosulphate - chlorine gas)
- B. 75 October 1944  
Gray, W.E. and Pringle, G.E.  
*Note on Observations of the Boundary Layer on a Fighter with Low Drag Wings. (King Cobra.)*  
ARC 8153. Unpublished MOA Report.
- B. 76 March 1945  
Preston, J.H. and Sweeting, N.E.  
*Experiments on the Measurement of Transition Position by Chemical Methods.*  
ARC R & M 2014, ARC 8536.
- B. 77 June 1945  
Pringle, G.E. and Main-Smith, J.D.  
*Boundary Layer Transition Indicated by Sublimation.*  
ARC 8892. Unpublished MOA Report.
- B. 78 August 1945  
Richards, E.J. and Burstall, F.H.  
*The China Clay Method of Indicating Transition.*  
ARC R & M, 3126, ARC 8867.
- B. 79 July 1945  
Holder, D.W.  
*Transition Indication in the National Physical Laboratory 20 x 8 in. High Speed Tunnel.*  
ARC R & M 2079, ARC 8866.
- B. 80 August 1946  
Gray, W.E.  
*A Simple Visual Method of Recording Boundary Layer Transition (liquid film).*  
ARC 10028. Unpublished MOA Report.

- B.81 December 1946  
Merewether, E.R.A., Smith, J.H.F., Pankhurst, R.C. and Burstall, F.H.  
*A Note on the Toxic Effects of Some Chemicals Previously Recommended for use in Wind Tunnel Technique and on Vapour and Gas Explosion Risks in Wind Tunnels.*  
ARC R & M 2198.  
(Lead compounds, nitrobenzene, nitrotoluene, chloronaphthanes and glycols should all be avoided.)
- B.82 1947  
Pankhurst, R.C.  
*Cautionary Note Regarding Some Chemicals for Transition Indication.*  
Royal Aeronautical Society Journal 51 (1947), pp.651 - 652.
- B.83 1947  
Reif, E.F.  
*Nitrobenzene Dangers (letter to the Editor).*  
Royal Aeronautical Society Journal 51 (1947), pp.69.
- B.84 January 1947  
Gray, W.E.  
*Interim Note on Boundary Layer Transition Tests in Flight by the Chemical Method.*  
ARC 10233. Unpublished MOA Report.
- B.85 April 1949  
Dando, R.C.A.  
*Two Methods of Boundary Layer Transition Indication Suitable for Routine Tests in Flight.*  
ARC 12531. Unpublished MOA Report.
- B.86 March 1950  
Gazely, C.  
*The Use of the China Clay Lacquer Technique for Detecting Boundary Layer Transition.*  
General Electric Co., U.S.A., Report No. R49A0536.
- B.87 March 1950  
Gray, W.E.  
*Transition in Flight on a Laminar-Flow Wing of Low Waviness (King Cobra).*  
Unpublished MOA Report ARC 13221.  
(Improvement in flight technique in connection with the chemical methods of indicating transition.)
- B.88 May 1950  
Main-Smith, J.D.  
*Chemical Solids as Diffusible Coating Films for Visual Indication of Boundary Layer Transition in Air and Water.*  
ARC R & M 2755.

- B. 89 1951  
Wijker, H.  
*Survey of Transition Point Measurements at the N.L.L. Mainly for Two Dimensional Flow over a NACA 0018 Profile.*  
National Luchtvaartlaboratorium, Amsterdam, Report A.1269.  
(Methods used are China clay, H<sub>2</sub>S and smoke.)
- B. 90 February 1951  
Stalder, J.R. and Slack, E.G.  
*The Use of a Luminescent Lacquer for the Visual Indication of Boundary-Layer Transition.*  
NACA TN 2263.
- B. 91 August 1951  
Owen, P.R. and Omerod, A.O.  
*Evaporation from the Surface of a Body in an Airstream (with particular reference to the chemical method of indicating boundary layer transition).*  
ARC R & M 2875.
- B. 92 November 1951  
Murphy, J.S. and Phinney, R.E.  
*Visualization of Boundary Layer Flow.*  
Journal of the Aeronautical Sciences 18 (1951) 11 (November), pp.771 - 772.  
( 'China film' technique, a hybrid of the 'China clay' and 'liquid film' techniques.)
- B. 93 January 1952  
Britland, C.M. and Sibbald, P.A.  
*Preliminary Flight Tests to Determine the Position of Boundary Layer Transition on a Large Aircraft. (Armstrong Whitworth E9/44.)*  
Unpublished MOA Report ARC 15142.
- B. 94 September 1954  
Winter, K.G., Scott-Wilson, J.B. and Davies, F.V.  
*Methods of Determination and of Fixing Boundary Layer Transition on Wind Tunnel Models at Supersonic Speeds.*  
ARC CP 212  
AGARD AG 17/P7.  
(Sublimation and oil flow)
- B. 95 December 1954  
Murphy, J.S. and Smith, A.M.O.  
*Measurements of Shearing Stress by Means of an Evaporating Liquid Film.*  
Douglas Aircraft Co., U.S.A., Report No. ES. 17813.
- B. 96 July 1955  
Atkins, P.B. and Trayford, R.S.  
*A Method of Boundary Layer Flow Visualisation for Use in Flight.*  
A.R.L., Australia, Flight Note 22.  
(China clay method)

- B. 97      October 1955  
            Stalker, R.J.  
            *A Study of the China-film Technique for Flow Indication.*  
            A.R.L., Australia, Report A96 (TIL No. 1.56984).
- B. 98      April 1956  
            Friedman, A.E.  
            *Chemiluminescence as a Tool in the Study of Liquid Flow Boundaries.*  
            *Journal of Applied Physics* 27 (1956) No. 4, (April), p. 417.
- B. 99      August 1956  
            Stalker, R.J.  
            *A Note on the China-film Technique for Boundary Layer Indication.*  
            Royal Aeronautical Society Journal 60 (1956) 548 (August), pp. 543 - 544.
- B. 100     October 1957  
            Rygh, P.J. and Martin, R.E.  
            *The Use of Azobenzene to Provide a Visual Indication of Supersonic-Boundary-Layer Transition.*  
            California Institute of Technology Jet Prop. Lab. Prog. Report 20-335,  
            ASTIA AD 159,889.
- B. 101     January 1958  
            Cornillon, J.  
            *Extension de la Technique de l'Argile de Chine à l'Etude des Ecoulements et des Echauffements de Maquettes en Régime Supersonique.*  
            Docaéro January 1958, pp. 15 - 18.  
            (Extension of the china-clay technique)
- B. 102     November 1958  
            Van der Blik, J.A.  
            *Boundary Layer Transition on a 10-degree Cone in the NAE 30 x 16 in. Wind Tunnel.*  
            NAE, Canada, LR-232.  
            (Fluorescent lacquer technique, French chalk and lampblack and kerosene methods of visualization described)

## DISTRIBUTION

Copies of AGARD publications may be obtained in the various countries at the addresses given below.

On peut se procurer des exemplaires des publications de l'AGARD aux adresses suivantes.

BELGIUM BELGIQUE	Centre National d'Etudes et de Recherches Aéronautiques 11, rue d'Egmont, Bruxelles
CANADA	Director of Scientific Information Service Defense Research Board Department of National Defense 'A' Building, Ottawa, Ontario
DENMARK DANEMARK	Military Research Board Defense Staff Kastellet, Copenhagen Ø
FRANCE	O.N.E.R.A. (Direction) 25, Avenue de la Division Leclerc Châtillon-sous-Bagneux (Seine)
GERMANY ALLEMAGNE	Zentralstelle für Luftfahrt- dokumentation und -information München 27, Maria-Theresia Str. 21 Attn: Dr. H.J. Rautenberg
GREECE GRECE	Greek National Defense General Staff B. MECO Athens
ICELAND ISLANDE	Director of Aviation c/o Flugrad Reykjavik
ITALY ITALIE	Ufficio del Generale Ispettore del Genio Aeronautico Ministero Difesa Aeronautica Roma
LUXEMBURG LUXEMBOURG	Obtainable through Belgium
NETHERLANDS PAYS BAS	Netherlands Delegation to AGARD Michiel de Ruyterweg 10 Delft

NORWAY NORVEGE	Mr. O. Blichner Norwegian Defence Research Establishment Kjeller per Lilleström
PORTUGAL	Col. J.A. de Almeida Vianna (Delegado Nacional do 'AGARD') Direcção do Serviço de Material da F.A. Rua da Escola Politecnica, 42 Lisboa
TURKEY TURQUIE	Ministry of National Defence Ankara Attn. AGARD National Delegate
UNITED KINGDOM ROYAUME UNI	Ministry of Aviation T.I.L., Room 009A First Avenue House High Holborn London W.C.1
UNITED STATES ETATS UNIS	National Aeronautics and Space Administration (NASA) 1520 H Street, N.W. Washington 25, D.C.



<p>AGARDograph 70 North Atlantic Treaty Organization, Advisory Group for Aeronautical Research and Development FLOW VISUALIZATION IN WIND TUNNELS USING INDICATORS Compiled by R.L. Malby 1962 179 pp., Incl. 58 refs., 66 figs &amp; bibliography</p> <p>This AGARDograph describes various flow visualization techniques in current use in British wind tunnel practice which are not dealt with fully elsewhere. Emphasis is on such of these techniques that have been developed during recent years - particularly those devised for the understanding of separated flows. These include two of the most valuable methods for investigating three-dimensional</p> <p>P. T. O.</p>	<p>AGARDograph 70 North Atlantic Treaty Organization, Advisory Group for Aeronautical Research and Development FLOW VISUALIZATION IN WIND TUNNELS USING INDICATORS Compiled by R.L. Malby 1962 179 pp., Incl. 58 refs., 66 figs &amp; bibliography</p> <p>This AGARDograph describes various flow visualization techniques in current use in British wind tunnel practice which are not dealt with fully elsewhere. Emphasis is on such of these techniques that have been developed during recent years - particularly those devised for the understanding of separated flows. These include two of the most valuable methods for investigating three-dimensional</p> <p>P. T. O.</p>	<p>533 6 071 3 37855</p>	<p>533 6 071 3 37865</p>
<p>AGARDograph 70 North Atlantic Treaty Organization, Advisory Group for Aeronautical Research and Development FLOW VISUALIZATION IN WIND TUNNELS USING INDICATORS Compiled by R.L. Malby 1962 179 pp., Incl. 58 refs., 66 figs &amp; bibliography</p> <p>This AGARDograph describes various flow visualization techniques in current use in British wind tunnel practice which are not dealt with fully elsewhere. Emphasis is on such of these techniques that have been developed during recent years - particularly those devised for the understanding of separated flows. These include two of the most valuable methods for investigating three-dimensional</p> <p>P. T. O.</p>	<p>AGARDograph 70 North Atlantic Treaty Organization, Advisory Group for Aeronautical Research and Development FLOW VISUALIZATION IN WIND TUNNELS USING INDICATORS Compiled by R.L. Malby 1962 179 pp., Incl. 58 refs., 66 figs &amp; bibliography</p> <p>This AGARDograph describes various flow visualization techniques in current use in British wind tunnel practice which are not dealt with fully elsewhere. Emphasis is on such of these techniques that have been developed during recent years - particularly those devised for the understanding of separated flows. These include two of the most valuable methods for investigating three-dimensional</p> <p>P. T. O.</p>	<p>533 6 071 3 37865</p>	<p>533 6 071 3 37855</p>

flow, namely, the vapour screen and surface oil flow techniques. Other techniques described are various techniques for locating boundary-layer transition, and smoke techniques for use in low-speed wind tunnels. Included in the AGARDograph are many references, and also an extensive Bibliography covering the complete range of indicator techniques.

April 1962.

flow, namely, the vapour screen and surface oil flow techniques. Other techniques described are various techniques for locating boundary-layer transition, and smoke techniques for use in low-speed wind tunnels. Included in the AGARDograph are many references, and also an extensive Bibliography covering the complete range of indicator techniques.

April 1962.

flow, namely, the vapour screen and surface oil flow techniques. Other techniques described are various techniques for locating boundary-layer transition, and smoke techniques for use in low-speed wind tunnels. Included in the AGARDograph are many references, and also an extensive Bibliography covering the complete range of indicator techniques.

April 1962.

flow, namely, the vapour screen and surface oil flow techniques. Other techniques described are various techniques for locating boundary-layer transition, and smoke techniques for use in low-speed wind tunnels. Included in the AGARDograph are many references, and also an extensive Bibliography covering the complete range of indicator techniques.

April 1962.

<p>AGARDograph 70 North Atlantic Treaty Organization, Advisory Group for Aeronautical Research and Development: FLOW VISUALIZATION IN WIND TUNNELS USING INDICATORS Compiled by R. L. Maltby 1962 179 pp., incl. 58 refs., 66 figs &amp; bibliography</p> <p>This AGARDograph describes various flow visualization techniques in current use in British wind tunnel practice which are not dealt with fully elsewhere. Emphasis is on such of these techniques that have been developed during recent years - particularly those devised for the understanding of separated flows. These include two of the most valuable methods for investigating three-dimensional</p> <p>P.T.O.</p>	<p>532 6 071 3 21825</p>	<p>AGARDograph 70 North Atlantic Treaty Organization, Advisory Group for Aeronautical Research and Development: FLOW VISUALIZATION IN WIND TUNNELS USING INDICATORS Compiled by R. L. Maltby 1962 179 pp., incl. 58 refs., 66 figs &amp; bibliography</p> <p>This AGARDograph describes various flow visualization techniques in current use in British wind tunnel practice which are not dealt with fully elsewhere. Emphasis is on such of these techniques that have been developed during recent years - particularly those devised for the understanding of separated flows. These include two of the most valuable methods for investigating three-dimensional</p> <p>P.T.O.</p>	<p>532 6 071 3 21825</p>
<p>AGARDograph 70 North Atlantic Treaty Organization, Advisory Group for Aeronautical Research and Development: FLOW VISUALIZATION IN WIND TUNNELS USING INDICATORS Compiled by R. L. Maltby 1962 179 pp., incl. 58 refs., 66 figs &amp; bibliography</p> <p>This AGARDograph describes various flow visualization techniques in current use in British wind tunnel practice which are not dealt with fully elsewhere. Emphasis is on such of these techniques that have been developed during recent years - particularly those devised for the understanding of separated flows. These include two of the most valuable methods for investigating three-dimensional</p> <p>P.T.O.</p>	<p>532 6 071 3 21825</p>	<p>AGARDograph 70 North Atlantic Treaty Organization, Advisory Group for Aeronautical Research and Development: FLOW VISUALIZATION IN WIND TUNNELS USING INDICATORS Compiled by R. L. Maltby 1962 179 pp., incl. 58 refs., 66 figs &amp; bibliography</p> <p>This AGARDograph describes various flow visualization techniques in current use in British wind tunnel practice which are not dealt with fully elsewhere. Emphasis is on such of these techniques that have been developed during recent years - particularly those devised for the understanding of separated flows. These include two of the most valuable methods for investigating three-dimensional</p> <p>P.T.O.</p>	<p>532 6 071 3 21825</p>

flow, namely, the vapour screen and surface oil flow techniques. Other techniques described are various techniques for locating boundary-layer transition, and smoke techniques for use in low-speed wind tunnels. Included in the bibliography are many references, and also an extensive bibliography covering the complete range of indicator techniques.

April 1962.

flow, namely, the vapour screen and surface oil flow techniques. Other techniques described are various techniques for locating boundary-layer transition, and smoke techniques for use in low-speed wind tunnels. Included in the bibliography are many references, and also an extensive bibliography covering the complete range of indicator techniques.

April 1962.

flow, namely, the vapour screen and surface oil flow techniques. Other techniques described are various techniques for locating boundary-layer transition, and smoke techniques for use in low-speed wind tunnels. Included in the bibliography are many references, and also an extensive bibliography covering the complete range of indicator techniques.

April 1962.

flow, namely, the vapour screen and surface oil flow techniques. Other techniques described are various techniques for locating boundary-layer transition, and smoke techniques for use in low-speed wind tunnels. Included in the bibliography are many references, and also an extensive bibliography covering the complete range of indicator techniques.

April 1962.